NUREG/CR-1163
PNL-2755

/-

PCI Fuel Failure Analysis: A Report on a Cooperative Program Undertaken by Pacific Northwest Laboratory and Chalk River Nuclear Laboratories

Compiled by C. L. Mohr,
P. J. Pankaskie, Contributing Author, PNL
P. G. Heasler, Contributing Author, PNL
J. C. Wood, Contributing Author, CRNL/AECL

Pacific Northwest Laboratory

Prepared for
U. S. Nuclear Regulatory Commission

Available from

GPO Sales Program
Division of Technical Information and Document Control
U. S. Nuclear Regulatory Commission
Washington, D. C. 20555

and

National Technical Information Service
Springfield, Virginia 22161

NUREG/CR-1163
PNL-2755

PCI Fuel Failure Analysis: A Report on a Cooperative Program Undertaken by Pacific Northwest Laboratory and Chalk River Nuclear Laboratories

Manuscript Completed: December 1979
Date Published: December 1979

Compiled by
C. L. Mohr
P. J. Pankaskie, Contributing Author, PNL
P. G. Heasler, Contributing Author, PNL
J. C. Wood, Contributing Author, CRNL/AECL

Pacific Northwest Laboratory
Richland, WA 99352

Prepared for
Division of Systems Safety
Office of Nuclear Reactor Regulation
U.S. Nuclear Regulatory Commission
Washington, D.C. 20555
NRC FIN No. B2150

ACKNOWLEDGMENTS

This work was performed in cooperation with the Chalk River Nuclear Laboratory, Atomic Energy of Canada, Ltd. for the Core Performance Branch, Division of Systems Safety, U.S. Nuclear Regulatory Commission (USNRC). The authors wish to acknowledge the support and encouragement of R. O. Meyer and M. Tokar and members of the Reactor Fuels section of the Core Performance Branch, and of A. S. Bain of the Chalk River Nuclear Laboratories. The authors also acknowledge the assistance of R. L. Goodman and N. J. Wildung of the Nuclear Fuels Section, Pacific Northwest Laboratory (PNL), for the GAPCON Thermal 3 transient simulations and for the computer analysis of the PCI data. The discussions with E. L. Courtright, C. R. Hann and C. L. Mohr are also acknowledged.

The authors also wish to acknowledge and express their appreciation to the Babcock & Wilcox Company, Combustion Engineering Company, Commonwealth Edison Company, Electric Power Research Institute, Exxon Nuclear Corporation, and the General Electric Company for permission to use their data, without which this study would not have been possible.

The authors also acknowledge the efforts of the editor of this report, R. H. Williams, PNL.

ABSTRACT

Reactor fuel failure data sets in the form of initial power (P_i) final power (P_f) transient increase in power (ΔP) and burnup (Bu) were obtained for pressurized heavy water reactors (PHWRs), boiling water reactors (BWRs), and pressurized water reactors (PWRs). These data sets were evaluated and used as the basis for developing two predictive fuel failure models, a graphical concept called the PCI-OGRAM, and a nonlinear regression based model called PROFIT.

The PCI-OGRAM is an extension of the FUELOGRAM developed by AECL. It is based on a critical threshold concept for stress dependent stress corrosion cracking. Thresholds are defined in terms of the minimum post-transient power (P_{fc}) and a critical minimum transient increases in power (ΔP_c). The model uses post transient power (P_f), transient increase in power (ΔP), burnup (Bu), and dwell time at the peak post transient power.

The PROFIT model, developed at Pacific Northwest Laboratory, is the result of applying standard statistical regression methods to the available PCI fuel failure data and an analysis of the environmental and strain rate dependent stress-strain properties of the Zircaloy cladding. The PROFIT model incorporates pre-transient power (P_i), transient increase in power (ΔP), and burnup (Bu) parameters, and introduces a strain-rate dependent, strain-energy-adsorption-to-failure (SEAF) concept as the mechanistic corollary of the power ramping rate ($\dot{P}$).

CONTENTS

FIGURES

TABLES

1.0 INTRODUCTION

P. J. Pankaskie, Contributing Author, PNL,
P. G. Heasler, Contributing Author, PNL,

Fuel failures, although fractionally small under current core/plant operating recommendations,[1-6] continue to be one of the principal economic restrictions on normal plant operations. The primary source of these fuel failures is generally attributed to pellet/cladding interactions (PCI) of thermomechanical and chemical origins.[7-25] Current operating restrictions are an acknowledgment that moderate rate fuel power increases and/or abnormal operating transients pose a potential for a significant incidence of fuel failures by PCI.

Considerable efforts have been applied over the past few years to experimental investigation of the origins and mechanisms of the PCI fuel failure phenomenon. From these efforts, operating recommendations and several empirical fuel failure models[15-18] have been developed. These PCI fuel failure models are all based on a combination of pre- and/or post-transient fuel rod/assembly power, burnup, and perhaps "dwell time" at the higher post-transient power. Specific fuel rod/assembly design parameters have not been explicitly included in any of the empirical PCI fuel failure models. Analytical approaches, based on first principles and constitutive material models, are not yet sophisticated enough to provide realistic estimates of the probability of fuel failure by PCI. With the exception of pellet/cladding interfacial lubricants and/or stress corrosion cracking inhibitors, PCI fuel failure studies have not, as yet disclosed any direct link or first order effect between typical fuel rod/assembly design parameters and the susceptibility to PCI failure.

Atomic Energy of Canada, Ltd. (AECL) has acquired sufficient fuel failure data from on-line refueling experience, and from exploratory experiments performed in the Chalk River Nuclear Laboratories' NRU reactor to develop an empirical PCI-fuel failure model for CANDU fuel in pressurized heavy water reactor (PHWR) plants. These plants operate in an essentially constant power,

base loaded mode, and the fuel in these plants rarely experiences a power transient other than what occurs during on-line refueling. The fuel burnup at which PCI failures have been observed in CANDU reactors ranges from about 1.5 GWd/MTM to 6.5 GWd/MTM.

By comparison, United States light water reactor (USLWR) fuel may experience one to numerous transient increases in power. PCI fuel failures have been observed in USLWR fuels at a burnup ranging from about 1.0 GWd/MTM to greater than 30.0 GWd/MTM.

In view of the apparent success of the AECL empirical PCI fuel failure model (FUELOGRAM) in predicting fuel failures for the on-line refueling transient in CANDU-PHWRs, a cooperative effort between AECL's Chalk River Nuclear Laboratories (CRNL) and Pacific Northwest Laboratory (PNL) was undertaken to:

1. Assess the applicability of the AECL empirical fuel failure model (i.e., FUELOGRAM developed for CANDU-PHWR fuels) to USLWR fuels.
2. Review and evaluate the bases and derivation of the AECL PCI fuel failure model and, if possible, adapt the model for use by the U.S. Nuclear Regulatory Commission (USNRC) as a tool in the evaluation of LWR fuel behavior.
3. Review and evaluate USLWR and CANDU-PHWR fuels behavior data, computer codes, and other pertinent information available at AECL and the USNRC.

Section 2 of this report describes the data that were provided for use in this study. Five PCI data sets were examined. Four data sets were derived from commercial power plants, the fifth data set consists of a single fuel rod and one of a kind experimental irradiations. The operating variables common to all five data sets are:

- power (P), either pre-transient (P_i) and/or post-transient (P_f)
- the transient increase in power (ΔP)
- the fuel burnup (Bu)

Early in this study, it was discovered that the FUELOGRAM, derived from PCI fuel failure data for CANDU fuel, was uniquely applicable only to the PHWR on-line refueling operations. CRNL however concluded that the FUELOGRAM could be extended to LWR fuel by applying the FUELOGRAM methodology to PCI data from light water reactors. The result is the PCI-OGRAM model, which is described in detail in Section 3 of this report.

Based on an examination of the bases and derivation of both the FUELOGRAM and the PCI fuel failure data, PNL concluded that an analytical approach was more appropriate for assessing the likelihood of PCI fuel failure in LWR fuel. The result of this effort is the PROFIT model, described in Section 4.

Comparisons of the estimated likelihood of PCI fuel failure of the PCI-OGRAM model, the PROFIT model, and two other proprietary models are shown in Section 5.

Sections 1, 2 and 4 of this report were prepared by P. J. Pankaskie and P. G. Heasler, PNL. Sections 3 and 5 were prepared by J. C. Wood, CRNL. The sections were prepared independently by the respective contributors and do not attempt to represent a consensus opinion. This report is intended to serve in a "forum capacity" to help promote and expand communications of concepts applicable to the PCI fuel failure phenomenon.

2.0 THE DATA BASE

P. J. Pankaskie, Empirical Modeling
P. G. Heasler, Statistical Analyses

2.1 INTRODUCTION

Five fuel failure data sets were available for examination in the course of this effort. These five data sets encompass fuels designed for duty in pressurized heavy water reactors (PHWRs), pressurized light water reactors (PWRs), and boiling light water reactors (BWRs). Many of the characteristic fuel design parameters, typical of these fuels from which most of the PCI fuel failure data were derived, are shown in Table 2.1

Four of the five data sets, hereafter identified as Data Sets 1 through 4, were derived from commercial use in both PHWRs and light water reactors (LWRs) and are therefore considered to be usable either in the evaluation of the FUELOGRAM model or in the development of a PCI-fuel failure model for application to LWR fuel. Data Set 5 consists primarily of single fuel rod failures from one-of-a-kind experiments such as the Halden IFA-405 tests and other experimental irradiations.

The common parameters reported for all five data sets are:

- the initial, pre-transient power (P_i) and the peak or final, post-transient power (P_f)
- the transient increase in power (ΔP)
- the fuel burnup (Bu).

These data sets did not include either qualitatively or quantitatively significant amounts of information relative to other operating variables such as:

- power ramping rate ($\dot{P}$)
- time-to-failure (TTF)

Nor did these data sets include significant amounts of information relative to fuel design variables such as:

- prepressurization
- pellet/cladding interfacial lubricants, surface coatings, and/or SCC inhibitors
- annular, chamfered, etc. fuel pellet geometries
- vibrationally compacted particle fuel.

TABLE 2.1. Fuel Design Parameters

Parameters	Reactor Types PHWR	PWR	BWR
Cladding			
Material	Zircaloy-4	Zircaloy-4	Zircaloy-2
Outside diameter	0.60 in.	0.42 in.	0.56 in.
Wall thickness	0.015 in.	0.024 in.	0.037 in.
R/t	20	9	7
Fuel Pellet			
Material	UO_2	UO_2	UO_2
Density	95%	95%	95%
Diameters	0.56 in.	0.36 in.	0.48 in.
Fuel Rod			
Pellet-cladding gap	0.006 in.	0.007 in.	0.009 in.
Active fuel length	20 in.	144 in.	144 in.
Pressurization	(1 atm)	(1 atm)	(1 atm)

In Data Set 1, a "dwell time" parameter was included. The dwell time is the result of on-line refueling in pressure-tube type PHWRs. In on-line refueling, the fuel, which experiences the transient increase in power, is moved from its low pre-transient power position into the peak, axial power position within the pressure-tube fuel channel, where it "dwells" for approximately 18 minutes before it is moved to its final, lower power position. A very few time-to-fail (TTF) and power ramping rate ($\dot{P}$) data points were reported in Data Set 1.

2.2 GENERAL CHARACTERISTICS OF THE DATA SETS

The five data sets examined and used in this effort encompass a substantial diversity not only in fuel design parameters (see Table 2.1), but also in operating conditions under which the fuel failures occurred.

These five data sets are generally characterized as follows:

Data Set 1

This data set consists entirely of fuel failures that occurred as a result of the increase in fuel rod/assembly power accompanying on-line refueling in PHWR plants. The data set is characterized by:

1. Relatively low burnup. For all fuel, failed and non-failed, the burnup is relatively low by comparison to LWR fuels. The peak burnup in this data set is less than 7.0 GWd/MTM. With respect to burnup, this data set may be subdivided into one subset with an average burnup of 2.3 GWd/MTM and a second subset with an average burnup of 5.6 GWd/MTM. (Although the fuel burnup is substantially less than for LWR fuels, this aspect is not a major limitation because the burnup effect on PCI failure appears to diminish rapidly after 5.0 GWd/MTM.)

2. Fuel that does not experience any significant power transient prior to on-line refueling. PHWR plants operate primarily in a base-loaded mode (that is, approximately fixed power output), and therefore the fuel does not experience any significant power transient prior to on-line refueling. All failures in Data Set 1 occurred during the increase in power accompanying on-line refueling. Thus, each of the two data subsets consist of failures that resulted from a repetition of two nearly identical power transients.

3. Fuel rod failures that occur almost exclusively within the outer sixteen rod ring of the fuel assembly. All sixteen outer ring fuel rods experienced almost the same conditions throughout the on-line refueling transient to provide the best fuel rod failure statistics for this data set. The absence of PCI failures in any of the inner and intermediate fuel rod rings within the fuel assembly could provide additional information as to the range of P_f and/or ΔP conditions for PCI fuel rod failure.

4. The operating parameters (P, ΔP and Bu) were determined by calculations using proprietary core/fuel assembly simulator computer models. The values reported apply only to the sixteen outer ring fuel rods and are averaged over the length of the fuel assembly. The core kinetics computer codes have been indexed to actual fuel burnup as measured by analytical chemistry. The uncertainty in the calculated operating parameters, based on comparisons between measured and calculated fuel burnup, is estimated to be within 5%.

5. Failures that ocurred during the 18 minute dwell time. In the course of the on-line refueling operation, the fuel assemblies, which experience the transient increase in power, reside at the peak power position in the fuel channel for approximately 18 min before they are moved on to their final and slightly lower power position. For this data set, all failures were reported to have occurred sometime within this 18 min dwell time.

   Movement of a fuel assembly from the initial low power position to the peak power position within the fuel channel requires approximately 1-1/2 min. These data therefore could provide general information, although over a limited range of rates, for future evaluation of power ramp rate effects.

Data Set 2

This data set includes PCI failures that occurred under essentially normal plant operation. In general, this data set is characterized by:

1. Fuel failures that occurred over a rather wide range of fuel burnup (∿1.0 to ∿25 GWd/MTM).

2. Three fuel duty cycles. At the end of each fuel duty cycle, the fuel assemblies were examined and those that had sustained failure were retired from further duty.

3. Operating parameters (P, ΔP, Bu) were derived from calculations using a proprietary 3-D core simulator to obtain fuel assembly nodal powers (a node, as used here, is a 12-in. axial length of the fuel assembly). The fuel power was obtained by superimposing local rod power for two

positions of the control rods. The uncertainty in calculating the nodal power is estimated to be ±10%. The uncertainty in reported fuel burnup values is estimated to be in the 3% to 5% range. The values of the reported operating parameters in this data set apply to the fuel rod located in that corner of the fuel assembly adjacent to the orthogonal blades of the control element. The values for the operating parameters, P and ΔP, are for that specific 12 in. long axial segment (node) of the corner fuel rod that experiences the maximum increase in node power as a result of normal control element pattern sequences throughout the fuel cycle in which failure occurred. The value for the burnup parameter (Bu) is the average of the reported burnup immediately before and after the control element pattern sequencing for which the nodal power increase was a maximum for the fuel cycle. In each operating cycle, the corner fuel rod will experience more than one increase in node power as a result of the control element pattern sequencing. However, these increases in nodal power may not occur more than once within the same node. Unless the "failure transient" was identified by a primary coolant system radioactivity increase coincident with the increase in power and the confirmation of failure in end-of-cycle inspections, it was assumed that failure occurred during the most severe nodal power increase.

Data Sets 3 and 4

These two data sets are similar in that many and perhaps all of the fuel failures occurred as a result of specific and atypical transients in similar reactor plants. These data sets are characterized as follows:

1. Operating parameters (P, ΔP and Bu) were determined by calculations using a proprietary core/fuel assembly simulator computer model. The simulator computer model was used to calculate the operating parameters for each of the 12 axial nodes in each fuel assembly. Inasmuch as the simulator computer models cannot track transient xenon, calculations were made assuming both zero and equilibrium xenon at each axial node. The actual operating power (P and ΔP) at each axial node was then estimated, with respect to zero and equilibrium xenon, using a transient xenon computer model which

had been subsequently calibrated in a similar reactor subjected to the transients represented in Data Sets 3 and 4. The uncertainty in calculating the operating parameters is estimated to be within 5%.

2. For both data sets, the duration of the transient was estimated to be 5 hour or less. The actual time-to-fail for any of the failures is unknown, although all failures are presumed to have failed within the approximate 5-hour duration of the transients.

3. Both data sets encompass a relatively broad range of pre-transient and transient increases in power but only a relatively limited range of fuel burnup. The pre-transient power (P_i) ranged from ~5 kW/ft to ~12kW/ft. The transient increase in power (ΔP) ranged from ~1 kW/ft to 10 kW/ft. The fuel burnup ranged from 5 GWd/MTM to 12 GWd/MTM.

Data Set 5

This data set consists largely of failures derived from power ramping experiments conducted in both test and commercial reactors. The data to a large extent were derived from single fuel rods in one-of-a-kind experiments. This data set is characterized by the following:

1. In at least some cases, the immediate pre-transient fuel rod power appears to have been rather severely suppressed. The fuel rod pre-transient power suppression is estimated to be about 25%, but no values were reported.

2. In power ramping experiments, the power ramps were deliberate and pre-programmed. In at least some of these experiments, the power ramp increases were not continuous throughout the experiment. We do not know what effect this discontinuity in power increase has on the susceptibility of a fuel rod to PCI failure.

3. This data set included 12, "time-to-failure" data points. In each instance, the reported time-to-failure is actually the period of time following the power increase when failure was indicated by the detection of the tell-tale fission products in the coolant.

2.3 STATISTICAL ANALYSIS

The data for each of the data sets were examined using standard statistical techniques. The procedures give an indication for the grouping of the data and the relative spread of each of the points.

As part of this analysis, the mean standard deviation, and minimum and maximum value of each parameter, as well as for histograms, were computed and are reported in detail in Appendix A. The results of this analysis are summarized in Tables 2.2 and 2.3.

2.4 DATA QUALIFICATIONS AND LIMITATIONS

The general data characteristics for Data Sets 1, 2, 3, 4, and 5 are given in Table 2.2 and 2.3.

For the five data sets shown, the failed fractions range from about 0.12 to 0.48 and appear to be generally greater than those reported for the nuclear industry as a whole.[1-6] Some of these data are considered to be the result of atypical reactor plant operation and therefore the failed fraction may reasonably be expected to be greater. For the remainder of these data, one presumes that the sampling may have been atypical.

As shown in Table 2.1, there is considerable diversity in fuel designs. Considering the diversity in both fuel designs and transient conditions from which these data were derived, it is doubtful that any one data set and Data Set 5 in particular would be wholly representative of the PCI fuel failure phenomenon.

- Figure 2.1 shows the composite data, Data Sets 1 through 5, collapsed on the P_f versus Bu, P_f versus ΔP, and ΔP versus Bu planes.
- Figure 2.2 shows the composite data, Data Sets 1 through 5 in an isometric view using the parameters P_f, ΔP and Bu.
- Figure 2.3 shows the composite data collapsed on the P_i versus Bu, P_i versus ΔP, and ΔP versus Bu planes.
- Figure 2.4 shows the composite data in an isometric view using the parameter P_i, ΔP and Bu.

TABLE 2.2. Data Set Characteristics

Data Set Identification	No. of Bundles In Set	No. of Bundles That Failed	No. of Bundles Did Not Fail	Failed Fraction
1	104	46	58[a]	0.44[a]
2	572	67	505	0.12
3	518	134	384	0.26
4	481	101	380	0.21
5	119	57	62	0.48

TABLE 2.3. Numerical Characterization of Each Data Set

Date Set Identification	Initial Power kW/ft				Power kW/ft				Burnup GWd/MTM			
	X	σ	Min	Max	X	σ	Min	Max	X	σ	Min	Max
1	6.1	2.5	0.3	10.3	8.3	3.3	0.5	14.7	4.1	1.5	2	6.3
2	2.9	1.1	0.8	8.0	5.5	2.8	0	11.5	15.4	5.1	1.4	25.5
3	8.8	1.5	6.6	15.0	2.8	1.1	0.3	6.9	11.2	1.6	5.5	12.0
4	6.2	0.8	2.9	9.4	4.2	2.1	1.2	10.5	11.7	0.6	7.7	11.8
5	10.0	2.7	4.6	19.2	6.6	3.0	0.9	16.3	8.2	5.5	0.9	31.6

where X = mean value

σ = standard deviation

Min = minimum value in the Data Set

Max = maximum value in the Data Set

(a) Fifty-eight (58) bundles were ramped in the same fuel channels as the defects at the same time and did not fail. Five thousand (5000) other bundles exposed to power ramps have also remained intact.

In these figures, Data Set 1 is identified by the numeral 1 for non-failures and by the letter A for failures. The remaining data sets are similarly identified by their set number, denoting non-failure, and a corresponding set letter denoting failures. As shown in Figures 2.1 through 2.4, each data set occupies a limited volume of three dimensional space defined by the coordinates P (either P_i or P_f), ΔP and Bu. Under these circumstances, it is doubtful that any one data set would be wholly representative and fully adequate to describe PCI fuel failure.

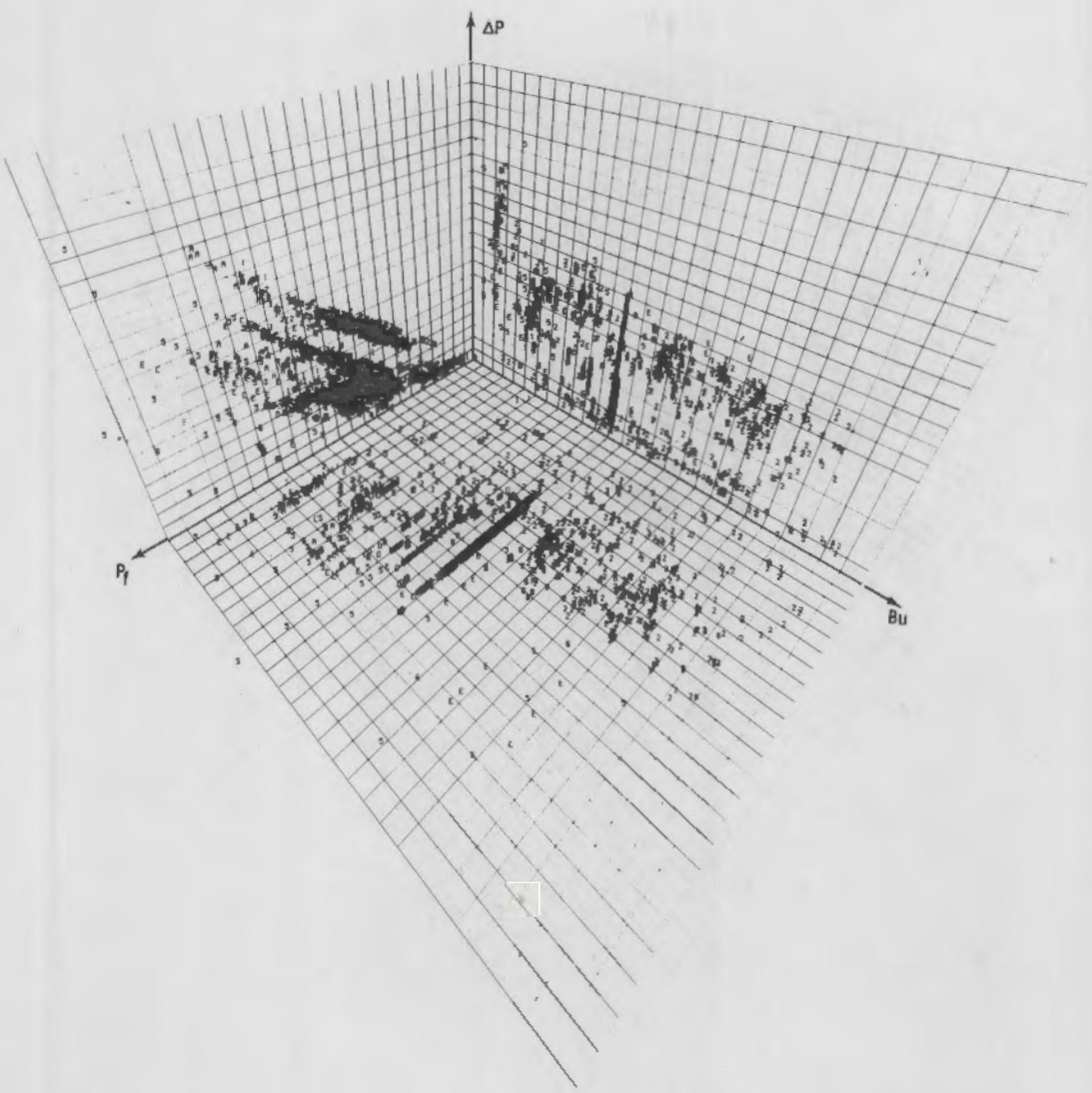

FIGURE 2.1. Data Sets 1 Through 5 are Shown Collapsed on the P_f Versus Bu, P_f Versus ΔP and ΔP Versus Bu Planes. Non-Failed and failed data are identified by number and letter, respectively.

The five data sets appear to be generally incomplete relative to the power ramping rate ($\dot{P}$) and the time-to-failure (TTF) parameters, which, based on physical and mechanistic consideration, appear to be of significance in the

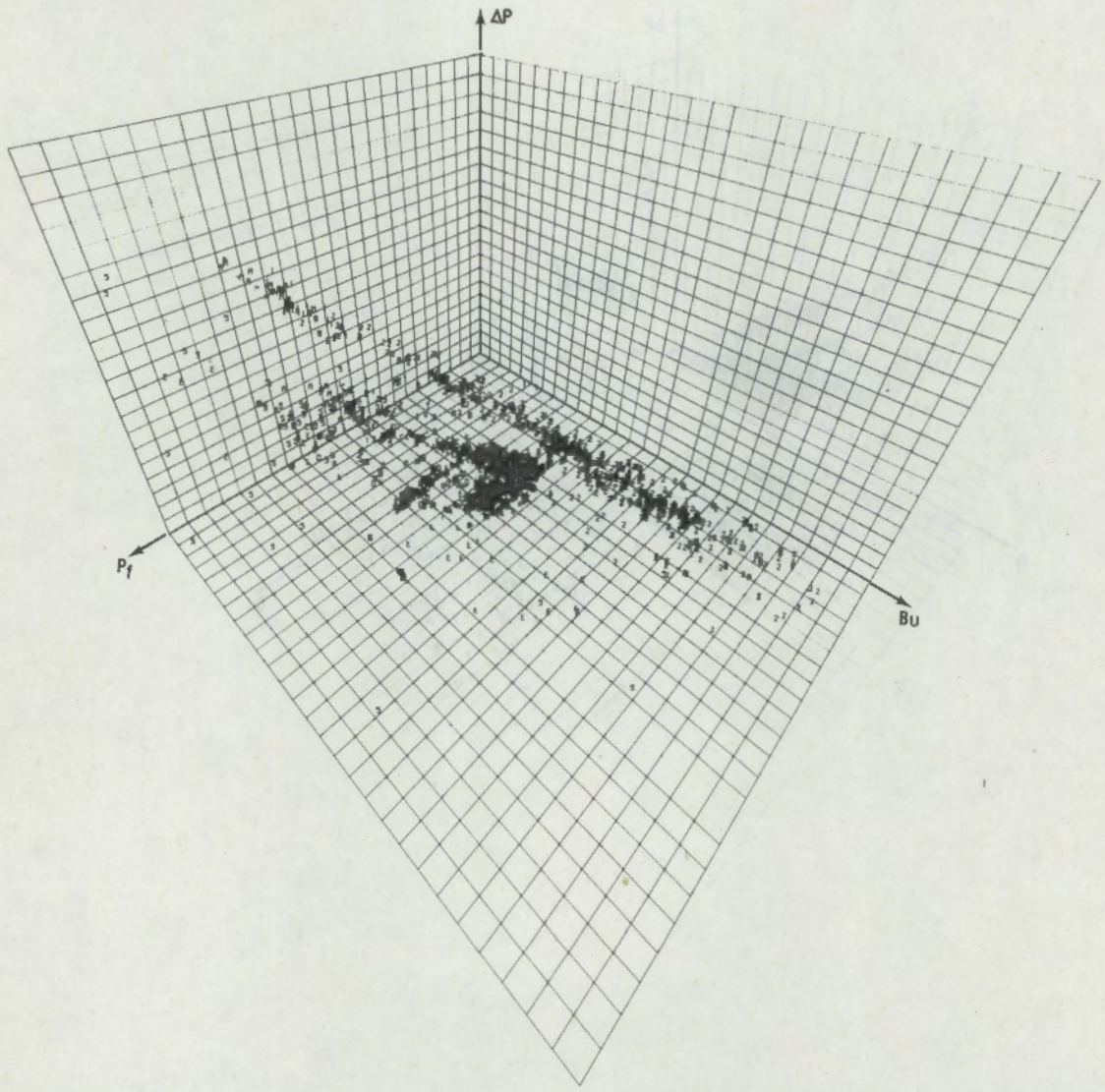

FIGURE 2.2. Data Sets 1 Through 5 are Shown in an Isometric View Using the parameters P_f, ΔP and Bu. Non-Failed and failed data are identified by number and letter, respectively.

PCI fuel failure phenomenon. Data Sets 1 and 5 include very limited information relative to $(\dot{P})$ and TTF. The range of the $(\dot{P})$ and TTF parameter values appears to be too small to be significant in modeling the PCI fuel failure phenomenon.

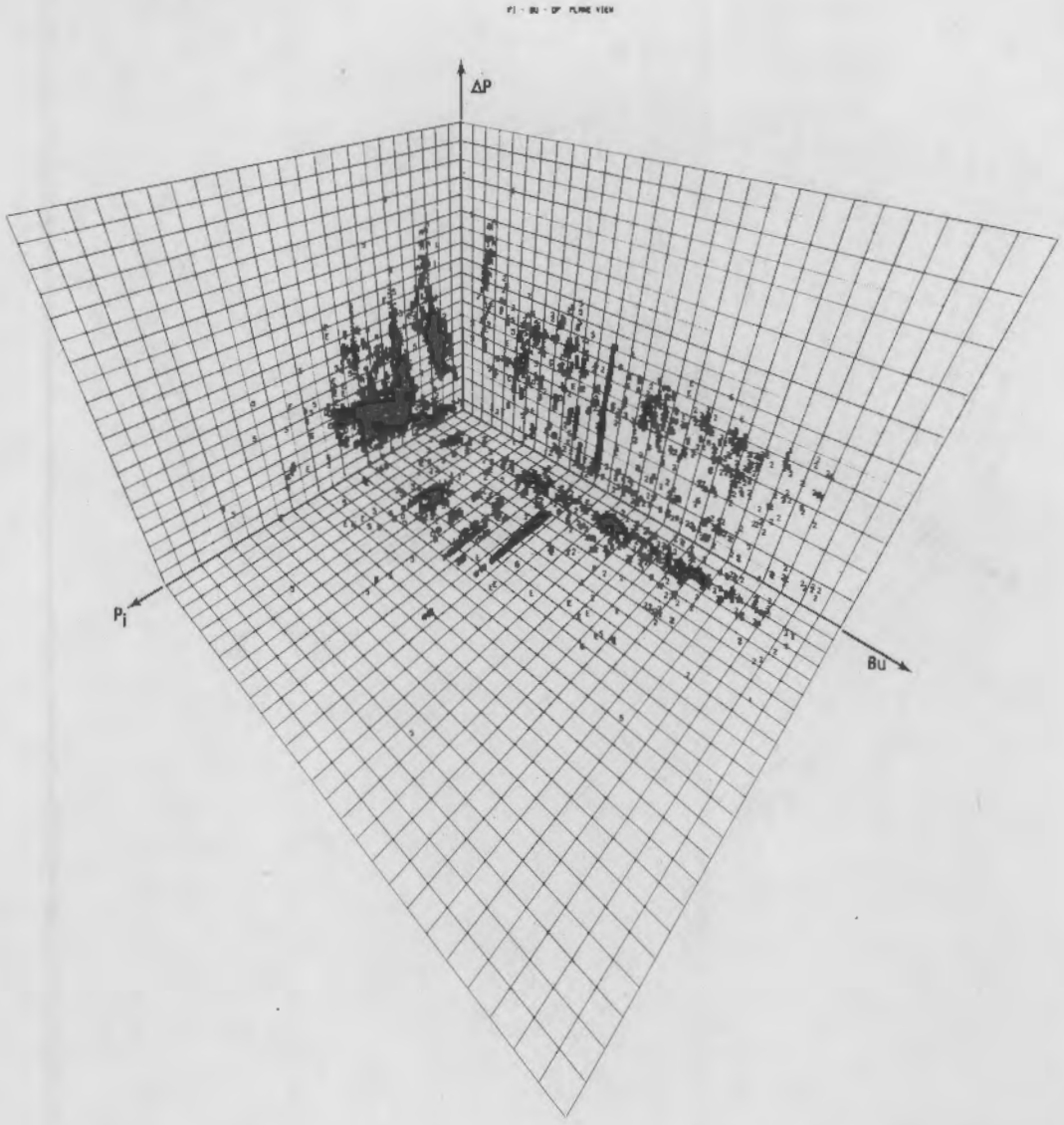

FIGURE 2.3. Data Sets 1 Through 5 are Shown Collapsed on the P_i Versus Bu, P_i Versus ΔP, and ΔP Versus Bu Planes. Non-Failed and failed data Are identified by number and letter, respectively.

Data Set 2 and to a lesser extent, Data Sets 3 and 4, include some information as to prior increases in fuel rod/assembly power (i.e., power ramp history). The significance of prior power ramp history relative to PCI fuel failure, is uncertain. There are a few post-irradiation-examination (PIE) observations showing that part-through-wall cracking of the Zry cladding or

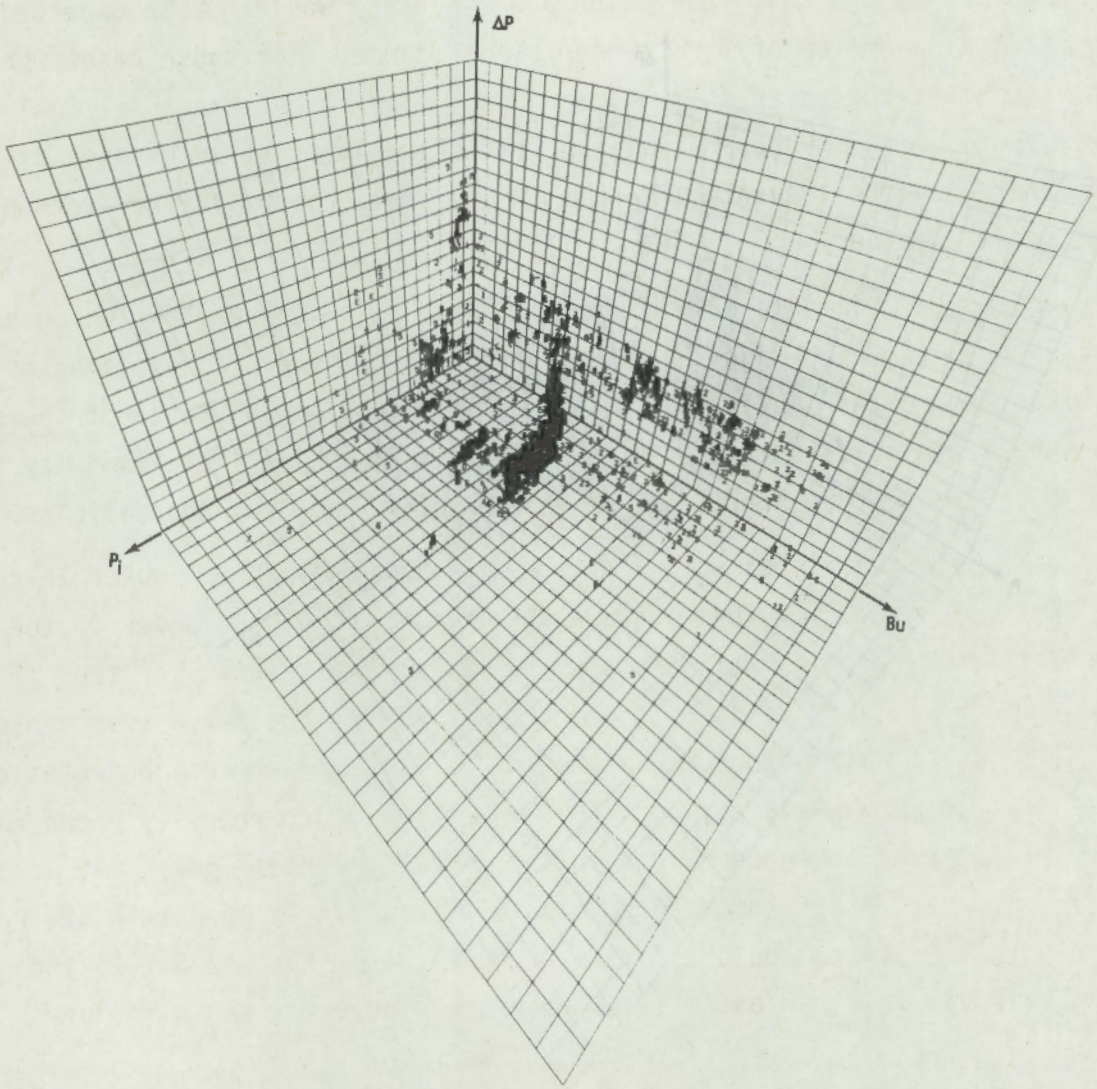

FIGURE 2.4. Data Sets 1 Through 5 are Shown in an isometric View Using the Parameter P_j, ΔP and Bu. Non-Failed and failed data are identified by number and letter, respectively.

other undefined damage may occur as a result of a transient increase in fuel rod power. These observations, however, are not sufficient to provide quantification of the incidence of part-through-wall cracking of the Zry cladding and the severity of the transient increase in power. Futhermore, our examination of Data Set 2, showed that repeated maximum increases in power rarely

occurred within the same axial node of a fuel rod. If the Data Set 2 observations are generally typical, then prior power history would not be expected to be an operating parameter of first order significance. For those cases where repeated transient increases in power may occur within the same axial fuel rod/assembly node, it may be possible to statistically treat such cases as separate and independent events, wherein the failure probability for each of the events are combined.

The absence of adequate information relative to all parameters which are postulated to be of major significance in modeling PCI fuel failure imposes some limitations on the applicability of standard statistical tests of these data for characteristics such as homogenity, goodness-of-fit, etc. and may be expected to increase the uncertainty in estimates of failure probabilities.

For Data Set 1, failures were reported to occur only in the outer 16-rod ring of the fuel assembly. This observation suggests that the power in the intermediate 8-rod ring may define a lower bound on the severity of the transient for PCI failure at power ramping rates within the range represented in Data Set 1. For Data Sets 2 through 5, neither the power ramping rates nor the fuel rod nodal power(s), at which failure actually occurred, is known with certainty even though the uncertainty in the calculated nodal power may be small. If, however, $\dot{P}$ for some of these data were known to be within the $\dot{P}$ range for Data Set 1, one could estimate, by comparison to Data Set 1, the uncertainty in the fuel rod/assembly average nodal power at which failure actually occurred.

For Data Set 1, failures were reported to occur only in the outer 16-rod ring of the fuel assembly. The number of fuel rod failures in an assembly ranged from 2 to 16. There is no obvious relationshiip between the number of the fuel rod failures in an assembly and the severity (i.e., P_f, ΔP) of the transient for the fuel assembly. The uncertainty in the detection and identification of failed fuel rods, by current methods, has not yet been quantified. It is, at present, unknown whether the absence of any distinct relationship between the number of failed fuel rods in an assembly and the severity of the

failed fuel rods, can be attributed to uncertainty in detection of failed fuel rods or some, as yet, unidentified parameter of significance in affecting PCI fuel failure.

In Data Sets 2 through 5, failures were reported to occur in transients which were significantly less severe than experienced by the intermediate 8-rod ring of CANDU fuel assemblies (Data Set 1) in on-line refueling transients. This observation suggests that the lower bound transient conditions P, ΔP, for failure in LWR fuels may be significantly lower than for CANDU fuels. The basis for this apparent difference is unknown. Differences in some operating parameters, such as power ramping rate, prior operating power history, etc., may account, at least in part, for the differences in the apparent failure threshold. There may also be other physical factors such as the vertical versus horizontal orientation of the fuels in LWR versus PHWR plants which may account to some extent for the apparent failure threshold differences.

Data Sets 2 through 4 do not include information as to either the number of fuel rod failures or their location within the fuel assembly. There appears to be a general consensus that failure is most likely to occur in the fuel rod within an assembly which experiences the most severe transient increase in power and at the axial node where the power is a maximum. Inasmuch as the operating parameters (P, ΔP and Bu) reported in Data Set 2 are for the single fuel rod nearest the intersection of the orthogonal blades of the control element, then Data Sets 1, 2 and 5 are considered to be substantially representative of the conditions (P, ΔP) for specific fuel rod failures. Data Sets 3 and 4 are considered to be somewhat less representative of specific fuel rod failure conditions (P, ΔP) inasmuch as the reported operating parameters (P, ΔP and Bu) are more characteristics of the fuel assembly peak power node than the fuel rod peak power node.

In summary, the greatest uncertainties in the composite data set appear to be:

1. the actual fuel rod power at which failure occurred,
2. the time, following the increase in power, at which failure occurred,
3. the rate of the increase in power.

Although the apparent failure thresholds for LWR fuel appears to be lower than for the CANDU fuel, these data do not show any obvious pattern or other direct link between the fuel design parameters, represented in these data, and the susceptibility to failure.

3.0 APPLICATION OF CANDU FUELOGRAM METHODOLOGY TO PCI DATA FROM LIGHT WATER REACTORS

J. C. Wood, Contributing Author, CRNL

3.1 PCI-OGRAM

The FUELOGRAM model[21] was derived to predict PCI defect probabilities for (CANDU) fuel bundles that had experienced power increases after being irradiated to appreciable burnups (mostly in the range 4.2 ±2.5 GWd/MTM (100 ±60 MWh/kgU). Defect probability was found to depend on the power increase (ΔP), ramped power (P_f),[a] and the fuel burnup (Bu), of the most highly rated rods in the bundle or assembly. Defect probability also depended on the time the fuel remained at the ramped power. While it was clearly inappropriate to extrapolate from the FUELOGRAMS to predict fuel performance at burnups up to 25 GWd/MTM (600 MWh/kgU), we considered it worthwhile to use the FUELOGRAM methodology on PCI fuel performance data from light water reactors. The resultant extended LWR FUELOGRAMS are termed PCI-OGRAMS.

3.2 SCRUTINY AND ORGANIZATION OF THE DATA

The most complete set of data in terms of powers, power changes, and burnup was Data Set 2. Also, since the power changes arose in normal operation, the time that the fuel remained at the ramped powers was appreciable. (It was deduced from CANDU experience that a dwell time of 2-1/2 hr would include 99.7% of the defects that would have occurred in essentially infinite hold times.) The basic Set 2 data were in the form of a comprehensive and detailed computer printout showing powers at various nodes in each fuel assembly as a function of burnup. The power increases, powers, and burnups judged to be most severe (in the reactor cycle immediately preceding testing of whether if the assembly was intact or defective) were extracted from the printout. Power increases that occurred at the very start of a reactor cycle were discounted because very slow startup rates prevented defects at that time.

(a) In this section P and P_f represent the same power.

Of the 302 assemblies, 65 had been confirmed defective. These data were plotted in Figures 3.1 and 3.2 as power and power increase versus burnup and threshold curves were drawn beneath the defects (except that two data points were ignored because they were sufficiently below the rest, that they possibly represented defects other than PCI). Above the threshold curves in Figures 3.1 and 3.2, dashed lines were drawn at equal intervals of 0.6 kW/ft (2 kW/m) above them. At low burnup levels, the data were sparse, so the CANDU thresholds[21] were drawn making a smooth joint with the P_f versus Bu curve (Figure 3.1) but effecting a sudden change of slope in the ΔP versus Bu threshold (Figure 3.2). The discontinuity of slope of the ΔP threshold curve occurred

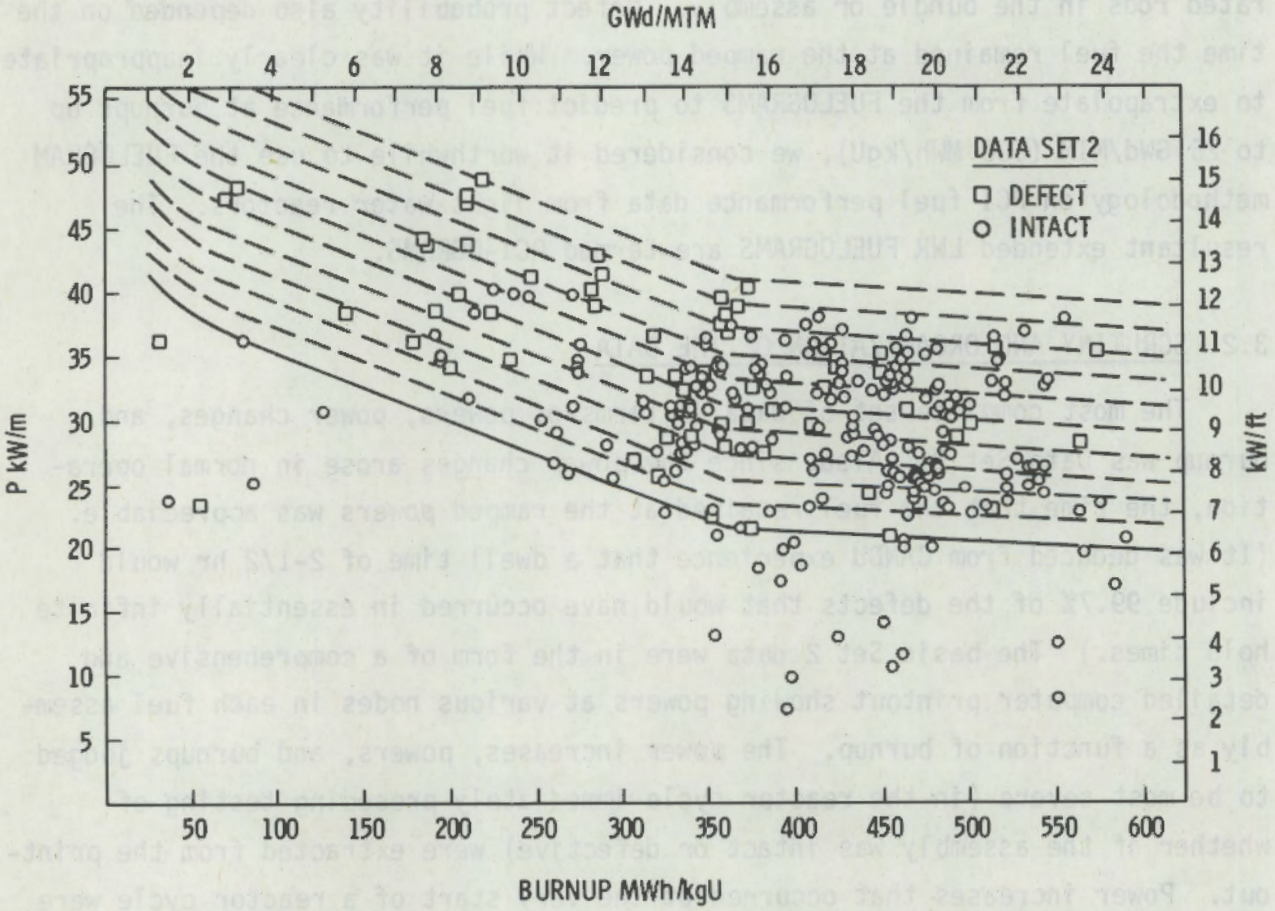

FIGURE 3.1. The Distributions of Ramped Powers and Burnups of Defective and Intact Assemblies. The threshold line drawn beneath the defects is curved at the upper left side to comply with the CANDU threshold.

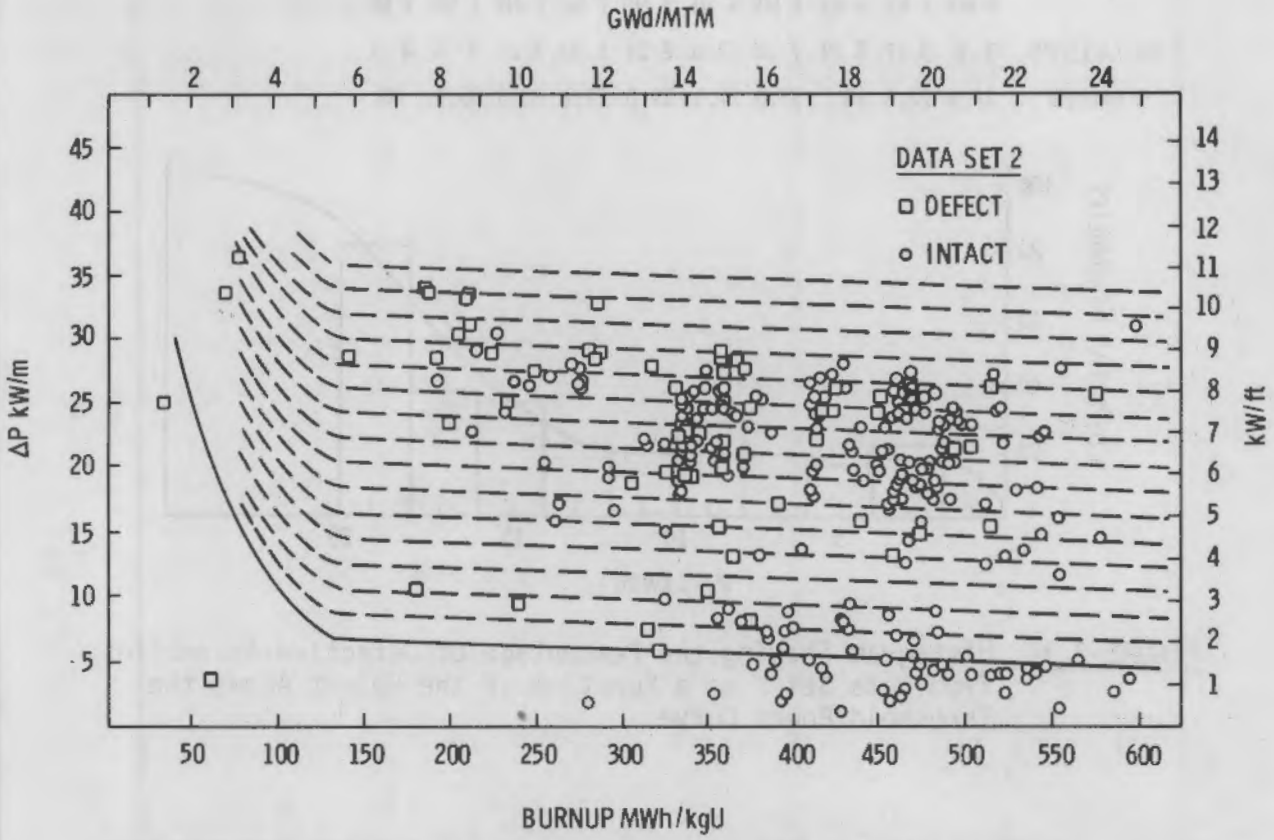

FIGURE 3.2. The Distribution of Defects and Non-Defects as a Function of the Power Increase and Burnup. The curved part of the threshold on the left complies with CANDU data.

because the Data Set 2 fuel did not suffer "ripple defects"[21] or, more likely, the "ripple defects" occurred in fuel that also experienced larger power increases, thereby masking the occurrence of "ripple defects" ("ripple defects" occurred in CANDU fuel during ostensibly steady high-power operation and are possibly due to unrecorded power fluctuations or "flux ripple").

Histograms were plotted (Figures 3.3 and 3.4) showing the percentages of defective fuel assemblies as a function of the height above the threshold power curve ($P-P_c$) in Figure 3.3 and the power increase curve ($\Delta P-\Delta P_c$) in Figure 3.4. The numbers of failed and intact fuel assemblies included in each

	F	NF	F	NF	F	NF	F	NF	F	NF	F	NF	F	NF	F	NF	F	NF
NO. ASSY'S	3	9	5	17	5	29	7	34	12	31	8	34	8	30	8	16	5	9	4	1
% FAILED	27.3		22.8		14.7		17.0		27.9		19.0		21.1		33.3		35.7		80	

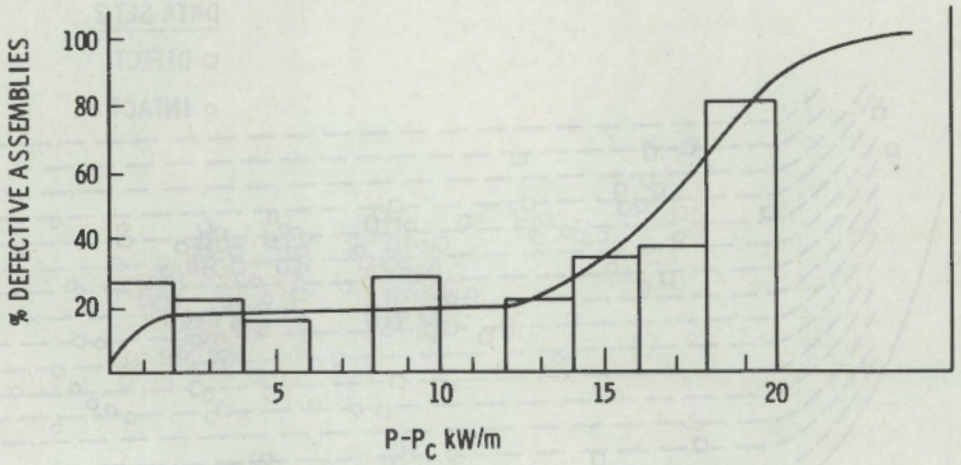

FIGURE 3.3. Histogram Showing the Percentage of Defective Assemblies from Data Set 2 as a Function of the Height Above the Threshold Power Curve

	F	NF	F	NF	F	NF	F	NF	F	NF	F	NF	F	NF	F	NF	F	NF	F	NF	F	NF	F	NF	F	NF
NO. ASSY'S	2	10	2	12	2	3	1	3	2	6	4	8	2	24	5	27	9	26	7	38	7	34	13	13	2	1	3	0	2	0
% FAILED	16.7		14.3		40		25		25		33		7.7		15.6		25.7		15.6		17.1		50		66		100		100	

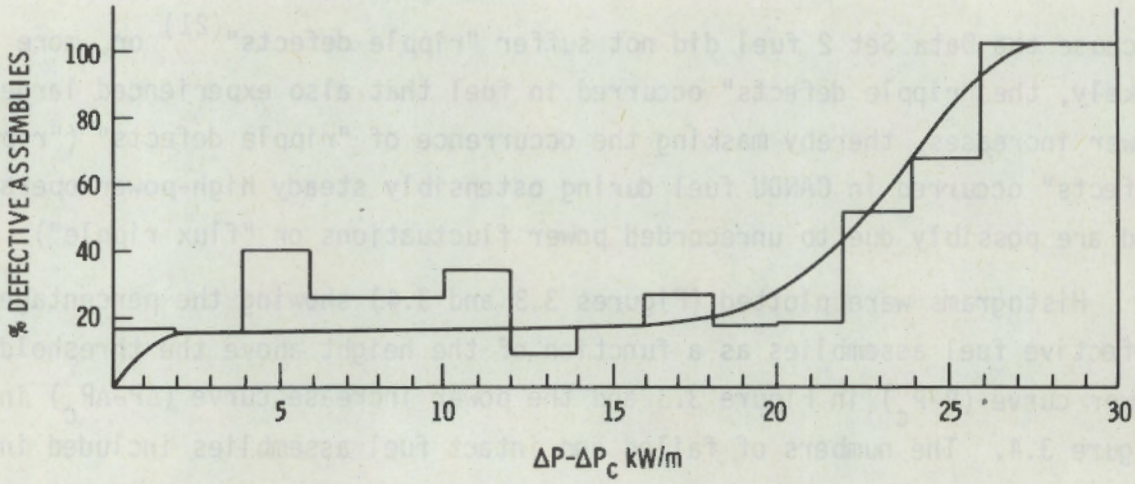

FIGURE 3.4. Histogram Showing the Percentages of Defective Assemblies from Data Set 2 as a Function of the Height Above the Threshold Power Increase Curve.

interval are shown above each histogram. The defect probability does not begin to rise steeply until reaching about 4 kW/ft (14 kW/m) above P_c or about 6 kW/ft (~20 kW/m) above ΔP_c. Also, there is an abrupt step in defect probability immediately above the defect threshold similar to the step increase previously observed with CANDU fuel.[21]

Additional power ramping data (Data Sets 3 and 4) were much less specific than Data Set 2 with regard to burnup, initial and final powers. Also, the dwell time at the ramped power was unknown (but thought to be short). Final powers had been calculated for Data Sets 3 and 4 assuming either that no xenon was present, or that the equilibrium amount of xenon was present. These estimates placed limits on the maximum powers attained during the overpower transients. Histograms shown in Figure 3.5 compare the three sets of LWR data in terms of the percentages of defective assemblies versus the heights above the respective threshold powers. The average defect probability curve obtained from Data Set 2 (Figure 3.5a) is reproduced on Figures 3.5b and 3.5c as a basis for comparison. The histograms represent power estimates assuming "no xenon" as full lines and "equilibrium xenon" as dashed lines. The Set 2 average curve underpredicts the defect threshold for Set 3 data but overpredicts for Set 4 data. Lateral shifting of the Set 3 data by 1 kW/ft (+ 3 kW/m) and Set 4 data by -1 kW/ft (-3 kW/m) would bring them into reasonable coincidence with the Set 2 defect threshold. It was sufficiently encouraging that the curve (Figure 3.5) derived from the most complete data set fell between the histograms from the other two that we preceeded to develop a model based on Data Sets 1 and 2. Data Sets 3 and 4 were considered unusable in the absence of knowledge of the dwell time at high power.

3.3 EQUATIONS USED TO PRODUCE PCI-OGRAMS

The equations defining the defect threshold criteria described in Figures 3.1 and 3.2 are given as follows:

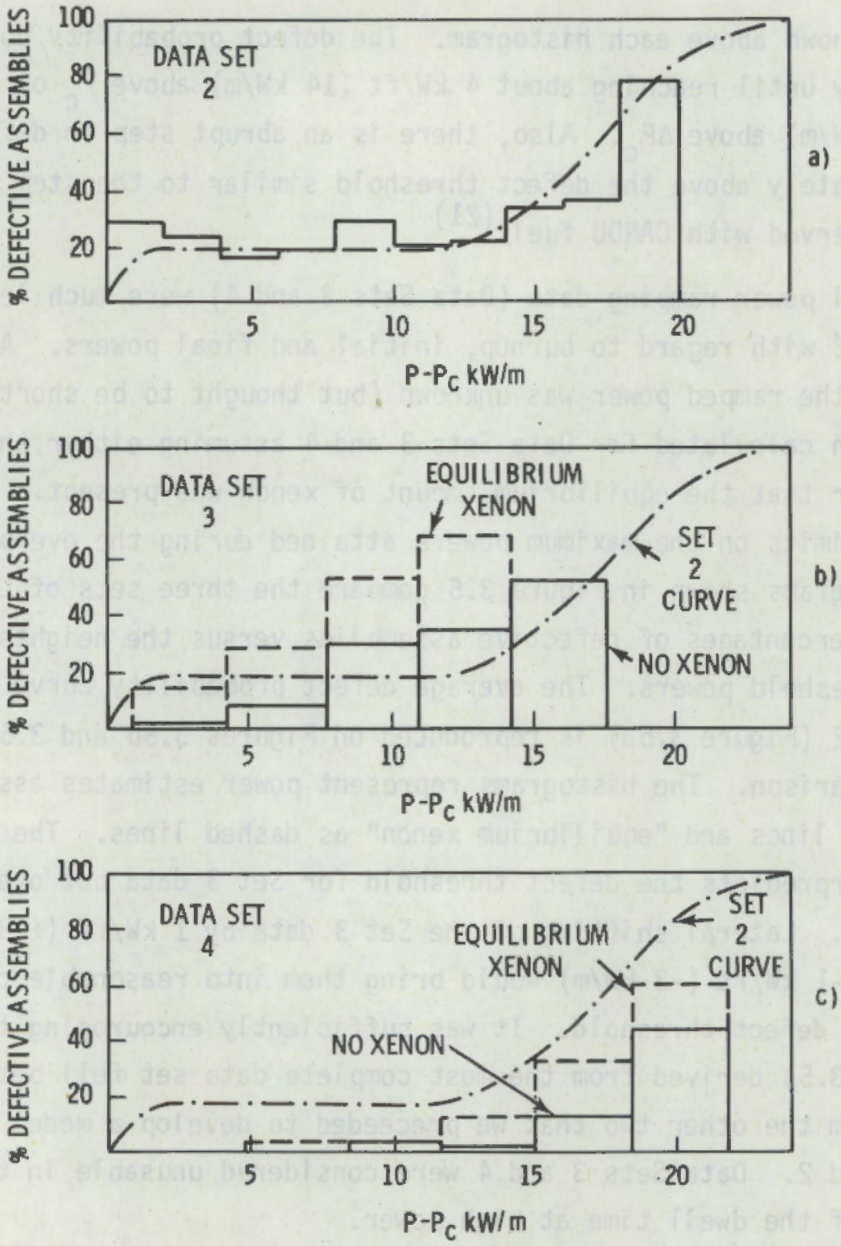

FIGURE 3.5. Comparison of Histograms Showing the Percentages of Defective Assemblies as a Function of the Heights Above the Respective Ramped Power Thresholds. The continuous and dashed histogram lines represent upper and lower limits to the estimates of ramped powers.

Valid Burnup Range	Critical Power Increase
GWd/MTM (MWh/KgU)	kW/ft (kW/m)
$1.25 < Bu < 5.42$	$\Delta P_c = \frac{18.55}{Bu} - 1.83$
$(30 < Bu < 130)$	$(\Delta P_c = \frac{1460}{Bu} - 6)$
$5.42 < Bu < 25.0$	$\Delta P_c - 2.16 - 3.07E\text{-}2 \cdot Bu$
$(130 < Bu < 600)$	$(\Delta P_c = 7.1 - 4.2 \times 10^{-3}\ Bu)$
$1.25 < Bu < 3.33$	$P_c - 11.16 + \frac{2.95}{Bu}$
$(30 < Bu < 80)$	$(P_c - 36.6 + \frac{232}{Bu})$
$3.33 < Bu < 15.0$	$P_c = 12.41 - 3.88E\text{-}1 \cdot Bu$
$(80 < Bu < 360)$	$(P_c = 40.7 - 5.3 \times 10^{-2}\ Bu)$
$15.0 < Bu < 25.0$	$P_c = 7.59 - 6.0E\text{-}2 \cdot Bu$
$(360 < Bu < 600)$	$(P_c = 24.9 - 8.2 \times 10^{-3}\ Bu)$

The above equations have been used to produce a PCI-OGRAM for $t \geq 2.5$ h pertinent to the performance of LWR and CANDU fuel (Figure 3.6). Since we think the same mechanism (fission product induced stress corrosion cracking) governs power ramping defects of LWR and CANDU fuel the time dependency should be the same. Therefore, benchmarking against the most accurately known data with a short-term hold at high power (Pickering 8-bundle shifting, t = 0.30h) the threshold criteria may be generalized to:

$1.25 < Bu < 3.33$	$P_c = 13.60 + \frac{2.95}{Bu} - 6.71\ [0.5\text{-}\exp(-23t)]$
$(30 < Bu < 80)$	$\left(P_c = 44.6 + \frac{232}{Bu} - 22\ [0.5\text{-}\exp(-2.3t)]\right)$
$1.50 < Bu < 3.33$	$P_c = 15.76 - 3.88\ 10^{-1}\ Bu - 6.71\ [0.5\text{-}\exp(-23t)]$

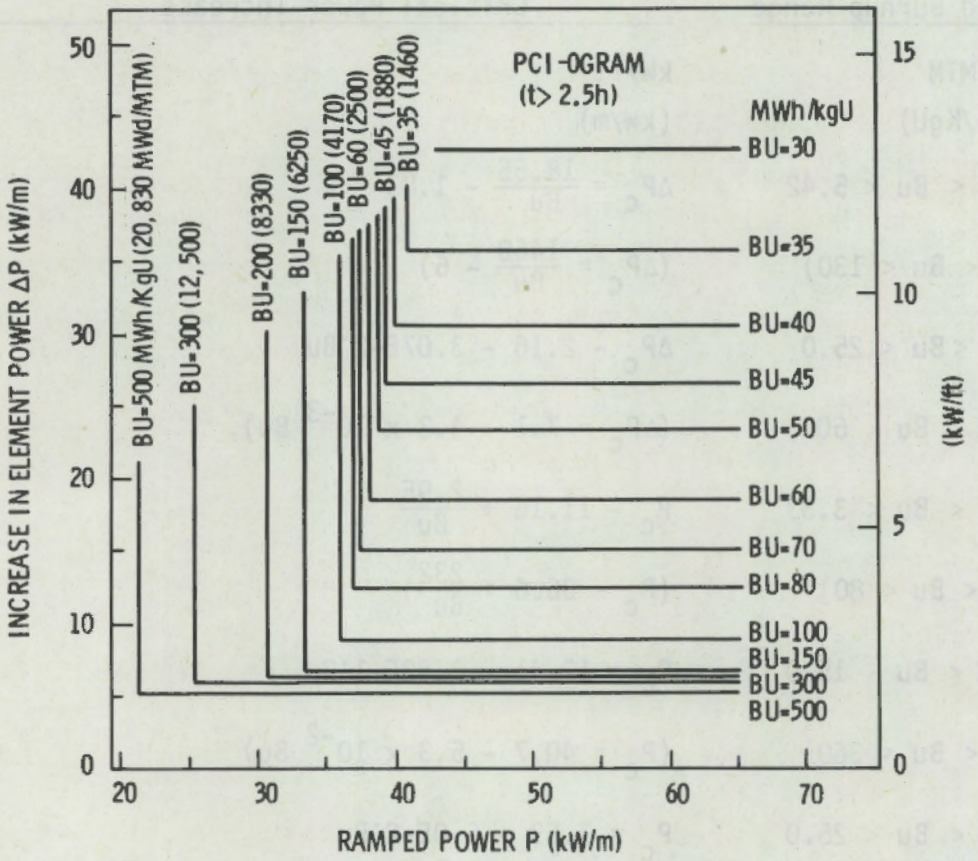

FIGURE 3.6. PCI-OGRAM Defining the Threshold Values of Ramped Power and Power Increase as a Function of Fuel Burnup. Dwell time $\geq$2.5 h at the ramped power.

$(80 < Bu < 360) \quad \left(P_c = 51.7 - 5.3 \times 10^{2}\ Bu - 22\ [0.5\text{-}\exp(2.3t)]\right.$

$15.0 < Bu < 25.0 \quad P_c = 10.95 - 6.0\ 10^{-2}\ Bu - 6.71\ [0.5\text{-}\exp(-23t)]$

$(360 < Bu < 600) \quad \left(P_c = 35.9 - 8.2 \times 10^{-3}\ Bu - 22\ [0.5\text{-}\exp(2.3t)]\right)$

$1.25 < Bu < 5.42 \quad \Delta P_c = 1.83 + \frac{18.55}{Bu} - 7.32\ [0.5\text{-}\exp(-2.3t)]$

$(30 < Bu < 130) \quad \left(\Delta P_c = 6 + \frac{1460}{Bu} - 24\ [0.5\text{-}\exp(-2.3t)]\right)$

$5.42 < Bu < 25.0 \quad \Delta P_c = 5.82 - 3.07\ 10^{-2}\ Bu - 7.32\ [0.5\text{-}\exp(-2.3t)]$

$(130 < Bu < 600) \quad \left(\Delta P_c = 19.1 - 4.2 \times 10^{-3} Bu - 24\ [0.5\text{-}\exp(2.3t)]\right)$

A set of 20 PCI-OGRAMS describing these criteria at various dwell times from 0.1 h to $\geq$ 2.5 h has been computed and a defect probability grid (Figure 3.7) has been generated (using Figures 3.3 and 3.4) which when overlaid on the PCI-OGRAM (Figure 3.6) allows direct reading of defect probabilities for LWR fuel. A defect may occur if a point (P, ΔP) is included in the "L" shape that defines values of ΔP_c and P_c at the burnup of the fuel rod concerned (Figure 3.6). In other words fuel defects can occur if both the criteria in terms of P and ΔP are satisfied, i.e.

$$P - P_c > 0 \quad \text{and} \quad \Delta P - \Delta P_c > 0$$

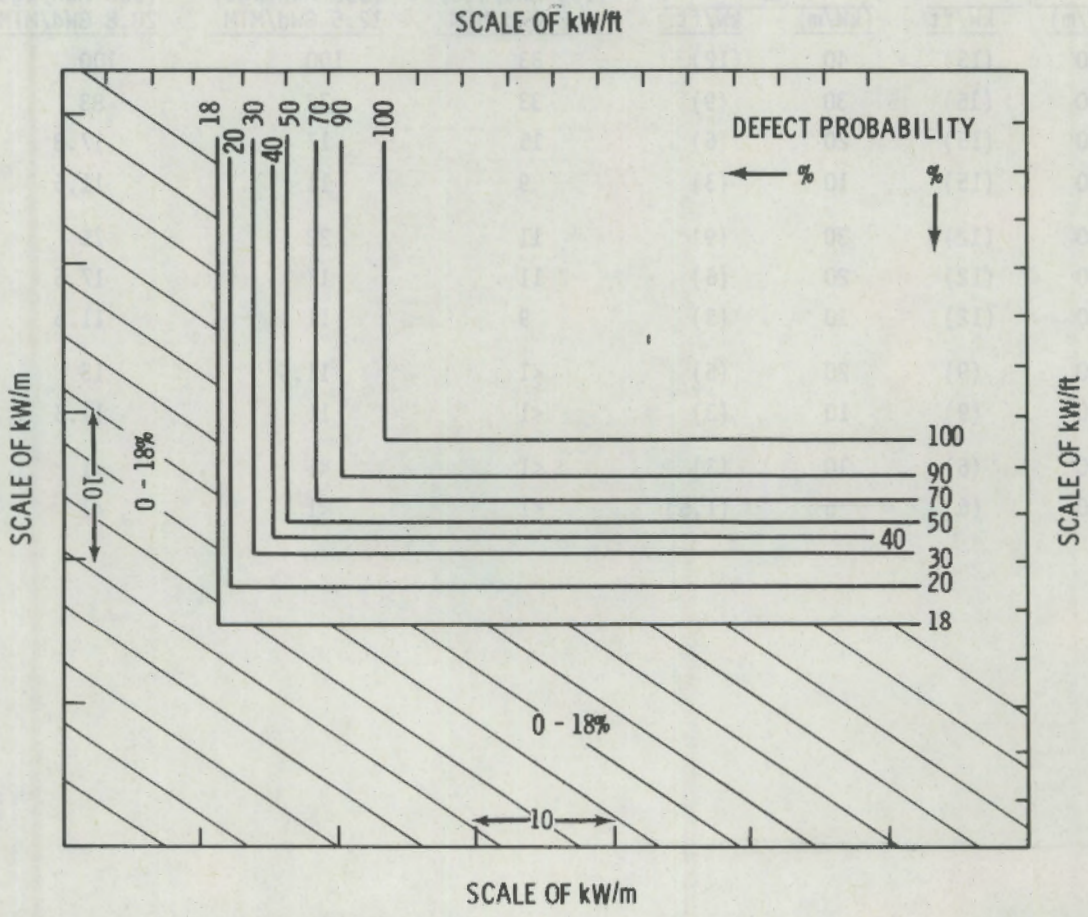

FIGURE 3.7. Defect Probability Grid to be Overlaid on the PCI-OGRAM (Figure 3.6) to Estimate Defect Probabilities of Ramped LWR Fuel. The axes of this grid are laid over the "L" shaped lines representing fuel burnup on the PCI-OGRAM.

The variable that controls the defect probability is the one that yields the lower probability.

Table 3.1 show defect probabilities predicted using the PCI-OGRAM model for various combinations of P_f and ΔP at three burnups. Graphical representation of defect probability as a function of P_f, ΔP and Bu will be included in Section 5.

TABLE 3.1. PCI-OGRAM Predictions of Defect Probabilities When the Dwell Time at High Power P_f Exceeds 2.5 hours

P_f		ΔP		Defect Probabilities %		
(kW/m)	kW/ft	(kW/m)	kW/ft	(100 MWh/kgU) 4.2 GWd/MTM	(300 MWh/kgU) 12.5 GWd/MTM	(500 MWh/kgU) 20.8 GWd/MTM
50	(15)	40	(12)	33	100	100
50	(15)	30	(9)	33	72	83
50	(15)	20	(6)	15	17	17.8
50	(15)	10	(3)	9	11	11.5
40	(12)	30	(9)	11	38	75
40	(12)	20	(6)	11	17	17.6
40	(12)	10	(3)	9	11	11.5
30	(9)	20	(6)	<1	11.5	15
30	(9)	10	(3)	<1	11	11.5
20	(6)	10	(3)	<1	<1	<1
20	(6)	5	(1.5)	<1	<1	<1

4.0 THE DEVELOPMENT OF THE PROFIT PCI FUEL FAILURE MODEL

P. J. Pankaskie, Empirical Modeling
P. G. Heasler, Statistical Analysis

Analytical and statistical methods generally constitute an approach to modeling physical phenomena, wherein individual data and/or sets may be treated in a logical and consistent manner. The procedure generally involves identification of some physical/mathematical relationship between measured variables. This approach can also provide an opportunity to easily include, in the phenomenological modeling, new and/or additional variables as they become available at some future time. Because it is still uncertain as to whether all of the variables of first order importance to the PCI fuel failure phenomenon have been identified, PNL chose the analytical/statistical approach in preference to the graphical approach.

4.1 MODELING CONSIDERATIONS

PCI fuel failures have been modeled empirically[21,22] in terms of operating parameters such as:

- the post-transient fuel rod/assembly power (P_f)
- the transient increase in fuel rod/assembly power (ΔP)
- the fuel rod/assembly burnup (Bu)
- the "dwell" time at the peak post-transient power or the delay between the transient and failure.

Exploratory and experimental efforts have been undertaken in attempts to identify and quantify mechanisms by which PCI fuel failures occur. These efforts, as yet, have not been fully successful. There appears to be a general consensus that thermomechanical and thermochemical mechanisms play key roles in PCI fuel failure.

It has been postulated that the operating parameters that were available for this study, and that have been used in empirical fuel failure modeling,

are the corollary of certain thermomechanical and thermochemical fuel behavior mechanisms.[42] The postulated mechanistic corollaries are as follows:

- The mechanistic corollary to the post-transient fuel rod/assembly power (P_f) is the fuel temperature for relatively prompt fission product release from the fuel.

  This temperature appears to be the temperature at which thermally activated solid state reactions, diffusional processes, knockout-recoil mechanisms, etc., begin to occur at significant rates. The fission products of concern appear to be those which are chemically aggressive to the Zry cladding (e.g., I_2, Cd, etc.). These considerations imply that, whenever the fuel rod/assembly power (P_f) is used as one of the PCI fuel failure modeling parameters, the values chosen for P_f must correspond to the fuel temperature. For example, in very fast transients caused by a sudden and substantial reactivity insertion, there is likely to be a significant mismatch between the heat generation rate and the actual temperatures corresponding to an equilibrium temperature within the fuel. It should also be noted that the post-transient power (P_f) is merely the sum of the pre-transient (P_i) and the transient increase (ΔP) in the fuel rod/assembly power.

- The mechanistic corollary to the transient increase (ΔP) in fuel rod/assembly power is the differential thermal expansion of the fuel and cladding.

  This differential expansion of the fuel and cladding provides the thermomechanical interaction forces to produce the stress and strains in the cladding which, in the presence of fast neutron radiation damage and/or chemically aggressive fission products, may promote failure of the Zry cladding. There may also be additional factors such as:

  - the thermal stress effect in promoting radial cracking of the fuel pellets, which are likely to cause stress and strain intensification in the Zry cladding at the crack location

- the thermal transient effect[42] in promoting the relatively prompt release of fission products, some of which are chemically aggressive to the Zry cladding.

- The mechanistic corollary to the fuel burnup (Bu) is postulated to be at least severalfold:
  - the accumulation of a fission product inventory within the fuel, some of which, when released, are chemically aggressive to the Zry cladding
  - the accumulation of fast neutron radiation damage of the Zry cladding and which tends to enhance such stress-strain anomalies as the yield point,[a] dislocation channeling as manifested by drop-in-load yielding and strain localization and the reduction in strain energy absorption to failure
  - cladding "creepdown" and fuel swelling which may promote harder interfacial contact between the fuel pellet and the cladding, and thereby intensify the thermomechanical interaction force accompanying a specific transient increase in power.

- The mechanistic corollary to the "dwell time," as reported for Data Set 1, has been postulated[42] to be the time-to-failure measured in a stress corrosion cracking test under a constant load, stress, or displacement in a chemically aggressive environment.

The chemically aggressive environment is postulated[11,16] to be fission product iodine, cadmium and/or other fission product species that tend to embrittle the Zry cladding. The source of the "critical" load, stress or displacement for stress corrosion cracking (SCC) is attributed to the differential thermal expansions of the fuel and cladding accompanying an increase in power.

(a) Drop-in-load yielding, as used here, is defined as that characteristic of certain metals and alloys, to continue to deform plastically under externally-applied loads that are smaller than that necessary to cause the initial yielding.

Considering their mechanistic corollaries, the above operating parameters have generally been considered to be the most pertinent for empirical modeling of PCI fuel failures. For these reasons, virtually all PCI fuel failure data are reported in terms of these operating parameters (P, ΔP, and Bu). Only Data Set 1 included a "dwell time" observation, and Data Set 5 included only a very few "time-to-failure" observations.

Data relative to other operating parameters or their mechanistic corollaries are either very sparce or nonexistent. There are, however, well known phenomenological aspects of the stress-strain behavior of Zry in nonaggressive, chemically aggressive, and neutron radiation environments, which show Zry to be very strain rate sensitive, particularly within the range of fuel operating temperatures. Using the same logic by which mechanistic corollaries to key operating parameters were identified, one may also postulate that the operating corollary to strain rate in the Zry cladding is the rate of increase ($\dot{P}$) in fuel rod/assembly power.

Based on the above considerations, empirical modeling of the available PCI fuel failure data should include consideration of the following operating parameters:

1. the pre-transient (P_i) and/or post-transient (P_f) power,
2. the increase in power (ΔP)
3. the fuel burnup (Bu)
4. the power ramping rate ($\dot{P}$)
5. the time-to-failure.

The above parameters were all considered in this attempt to model the PCI fuel failure phenomenon.

4.2 STATISTICAL ANALYSIS

The statistical model development is based on relating the failed and nonfailed data to the available reported operating parameters Bu, P, and ΔP. The procedure involves using an assumed form for the solution and using this to evaluate probability of failure for a given set of conditions. Because of

the limitation on the independent parameters P and Bu for each data set, no one data set is complete enough to be used solely in the development. All data must be treated equally.

The procedure involves the development of the most realistic functional relationship and then evaluating the data to see if they can be combined using this relationship.

A CHI-squared test of each data set, including both failed and nonfailed data, was performed to determine the relative degree of apparent homogenity between individual data sets, and to evaluate the use of these data for developing a statistical probability of failure model. The results of this work indicate whether these data, by themselves, can be used to estimate failure probabilities having known confidence limits.

If the answer to the homogenity test was negative (small values for the CHI-squared statistic), it would indicate that, although only three parameters were supplied, they would appear to be a composite data set, and that the individual data sets could be pooled together. Any probability estimates that might be generated from the data set would be reasonable and confidence limits determined.

If the answer to the homogenity test is positive (large values for the CHI-squared statistic), it would indicate that the three parameters alone do not constitute a complete composite data set, and these data alone should not be used for the development of a purely statistical failure model. It also suggests that the probabilities, having known confidence limits, could not be derived from these data.

In terms of predicting PCI fuel failure, a positive homogenity test would give a very strong indication that one, or more, first order parameters were missing from these data. In other words, P, ΔP, and Bu would not constitute a complete and composite data set for statistical model development. It would not preclude failure model development by some other technique, but it would make it difficult to evaluate the confidence limits on the predicted failure probability.

In this effort, three types of models were used in the analysis. A simple linear model in the three paramters P, ΔP, and Bu, a second order model, and the COSH model based on engineering considerations and other experimental data. Once the relationships were identified, a maximum likelihood technique was then used to fit these relationships to the data.

A goodness-of-fit statistic was calculated for each model fit. This statistic is only accurate when replicate measurements exist in the data, so it should not be viewed as an absolute measure of goodness-of-fit. However, the goodness-of-fit statistic from different model-fits can be compared to assess the different models. The results of this work indicate that any of the three models used seem to fit the data as well as the others (see Appendix B).

The test for homogenity of the three parameter data sets was made using the linear or main effects model. The results are shown in Table 4.1. The results suggest that the degree of homogenity is not great, and that the three-parameter data base does not account for the observed variability between the individual data sets.

TABLE 4.1. Test for Homogenity of Data Sets[a]

Data Set	Loglikelihood Table: -2 Loglikelihood for Combined Fit	Loglikelihood Table: -2 Loglikelihood for Individual Fits	Contribution of Data Set to Test Statistic
1	112.35	66.52	45.83
2	368.82	359.70	9.12
3	490.70	0	490.70
4	346.04	277.38	68.66
5	234.01	162.05	71.96
TOTAL	1551.91	865.65	T = 686.27

(a) This test for homogenity was conducted using the main effects model.

The conclusion of this statistical work indicates that P, ΔP and Bu are inadequate for developing a purely statistical model for estimating the probability of failure caused by PCI. It also suggests that it is not possible to calculate the error bands for failure probabilities that would be computed using only these three parameters.

The test statistic is T = 686.27. If the data sets were homogenous, T should be less that $X_{0.99}(16) = 32$, 99% of the time. Since T is bigger than 32, we can conclude that the data sets are not homogenous. (See Appendix B for detail of the calculations.)

4.3 EMPIRICAL MODELING OF THE PCI FAILURE PHENOMENON

The preceding statistical analyses of the available three-variable data (Data Sets 1 through 5) show that the PCI fuel failure phenomenon cannot be adequately modeled from three variable data by statistical methods alone. Data quantifying all other operating variables of first order importance in the PCI fuel failure phenomenon, would be necessary for the development of a purely statistical PCI fuel failure model. Additional three variable PCI data, even though they were infinitely more precise or covered a much broader range of the same three operating variables, would be of no greater value or further use in the development of a purely statistical PCI fuel fail- ure model. Under these circumstances, any PCI fuel failure modeling approach must include empirical methods.

4.3.1 Development of a Failure Function

The PCI fuel failure data available for this study were identified almost entirely by the operating variables P, ΔP and Bu. Data Set 1 included a "dwell time" observation. Only Data Set 5 included a very few "time-to-failure" observations. There were almost no data that included parameters such as:

- power ramping rate $(\dot{P})$[(a)]

(a) Data Set 1 includes this information, but the range of power ramping rates is less than an order of magnitude.

- fuel design effects such as: fuel-to-cladding gap size, interfacial lubricants or SCC inhibitors, prepressurization, etc.
- operating history for either failed or nonfailed fuel rods/assemblies
- neutronic aspects, such as local fuel rod power suppression, peak rod power positions, etc.

Two of the approaches by which the available three parameter (P, ΔP, and Bu) PCI fuel failure data may be evaluated and a failure function derived are:

1. A critical value threshold approach which requires assurance from some independent and/or alternate source that the PCI fuel failure phenomenon is "threshold" controlled, and assurance that the available data include critical value data points.
2. A regression or least squares surface fitting approach, which provides the best results when the data samples are of sufficient size and distribution, requires that the data are randomly distributed about the statistical mean surface/contour.

A threshold for PCI fuel failures may be estimated graphically by the development of its surface directly from the three-dimensional data coordinates, P, ΔP and Bu. Some apriori knowledge of the threshold surface/contour from an independent and/or alternate source, however, is necessary to be assured that the developed threshold surface is based on critical value data. In the absence of definitive apriori knowledge of the PCI failure threshold, it became necessary to evaluate the PCI failure data by analytical and statistical regression methods.

Taking into account the limitations of the data, the selection of the PCI fuel failure analysis approach was based on the following requirements, assumptions and/or critiera:

- the apriori assumption was made that each data point and each data set was as valid as any other, unless and/or until shown otherwise (in short, one model for all data)

- because each PCI fuel failure data point is spatially defined by the coordinates P, ΔP and Bu, there must be a unique relationship between these parameters
- the method must be mathematically and statistically consistent for assigning a unique and single valued failure probability
- the relationship between parameters should be substantiated by independent approaches and/or alternate fuel behavior parameters.

The approach was to determine, by regression analysis, the mean surface/contour for the PCI failure data in Data Sets 1 through 4 only. Data Set 5 was excluded because those data are far more experimental than statistical in character. If the four PCI failure data sets produce an acceptable mean surface/contour, then the combined failed and nonfailed data may be used to derive a failure function. The failure probabilities can then be estimated by means of this analytical function.

The initial effort was to segregate the data into relatively small and discrete burnup intervals and seek some pattern between the increase in power (ΔP), and either the initial pre-transient (P_i) power or the final post-transient (P_f) power. Figures 4.1 through 4.6 show the composite failed and nonfailed data segregated into discrete burnup intervals, and the data set identification number (DNF = did not fail; F = failed) for each data set. Inasmuch as the burnup effect appears to approach an asymptote within the range of about 5 to 10 GWd/MTM, all of the data within the range of $13.5 < Bu < 35.5$ GWd/MTM are shown in Figure 4.7. Least squares, linear and nonlinear regression methods, were applied to all of the failed data. The best fit to all of the failure data (taken from Data Sets 1 through 4) was obtained using least square, nonlinear regression methods and resulted in the following function:

$$\Delta P_{SM} = \frac{A}{2} \cdot \cosh\left(\frac{P_i - P_a}{A}\right) \qquad (4.1)$$

and:

$$P_a = B \left[1 + e^{-C \cdot Bu}\right] \quad (4.2)$$

where:

ΔP_{SM} = statistical mean transient increase in power for fuel failure

P_i = initial pre-transient power

Bu = fuel burnup

A,B,C = constant coefficients.

As shown in Figures 4.1 through 4.7, the ΔP_{SM} function is superimposed on the composite data at the averaged burnup for the PCI fuel failures within each burnup interval. Figure 4.8 is a computer-generated plot of ΔP versus P_i from the nonlinear regression analysis of all the PCI fuel failure data in Data Sets 1 through 4. On this plot, the zeros (0) and a few of the dollar ($) signs denote PCI failures, where these dollar signs represent two or more coincident failure data points. The asterisks (*) denote the ΔP_{SM} function. The bulk of the dollar ($) signs, particularly in the vicinity of the asterisks, indicate that the ΔP_{SM} function predicts the PCI failure observation. Figure 4.9 is a similarly generated plot of ΔP_{SM} versus Bu, in which the data are much more scattered. The burnup effect, however, does appear to approch an asymptote within about the 5 GWd/MTM to, perhaps, as high as 10 GWd/MTM burnup range. Figure 4.10 shows the general distribution of the PCI failure observations about the statistical mean ΔP for Data Sets 1 through 4. It is significant to note that the distribution about the mean is random.

4.3.2 Corroboration for the COSH Function

As shown in Table 3.1, there is considerable diversity in the three fuel designs from which the PCI fuel failure data were derived. There appears, also, to be significant diversity in the transients in which the failures occurred (see Section 1). As noted in Section 3, each data set occupies a rather limited volume of the three-dimensional space defined by the operating parameters P (either P_i or P_f), ΔP, and Bu. Under these circumstances, it seems unlikely that any individual data set would be wholly representative of

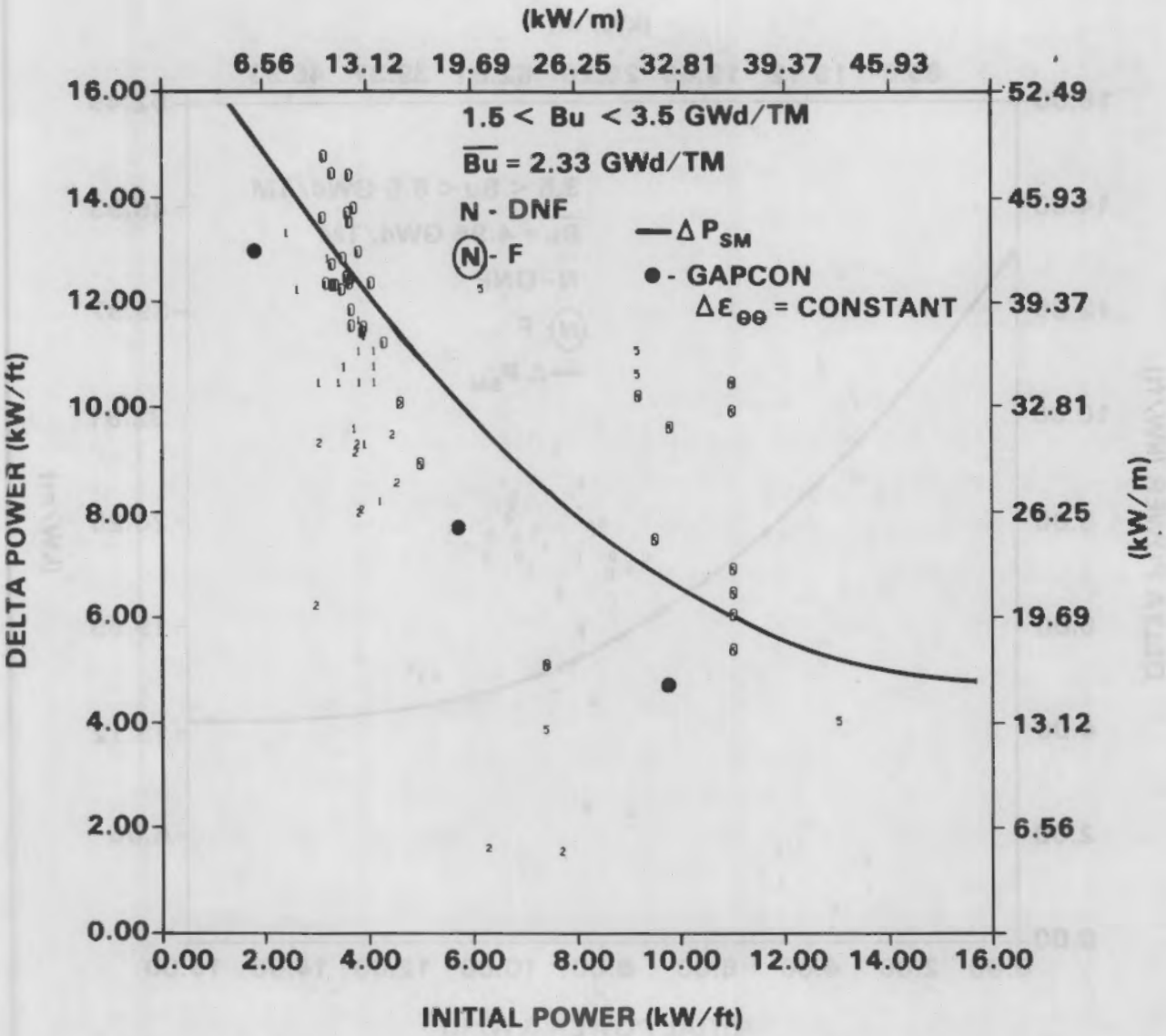

FIGURE 4.1. Shown Are All Failed (F) and Did Not Fail (DNF) Fuel Data for This Burnup Interval. Also shown is a least squares, nonlinear regression fit to the failed fuel data, and three GAPCON-THERMAL-3 transient simulations.

the PCI fuel failure phenomenon. Regression analyses of the data sets individually do indeed show some disparity in the statistical mean surface/contour for the Data Sets 1 through 4 for the failure data in each data set. Although the disparity in the statistical mean surface/contour was not generally great from data set to data set, it was considered necessary to attempt some

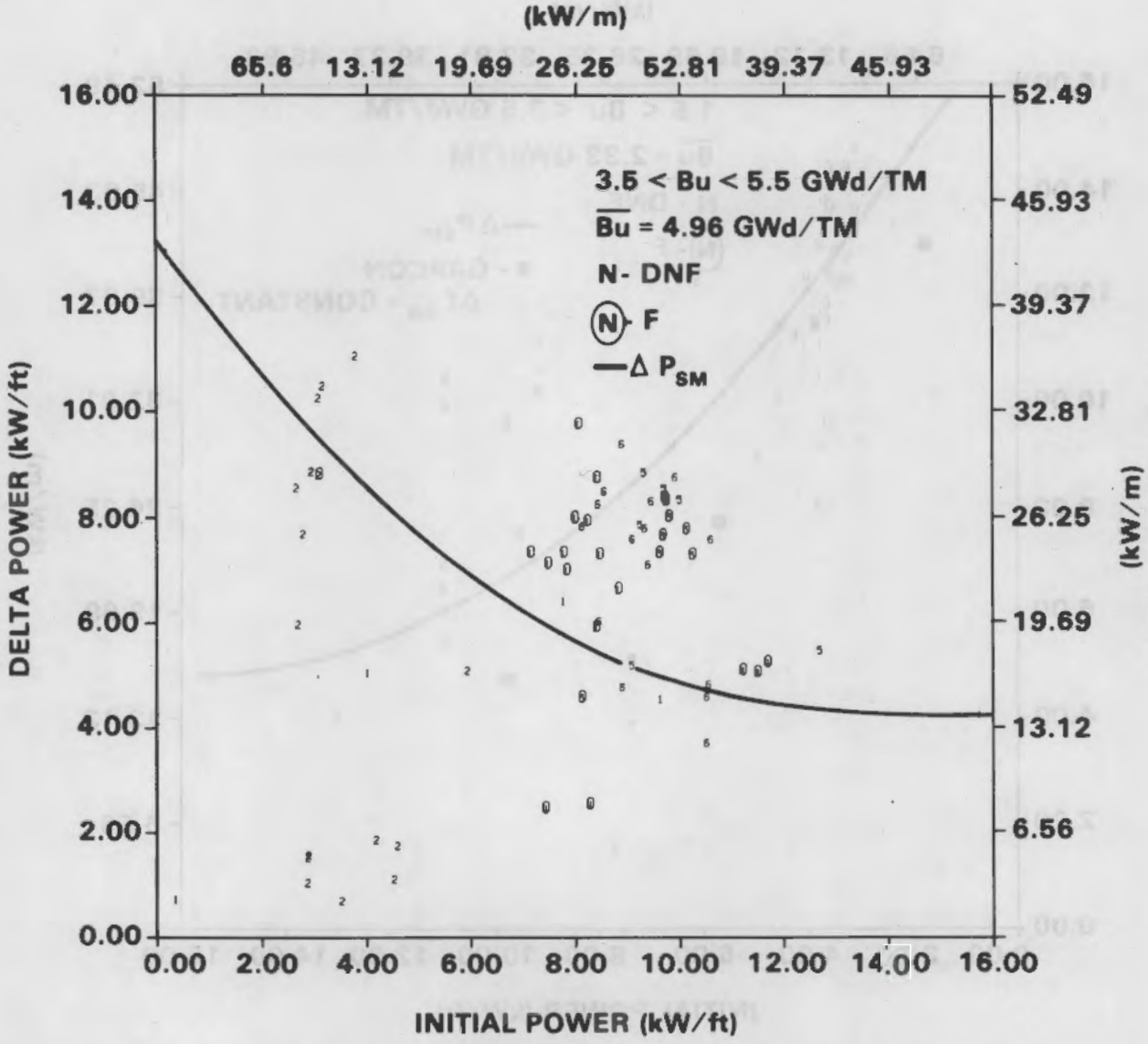

FIGURE 4.2. Shown Are All Failed (F) and Did Not Fail (DNF) Fuel Data for This Burnup Interval. Also shown is the least squares, nonlinear regression fit to the failed fuel data.

independent corroboration of the COSH function as derived from the combined failure data. To obtain some independent corroboration of the COSH function, a number of transient power increase simulations were analyzed with the GAPCON-THERMAL-3 fuel performance computer code.[43] In these transient simulations, a constant increment of circumferential strain ($\Delta\varepsilon_{\theta\theta}$), calculated by

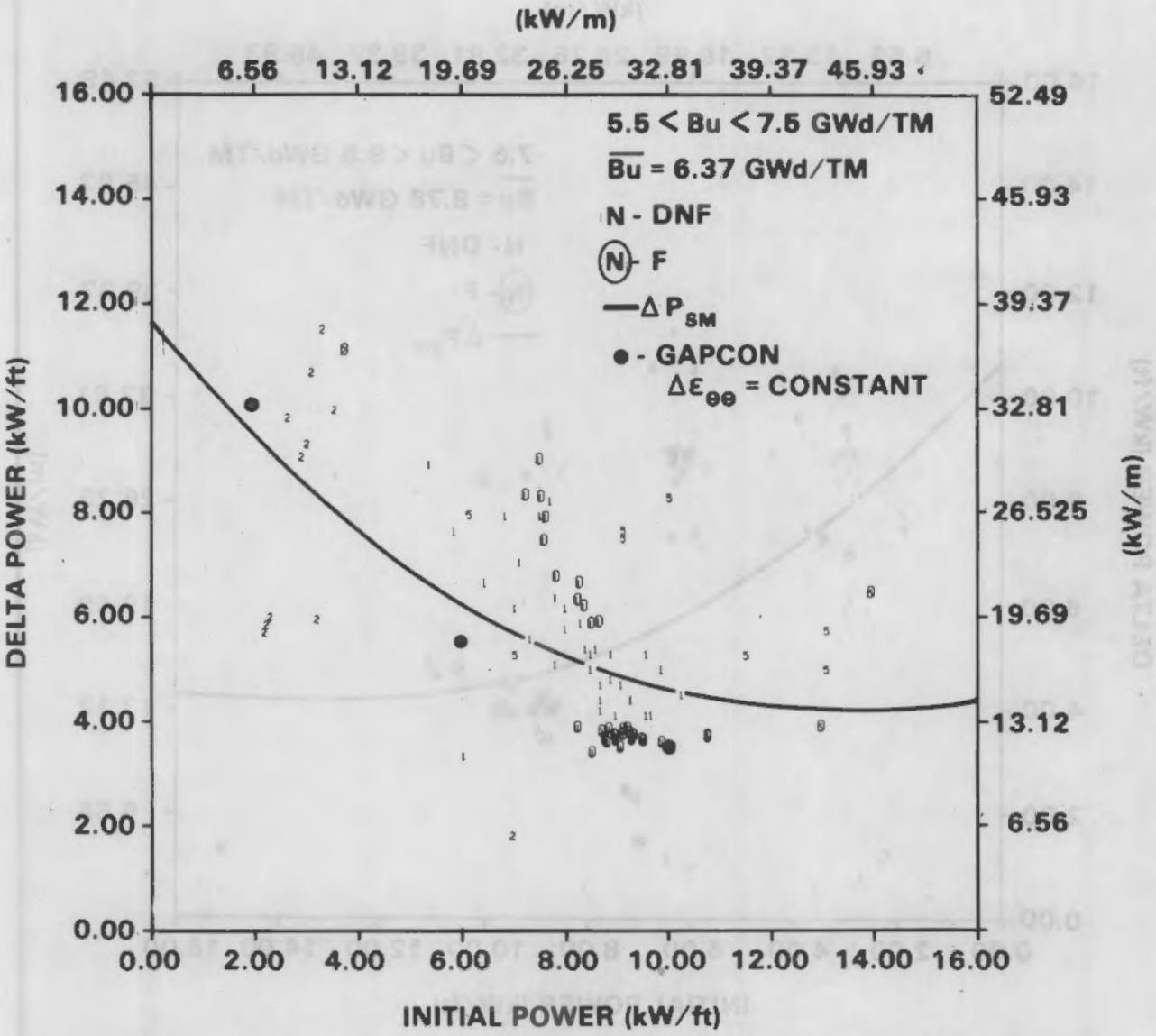

FIGURE 4.3. Shown Are All Failed (F) and Did Not Fail (DNF) Fuel Data for This Burnup Interval. Also shown is the least squares, nonlinear regression fit to the failed fuel data, and three GAPCON-THERMAL-3 transient simulations.

the code to occur in the transient only, was used as a criterion for equal severity of the transient. The choice of this criterion was based on the postulate that the differential thermal expansion of the fuel and cladding is the mechanistic corollary of the transient increase in power (ΔP). Therefore, the increment of circumferential strain ($\Delta\varepsilon_{\theta\theta}$), which occurs in the transient

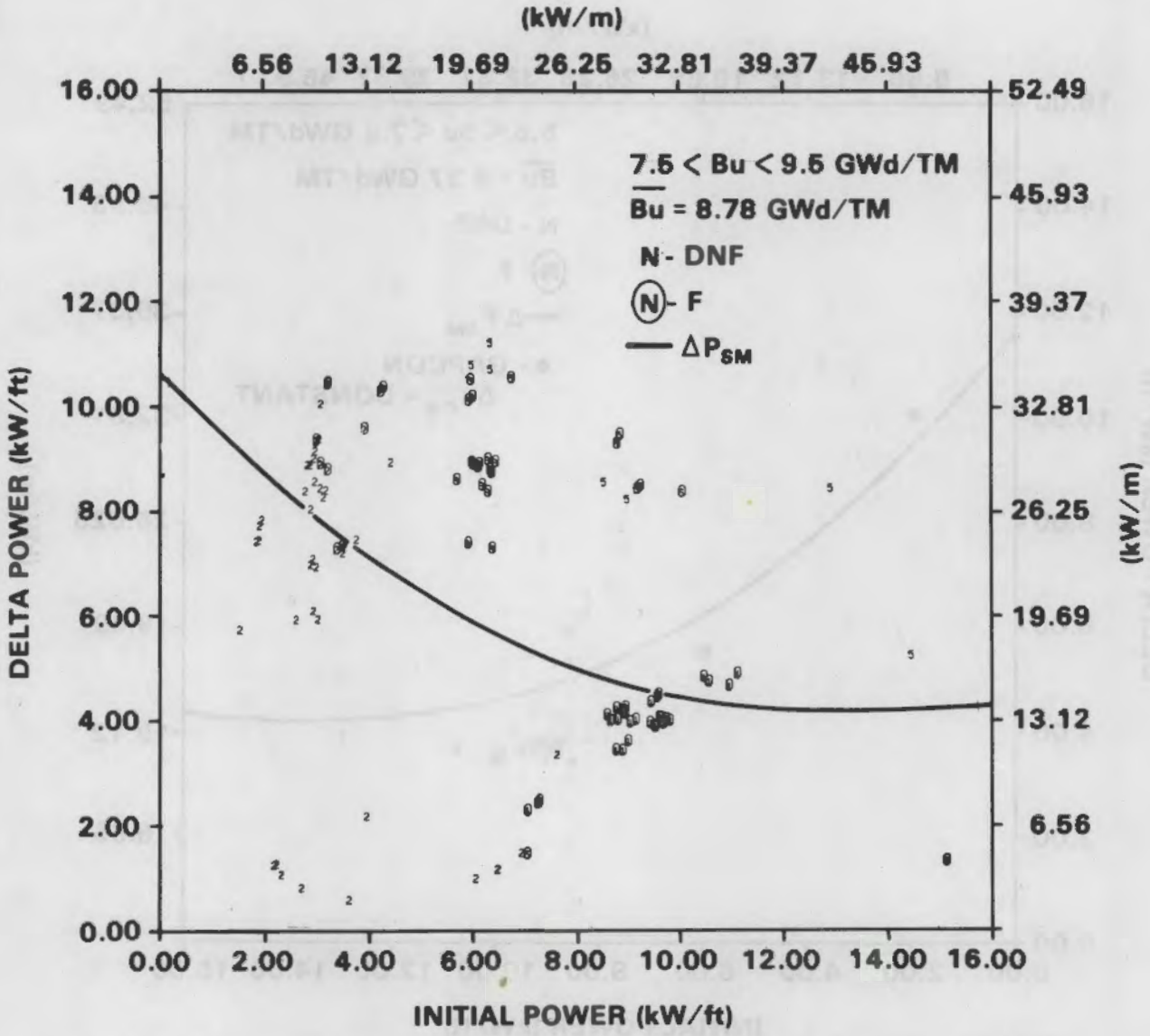

FIGURE 4.4. Shown Are All Failed (F) and Did Not Fail (DNF) Fuel Data for This Burnup Interval. Also shown is the least squares, nonlinear regression fit to the failed fuel data.

only, is a measure of that differential thermal expansion. The results of these transient simulations are shown in Figures 4.1, 4.3, and 4.5. The similarity between the COSH function for the composite PCI failure data and the transient simulations appears to provide assurance that the statistical mean failure surface/contour determined from the fuel failure data can be used as a basis for a failure probability function.

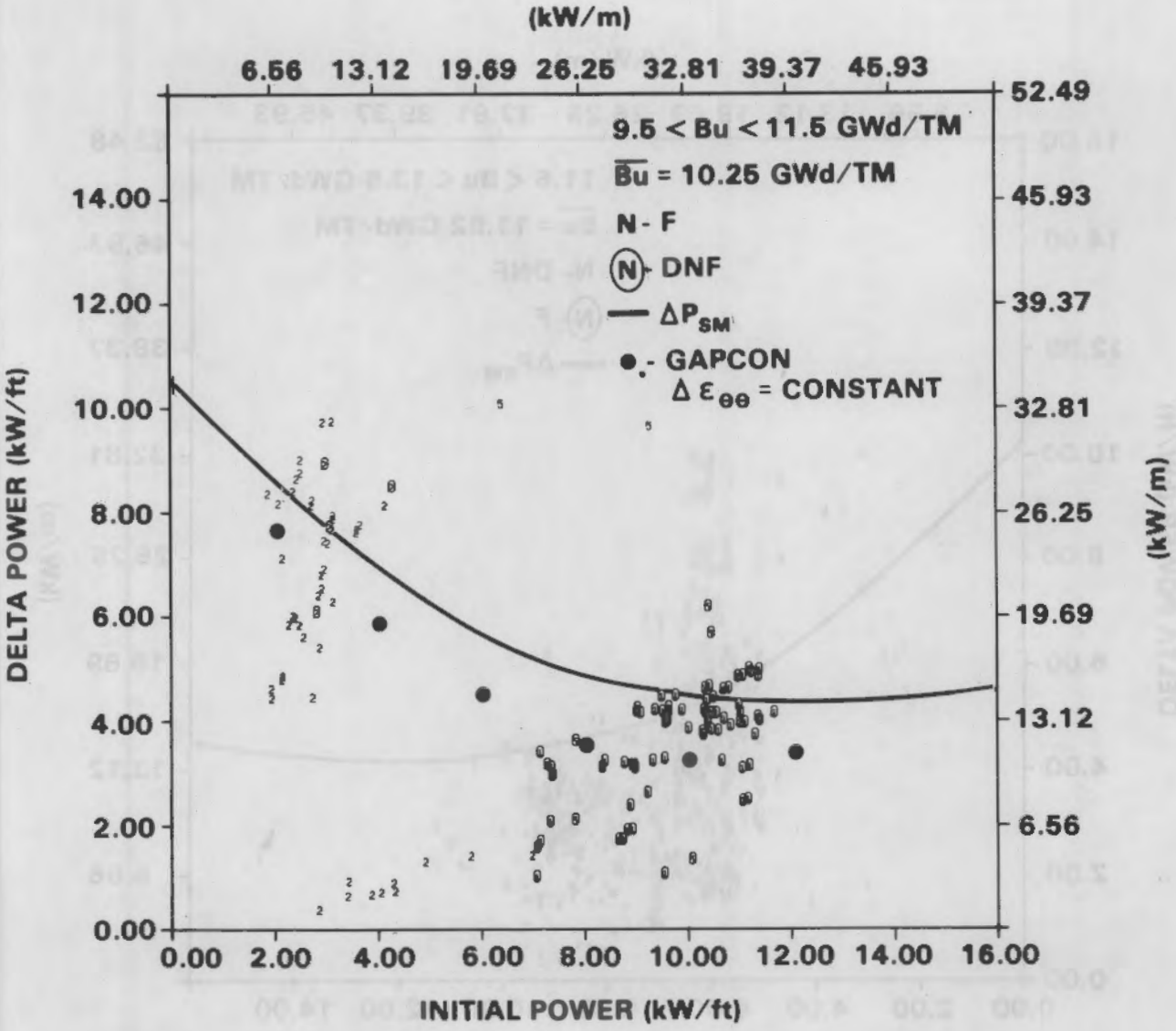

FIGURE 4.5. Shown Are All Failed (F) and Did Not Fail (DNF) Fuel Data for This Burnup Interval. Also shown is the least squares, nonlinear regression fit to the failed fuel data, and six transient simulations.

4.4 OTHER PCI FUEL FAILURE PARAMETERS

Several additional parameters have been identified in Section 4.1 as pertinent to defining the operating conditions under which PCI fuel failure may occur. Those operating parameters are the time-to-fail (TTF) and the power ramping rate ($\dot{P}$).

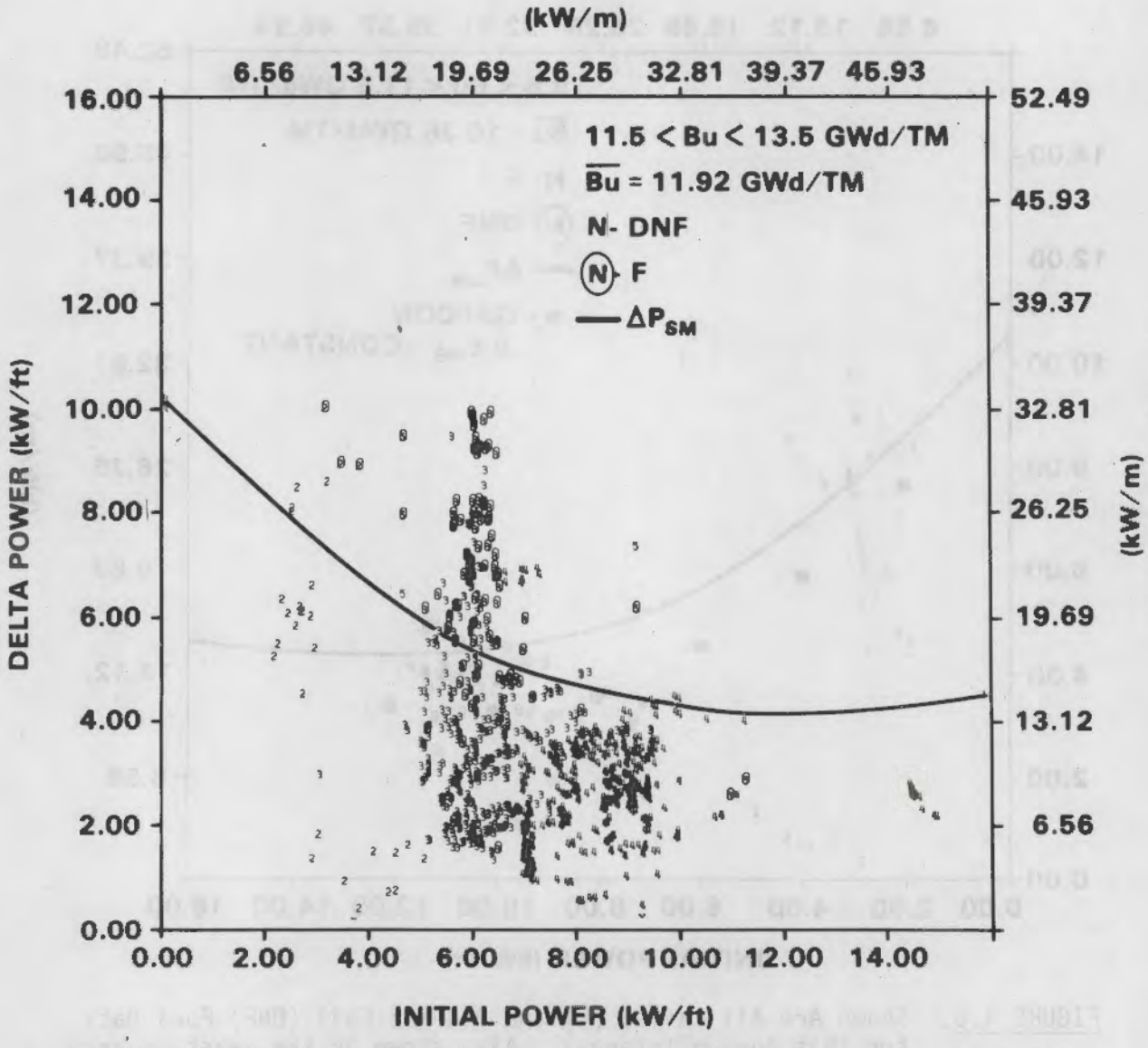

FIGURE 4.6. Shown Are All Failed (F) and Did Not Fail (DNF) Fuel Data for This Burnup Interval. Also shown is the least square, nonlinear regression fit to the failed fuel data.

4.4.1 Time-to-Fail Considerations

The FUELOGRAM includes a dwell time parameter used to modify the critical value thresholds, ΔP_c and ΔP_{fc}. This dwell time is unique to Data Set 1, and is the result of the on-line refueling operation in pressure-tube-type PHWRs. As noted in Section 2, all failures in Data Set 1 occurred within the 18-minute dwell time period during which the fuel resided at the peak power

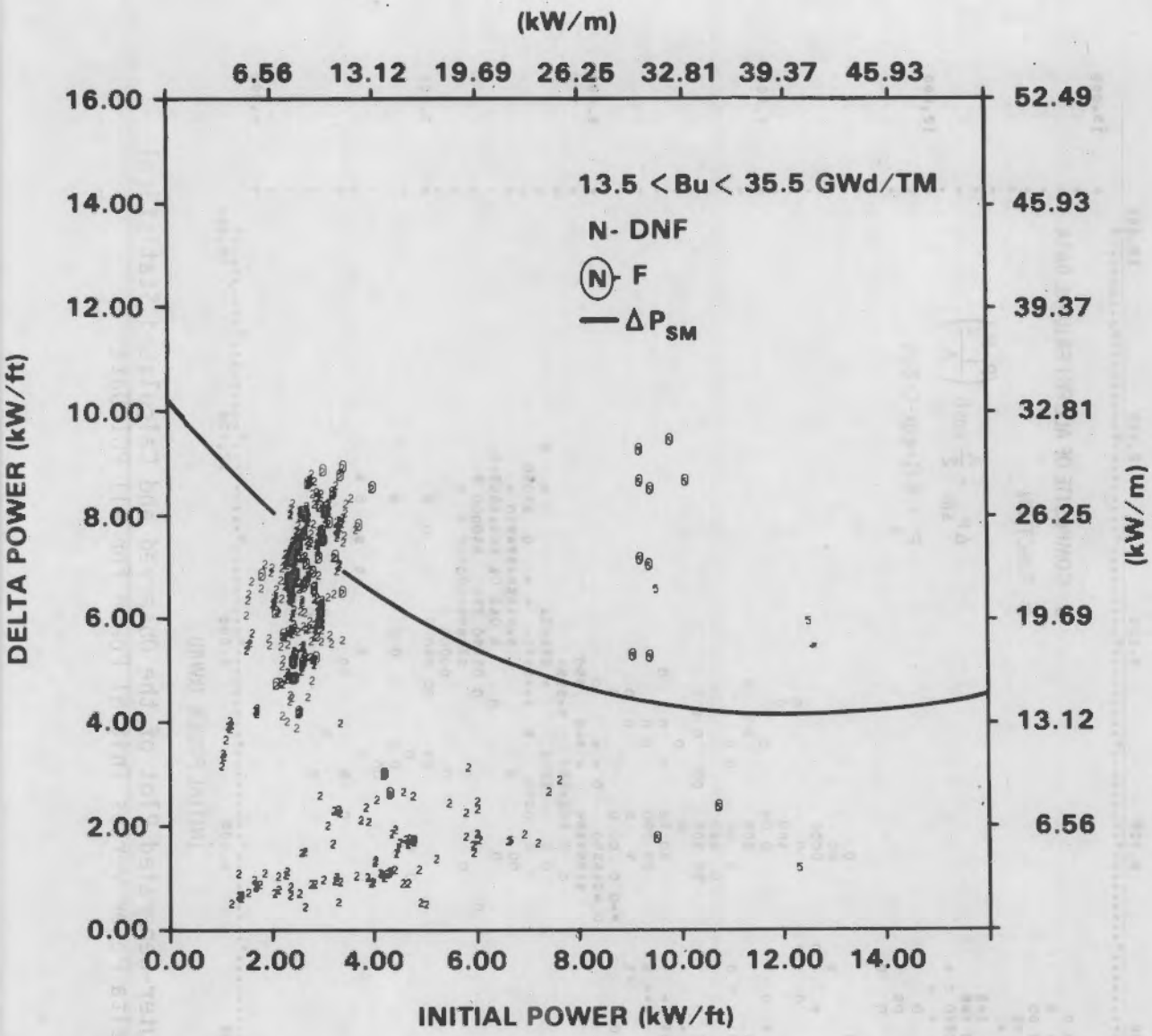

FIGURE 4.7. Shown Are All Failed (F) and Did Not Fail (DNF) Fuel Data for This Burnup Interval. Also shown is the least squares, nonlinear regression fit to the failed fuel data.

position within the pressure tube fuel channel. These failure observations, together with other experimental irradiations and iodine stress corrosion cracking (I_2SCC) laboratory experiments, were used to define a dwell time effect modification to the critical value thresholds, P_c and P_{fc}, as used in the FUELOGRAM. Since the SCC phenomenon (under conditions of constant load or stress) is time dependent, some time must elapse between the imposition of

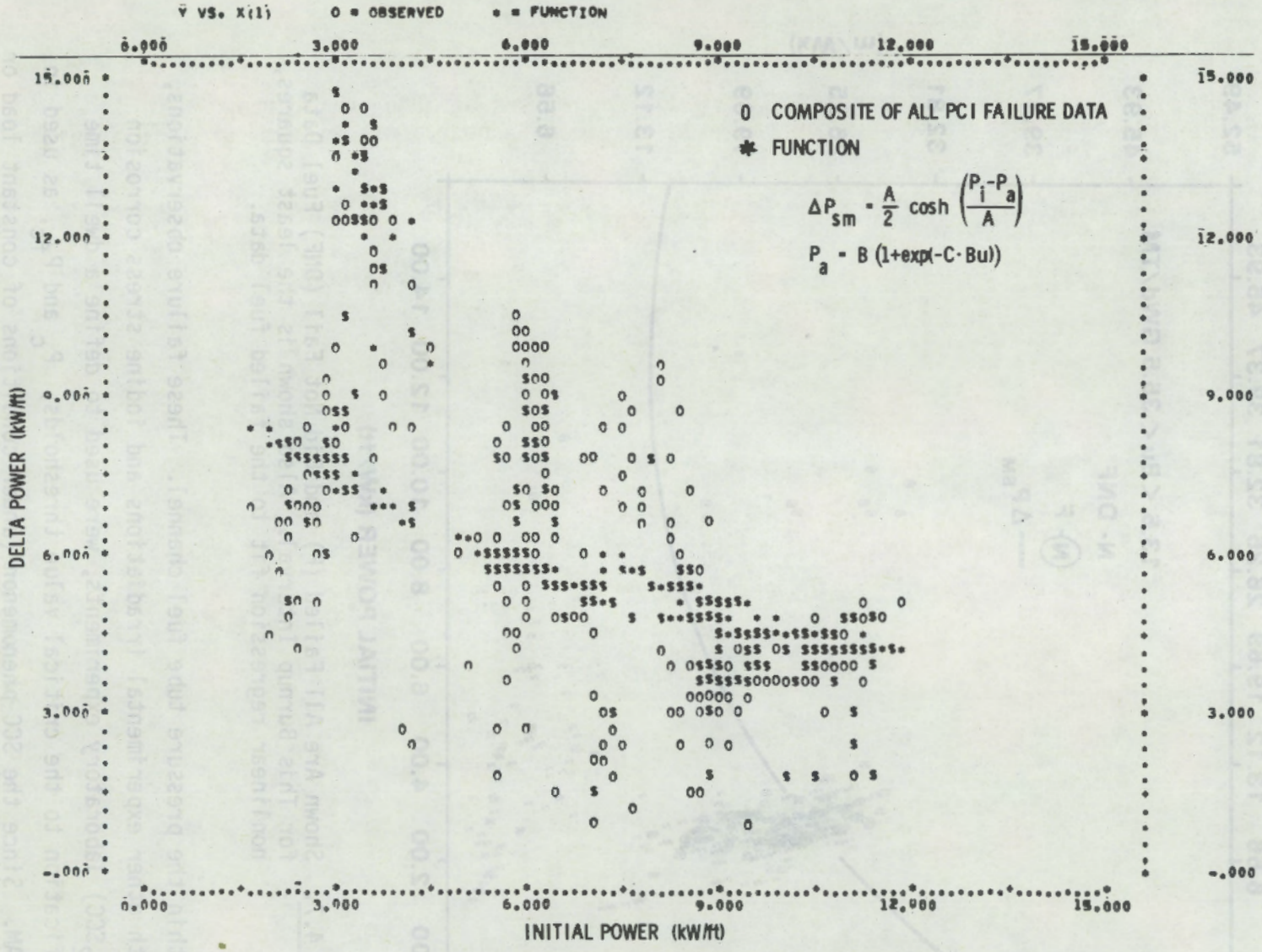

FIGURE 4.8. A Computer-Generated Plot of the Observed and Calculated Statistical Mean Delta Power versus Initial Power for All PCI Data

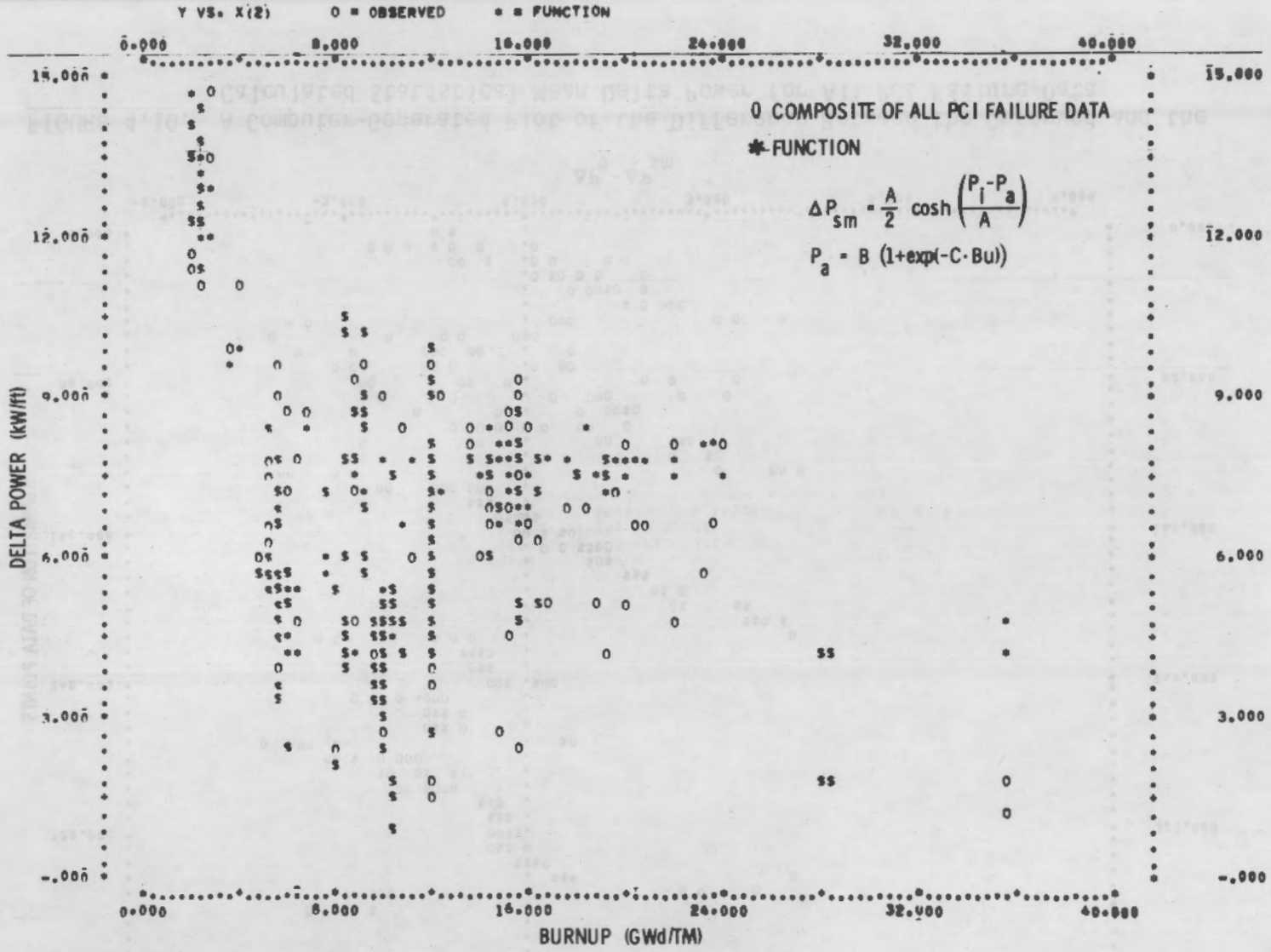

FIGURE 4.9. A Computer-Generated Plot of the Observed and the Calculated Statistical Mean Delta Power versus Burnup for All PCI Data

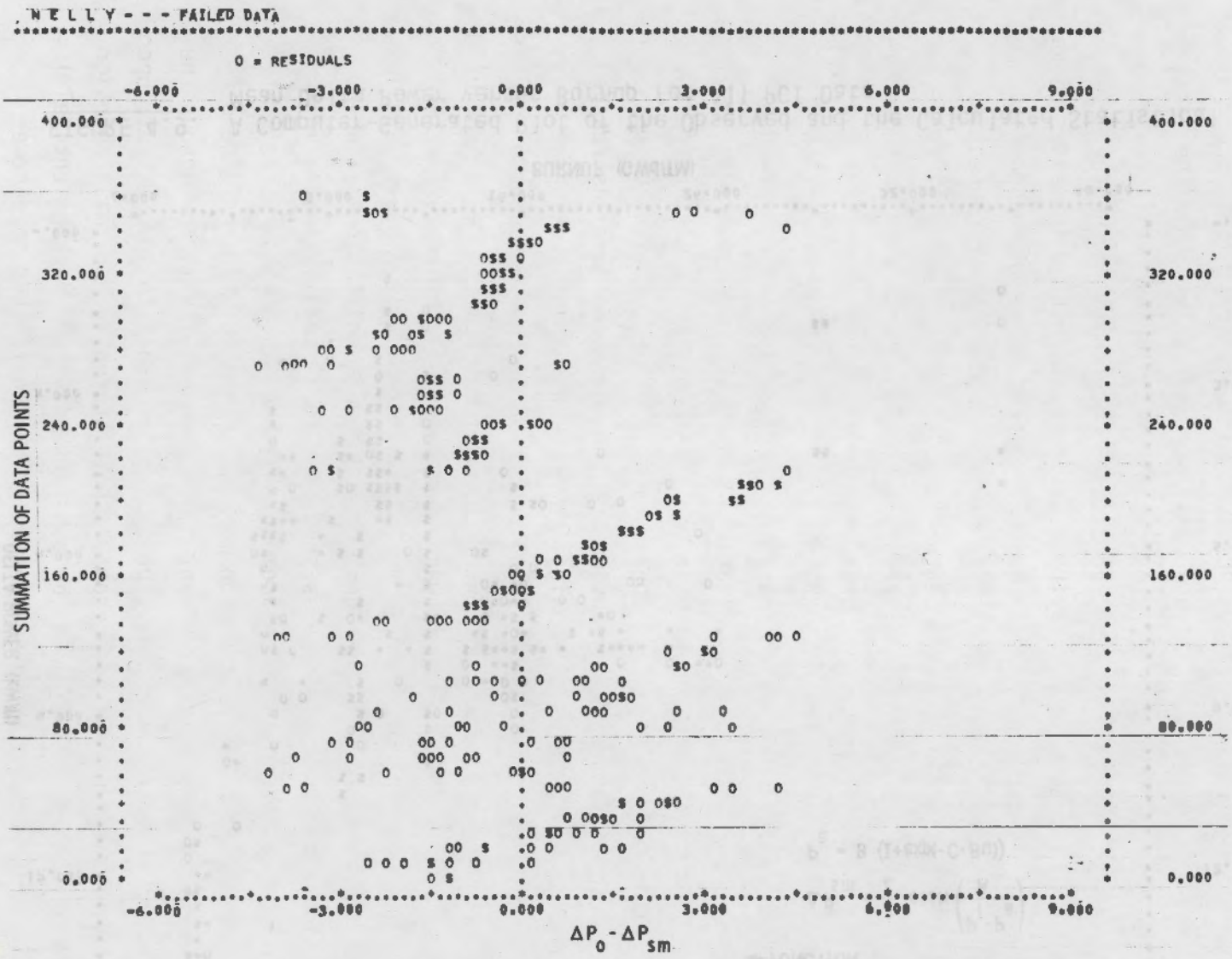

FIGURE 4.10. A Computer-Generated Plot of the Difference Between the Observed and the Calculated Statistical Mean Delta Power for All PCI Failure Data

the increase in power and subsequent failure if stress dependent I_2SCC is, in fact, the only mechanism by which PCI fuel failures occur.

An alternate viewpoint is that a PCI fuel failure, if it is to occur as the result of a transient increase in power, is most likely within the first quarter of the period of damped power oscillations following the increase in power. The neutron flux and the heat generation rate (HGR) in the fuel rise in response to an increase in reactivity. As the neutron flux increases above the pre-transient level, the ^{135}Xe is quickly reduced by an increased rate of neutron absorption. Because the ^{135}Xe neutron absorption cross-section is large, the reduction in ^{135}Xe concentration, below the ^{135}I to ^{135}Xe decay equilibrium, allows the flux/HGR to overshoot the final post-transient power. This increase in flux produces an increase in ^{135}I concentration. As the first quarter period is approached, the decay of the neutron absorption of ^{135}I to ^{135}Xe results in a greater than final equilibrium concentration of ^{135}Xe. This greater than final equilibrium concentration now exerts a damping effect and begins to cause a decrease in the flux/HGR. In this fashion, the over-and-undershoot in the flux/HGR continues in a damped oscillatory mode until the ^{135}I to ^{135}Xe decay equilibrium for the new power level is reached. Other factors, such as moderator density, rate of change in power, etc., may affect, to some degree, the magnitude and/or period of the damped power oscillations accompanying any change in power. For all rates of increase in flux/HGR, wherein there is no mismatch between power and fuel temperatures, the differential thermal expansion of the fuel and cladding will closely parallel the flux/HGR increase and the subsequent damped power oscillations. Under these conditions, the fuel cladding is subjected to a steadily increasing differential thermal expansion displacement, which peaks at about the first quarter of the damped power oscillation period. From that time on, the differential thermal expansion displacement diminishes cyclically throughout the remaining damped power oscillations. Depending, at least to some extent, upon the magnitude of the flux/HGR "overshoot," the differential thermal expansion displacement in the Zry cladding may be substantially (and perhaps entirely) removed at or prior to the three-quarter point in the first damped power oscillation period. Further removal of the differential thermal expansion

displacement will be accelerated by irradiation-enhanced stress relaxation. Therefore, assuming that the differential thermal expansion of the fuel and cladding is the source of the thermomechanical interaction for failure of the Zry cladding, failure then appears to be most likely within about the first quarter period of the damped power oscillations which accompany an increase in fuel rod/assembly power. These considerations suggest that the COSH failure function may be modified by a time-to-failure (TTF) parameter in a manner analogous to the dwell time parameter used in the FUELOGRAM. Alternatively, an adjunctive function might be chosen to aid in estimating the likelihood for failure. Because time-to-failure observations were very sparse within the available data, the adjunctive function approach was chosen. An adjunctive function, which currently appears to merit consideration, is a time-to-fail (TTF) function, tentatively defined as follows:

$$TTF = f\ (T,\ \Delta P,\ P_f) \qquad (4.3)$$

where:

TTF = time-to-fail

T = period of the damped power oscillations accompanying a transient increase in power

ΔP = transient increase in power

P_f = final, post-transient power.

If one assumes that the PCI fuel failure is principally dependent upon the severity of the thermomechanical interaction (i.e., differential thermal expansion of the fuel and cladding), the time-to-failure then may be expected to be primarily dependent upon the transient increase in power (ΔP). Alternatively, if one assumes that PCI fuel failure is principally dependent upon the severity of the thermo-chemical interaction (i.e., stress corrosion cracking by fission product I_2, Cd, etc.), the time-to-failure then may be expected to be primarily dependent upon the peak post-transient power (P_f). Available time-to-fail information in the five data sets are both sparse and uncertain.

In Data Set 1, all failures were reported to have occurred within the 18-minute dwell period during which the fuel resided at the axial peak power position within the pressure tube fuel channel. Assuming that, for the least severe transient (ΔP and P_f), the time-to-fail was equal to the 18-minute dwell time and one and one-half minutes for the most severe transient, the time-to-fail appears to be better defined by the ΔP parameter as follows:

$$TTF = a\, e^{b \cdot \Delta P} \qquad (4.4)$$

where:

TTF = time-to-fail, minutes

ΔP = transient increase in power, kW/ft

a = 90 minutes

b = -0.28.

Data Set 5 includes only a very few time-to-fail observations from "one-of-a-kind" experiments. Using these data, the time-to-fail appears to be better defined by the P_f parameter as follows:

$$TTF = \alpha \cdot e^{K (P_f - P_a)} \qquad (4.5)$$

where:

TTF = time-to-fail, minutes

P_f = final, post-transient power, kW/ft

P_a = burnup asymptote as defined in Equation 4.2, kW/ft

α = 48 minutes

K = -0.43.

The least squares, nonlinear regression fit of the sparse time-to-fail observations from Data Set 5 is shown in Figure 4.11. Figure 4.12 shows the statistical distribution of the time-to-fail observations about the statistical mean for the limited data. Clearly, one observation, at least, is at considerable variance with the general set of time-to-fail observations. Even

though, from a statistical viewpoint, Data Set 5 is the least reliable, it provides the only quantified time-to-fail observations. For this reason, Equation 4.5 appears to be the most appropriate adjunct function for use in estimating the probability of failure from a transient increase in power.

4.4.2 Strain Rate Considerations

There are at least two behavioral characteristics of Zry which are very strain-rate sensitive and appear to be of major significance to the PCI fuel failure phenomenon. These behavioral characteristics are: 1) strain rate dependent SCC embrittlement, and 2) strain rate dependent plastic deformation.

There is no consensus as to which of these two strain rate dependent behavioral characteristics dominate the Zry fuel cladding failure. Based on the available (but limited) data, both strain rate behavior characteristics appear to be of major importance and may even be synergistic.

4.4.2.1 Strain Rate Dependent SCC Embrittlement in Zry

One viewpoint is that the dominant failure mechanism in the PCI fuel failure phenomenon is stress corrosion cracking (SCC) and/or liquid/vapor metal (L/VME) embrittlement by fisson products, such as iodine, cadmium, etc., which may be more or less promptly released from the fuel during a power transient. Moreover, this viewpoint generally holds that a critical threshold stress within the Zircaloy cladding must exist for failure by the SCC mechanism. Considerable experimental effort has been expended in an attempt to establish the existence of and quantify the critical threshold stress for SCC. There is, however, a growing body of experimental data showing that strain rate and, perhaps, strain are key parameters in the stress corrosion phenomenon.[44-49]

Parkins[44] and others[45-48] have shown that the susceptibility of metal alloys to stress corroson cracking, as evidenced by a reduction in the tensile strength or fracture ductility is, among other factors, strongly and directly related to the strain rate imposed on the SCC test coupon. Scully, et al.[47] have shown experimentally in SCC tests on notch-defected coupons, that the stress corrosion cracking rate is determined by the crack tip strain rate and

not the absolute magnitude of the imposed body stress. Simulated fuel expansion experiments by Wood, et al.[17] show the effect of straining rate on the averaged circumferential strain at failure in Zry fuel cladding in an iodine environment. In I_2 SCC tests on unirradiated Zry, Peehs, et al.[49] observed a minimum in the relative uniform elongation at a critical strain rate. At either faster or slower strain rates the effective aggressiveness of the iodine is virtually eliminated. These data further suggest that the strain rate effect on the the reduction in relative uniform elongation is directly proportional to the iodine concentration. Coffin[50] observed that increasing temperature and decreasing strain rate enhance the embrittling effect of iodine on Zry.

In smooth bar specimens under tension, Parkins[44] observed that failure in an aggressive environment is preceded by the appearance of many surface cracks for all metal alloy systems investigated. Similar cracking behavior has been reported by Tomalin,[51] Lee and Adamson[52] with Zry in iodine, and by Grubb[16] in liquid cadmium and cadmium-cesium mixtures. By contrast, a notch-defected coupon was always observed to fail by cracking from the notch-root.[44,47] Cubicciotti, et al.[18] observed this behavior with Zry fuel cladding notched in the ID surface and tested under tension by internal pressurization with helium and iodine mixtures. Coffin[50] observed that microcracking was not observed at strains below about 0.6 to 0.7%. Zebroski and Roberts[53] have reported that the minimum strain for cracking the oxide surface film was about 0.4%. It was not reported as to whether this minimum strain for oxide cracking was observed in tests on irradiated or nonirradiated Zry. Cubicciotti, et al.[18] did experiments wherein the cracked oxide film was removed by ion milling to reveal the microcracking in the metal substrate. The microcracking in the metal substrate was observed only at second phase particle sites. It apparently was not determined whether the microcracking developed from fracturing of the second phase particle itself, or as decohesion of the second phase particle from the surrounding metal matrix. In any case, plastic deformation, as manifested by slip, appears to be necessary to

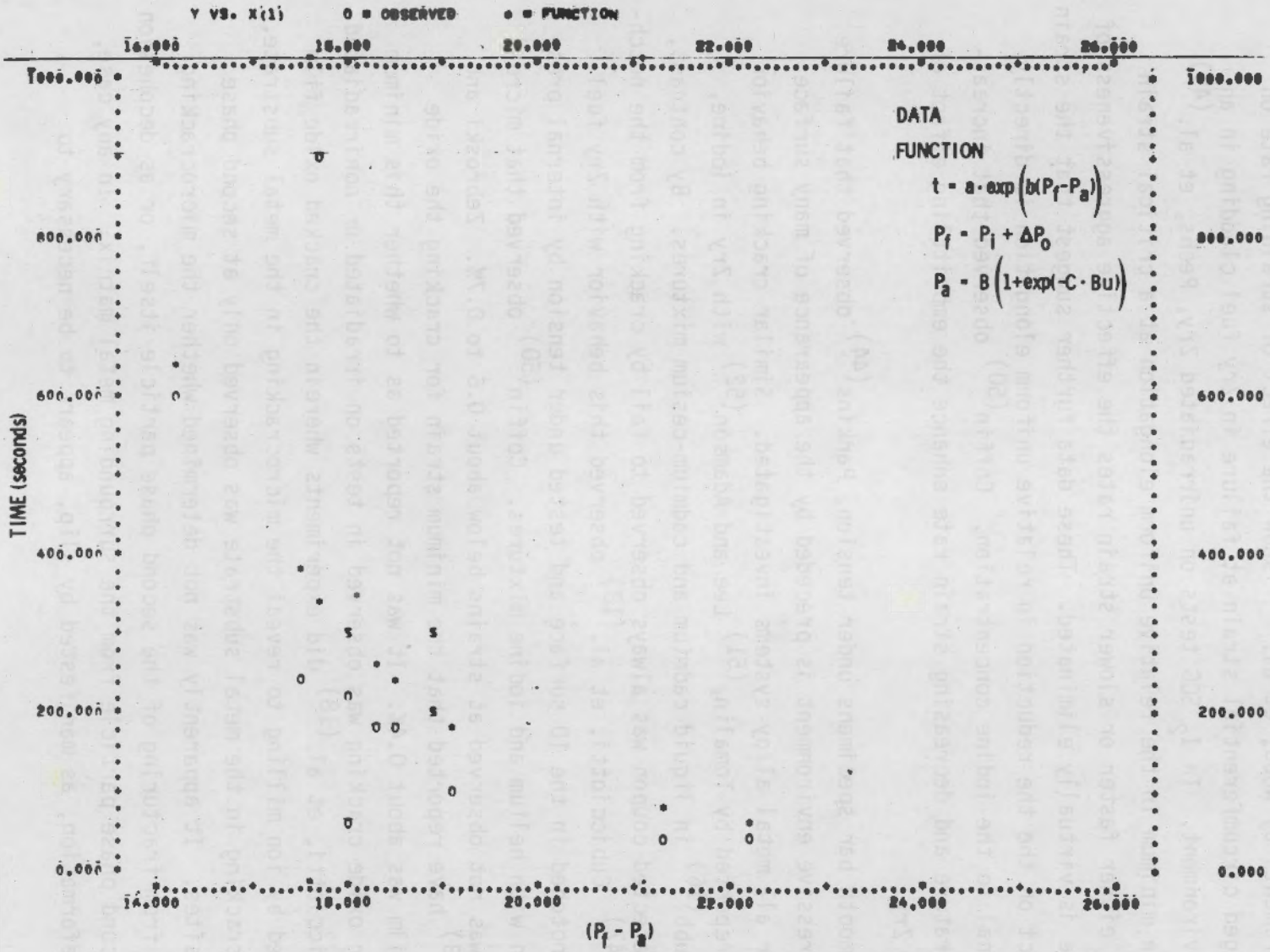

FIGURE 4.11. A Computer-Generated Plot of the Least Squares, Non-Linear Regression Fit of Equation 3.8 to Time-To-Fail Observations from Data Set 5

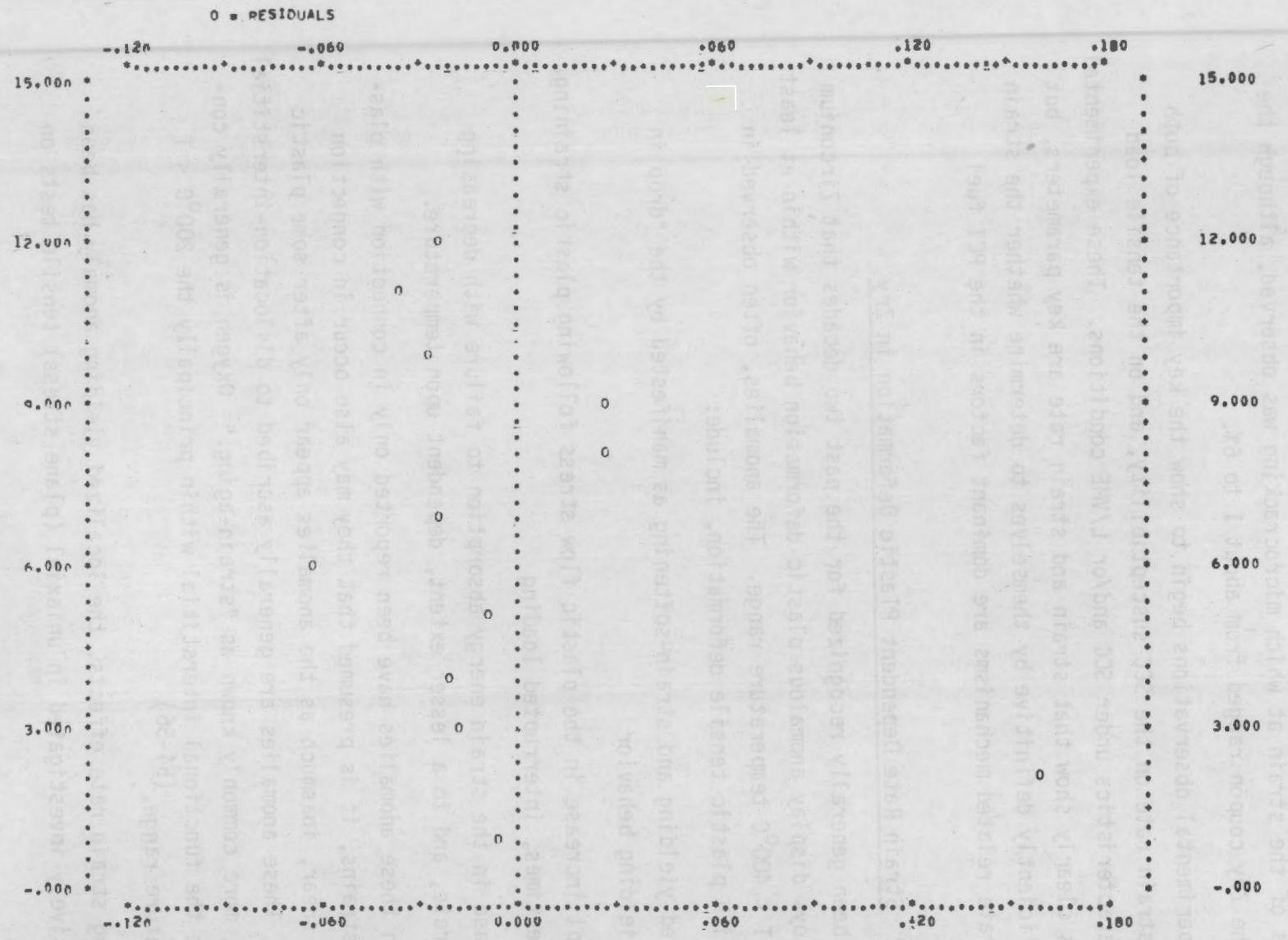

FIGURE 4.12. Statistical Distribution of the Time-To-Fail Observations About the Statistical Mean. All time-to-fail observations are from Data Set 5.

initiate microcracking by either process. In these experiments, there were no measurements of the strain at which microcracking was observed, although the strain in the Zry coupon ranged from about 1 to 6%.

The experimental observations begin to show the key importance of both strain and strain rate on the SCC susceptibility, and on the tensile load carrying characteristics under SCC and/or L/VME conditions. These experimental observations clearly show that strain and strain rate are key parameters, but are not sufficiently definitive by themselves to determine whether the strain and strain rate related mechanisms are dominant factors in the PCI fuel failures.

4.4.2.2 Strain Rate Dependent Plastic Deformation in Zry

It has been generally recognized for the past two decades that Zirconium and some alloys display anomalous plastic deformation behavior within at least the $200^{o}C < T < 400^{o}C$ temperature range. The anomalies, often observed in connection with plastic tensile deformation, include:

- localized yielding and strain-softening as manifested by the "drop in load" yielding behavior
- an abrupt increase in the plastic flow stress following plastic straining, and oftentimes, interrupted loading
- a decrease in the strain energy absorption to failure with decreasing strain rate, and to a lesser extent, dependent upon temperature.

Although these anomalies have been reported only in connection with plastic tensile strains, it is presumed that they may also occur in connection with plastic shear, inasmuch as the anomalies appear only after some plastic deformation. These anomalies are generally ascribed to dislocation-interstitial interactions, more commonly known as "strain-aging." Oxygen is generally considered to be the functional interstitial within principally the $200^{o}C < T < 400^{o}C$ temperature range.[54-56]

Excepting strain rate effects, the localized yielding anomaly has been fairly extensively investigated in uniaxial (plane stress) tensile tests on

both irradiated[57] and unirradiated[58-62] Zry, and are summarized as follows:

- The sharpness of the yield point and the magnitude of the yield drop appear to increase with increasing temperature and decrease with increasing strain hardenability. These effects appear to be dependent, to some extent at least, on the interstitial content.
- Localized yielding does not require large prior plastic strains, nor is it attributable to deformation by twinning.
- The yield drop appears to be inversely proportional to grain size, although a yield point has been observed in Zry single crystals.

Anisotropy effects on localized yielding have not been systematically explored. Considering the mechanisms postulated[58,59,61] to account for the localized yielding anomaly, a yield point is likely to be both more prevalent and pronounced in the hoop direction in Zry tubing.

The most significant observations from uniaxial (plane stress) tensile tests on irradiated Zry are summarized as follows:

- irradiation appears to lower the temperatures at which localized yielding occurs
- anisotropy/directional effects are retained.

In PIE uniaxial (plane stress) tensile tests on rolled sheet, Bement[57] further observed that the stress-strain behavior in the transverse direction was characterized by a sharp yield point and a single Luder's band[(a)], wherein all subsequent strain to failure was confined. In the longitudinal direction, however, the yield point at the same fluence was less pronounced and subsequent strain to failure was significantly less localized. This general stress-strain behavior was also observed in Hardy's[63] axial and transverse ring uniaxial (plane strain) tensile tests on Zry fuel clad tubing. There were slight differences in strain rates (0.017 min^{-1} and 0.05 min^{-1}, respectively) in the axial and transverse ring tests. Hardy's investigations also included biaxial stress tests by internal pressurizaton of the Zry fuel clad tubing. Except

(a) This is a manifestation of dislocation channeling.

for the effective strengthening by the biaxial stress state, the general stress-strain (and particularly, the yield point behavior) does not appear to be signficantly different from that in the transverse ring uniaxial tension tests. The effect of grain size on the stress-strain behavior was noted to be greater in the transverse ring uniaxial and internally pressurized biaxial stress tests than in the longitudinal uniaxial tension tests. There did not, however, appear to be any relative change in grain size effect by neutron irradiation.

Excepting strain rate effects over a wide range of strain rates, the flow stress anomaly ($\Delta\sigma/\sigma$) has been investigated in both uniaxial tensile and creep tests.[58] For unirradiated Zry, as determined from uniaxial tensile tests, the $\Delta\sigma/\sigma$ increases with temperature throughout about the $200^{o}C < T < 450^{o}C$ temperature range, aging time, aging stress, and strain rate. The range of strain rates over which the $\Delta\sigma/\sigma$ anomaly was examined was relatively small, ranging from 0.0064 min^{-1} to 0.24 min^{-1}. Based on PIE uniaxial (plane stress) tensile tests, Veever, et al.[55] concluded that the $\Delta\sigma/\sigma$ anomaly was reduced to insignificance after irradiation to a fluence ranging from 5.0 E 19 nvt to 1.0 E 19 nvt. As noted previously, radiation appears to lower the temperature at which the yield point, yield drop, and localized deformation occur. Based on this observation, is it not then also possible that radiation may cause a similar shift in the strain-aging temperature?

As determined in uniaxial tensile creep tests, the $\Delta\sigma/\sigma$ anomaly for unirradiated Zry is manifested by significant reductions in creep rates which, within the $200^{o}C < T < 450^{o}C$ temperature range, persist for very substantial times (i.e., >>1000 hrs.).[64-66] The time over which the reduced creep rates persist appears to be inversely proportional to temperature. The effect of neutron irradiation, as determined from influx, uniaxial tensile creep tests, is to markedly reduce the time (0 to 10 hrs) during which the creep rates are reduced.[65]

Strain energy absorption to failure has been generally regarded as a constitutive property of materials only in relation to impact and linear elastic fracture behavior. The yield strength and ductility (uniform and/or total

elongation and reduction in area) are generally regarded as the important constitutive properties in relation to stress-strain behavior. In a material which displays anomalous stress-strain behavior, the use of the yield and/or ultimate strength and ductility to fully define stress-strain behavior may be deceptive and misleading. Figure 4.13 shows three stress-strain curves which are postulated to be more or less characteristic of irradiated Zry at widely differing strain rates and plane stress conditions. The stress-strain curve for the intermediate strain rate is actually more or less characteristic of the stress-strain behavior in the transverse direction in rolled sheet observed by Bement,[57] and in the hoop direction fuel cladding observed by Hardy,[63] in irradiated Zry. The very low and very high strain rate stress-strain behavior for irradiated Zry has not been thoroughly or systematically explored.

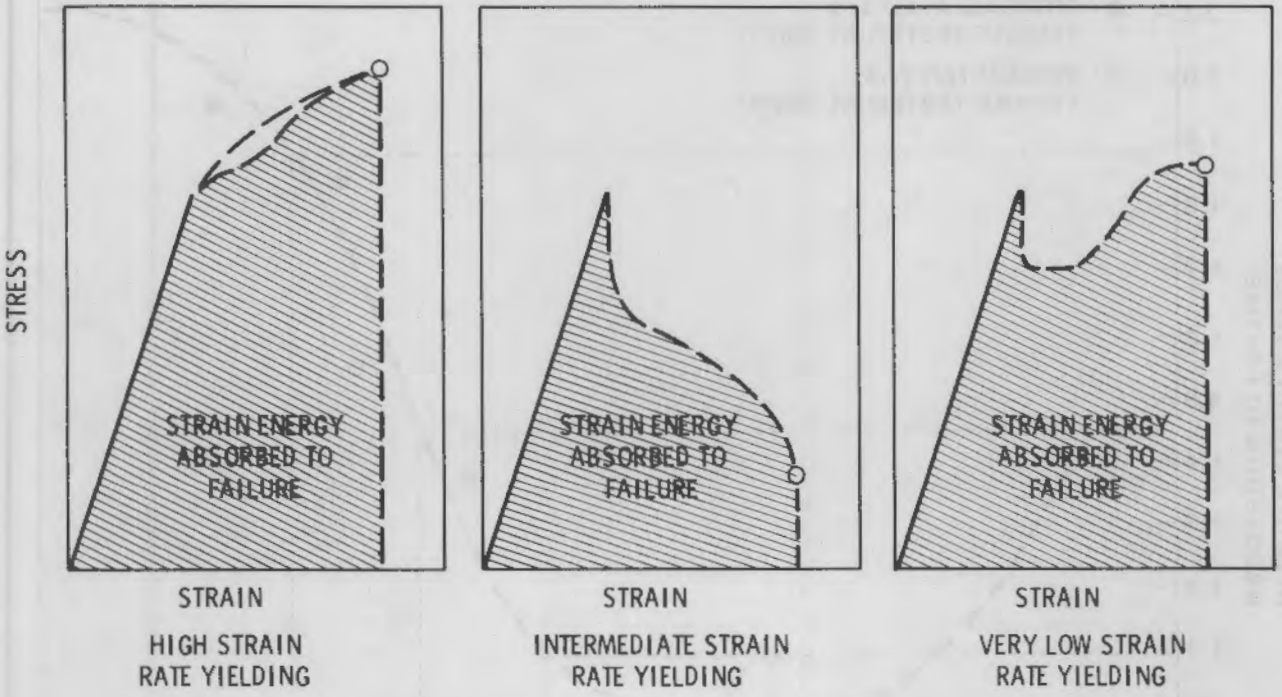

FIGURE 4.13. Postulated Tensile Stress-Strain Behavior for Irradiated Zry as Influenced by Strain Rate and the Localized Yielding Anomaly

The effect of strain rate on the tensile stress-strain behavior of Zry and some alloys was investigated to a limited extent by Lee.[67] All tests were at 350°C. All tensile coupons were taken from the transverse direction of rolled sheet. Monotonic strain rates ranged from 6.3E-5 min^{-1} to 6.3E-1 min^{-1}. Strain hardening occurred in all tests and the yield anomaly was noted only in the higher strain rate tests. The effect of strain rate on the tensile stress-strain behavior of irradiated Zr-4 was investigated to a lesser extent by Azzarto, et al.[68] The PIE tensile tests were at 282°C and strain rates ranging from 8.3E-8 min^{-1} to 5.0E-2 min^{-1}. Exposures ranged from 6.0E20 nvt to 9.4E20 nvt. The results of these two stress-strain behavior investigations are shown in Figure 4.14, where the strain energy

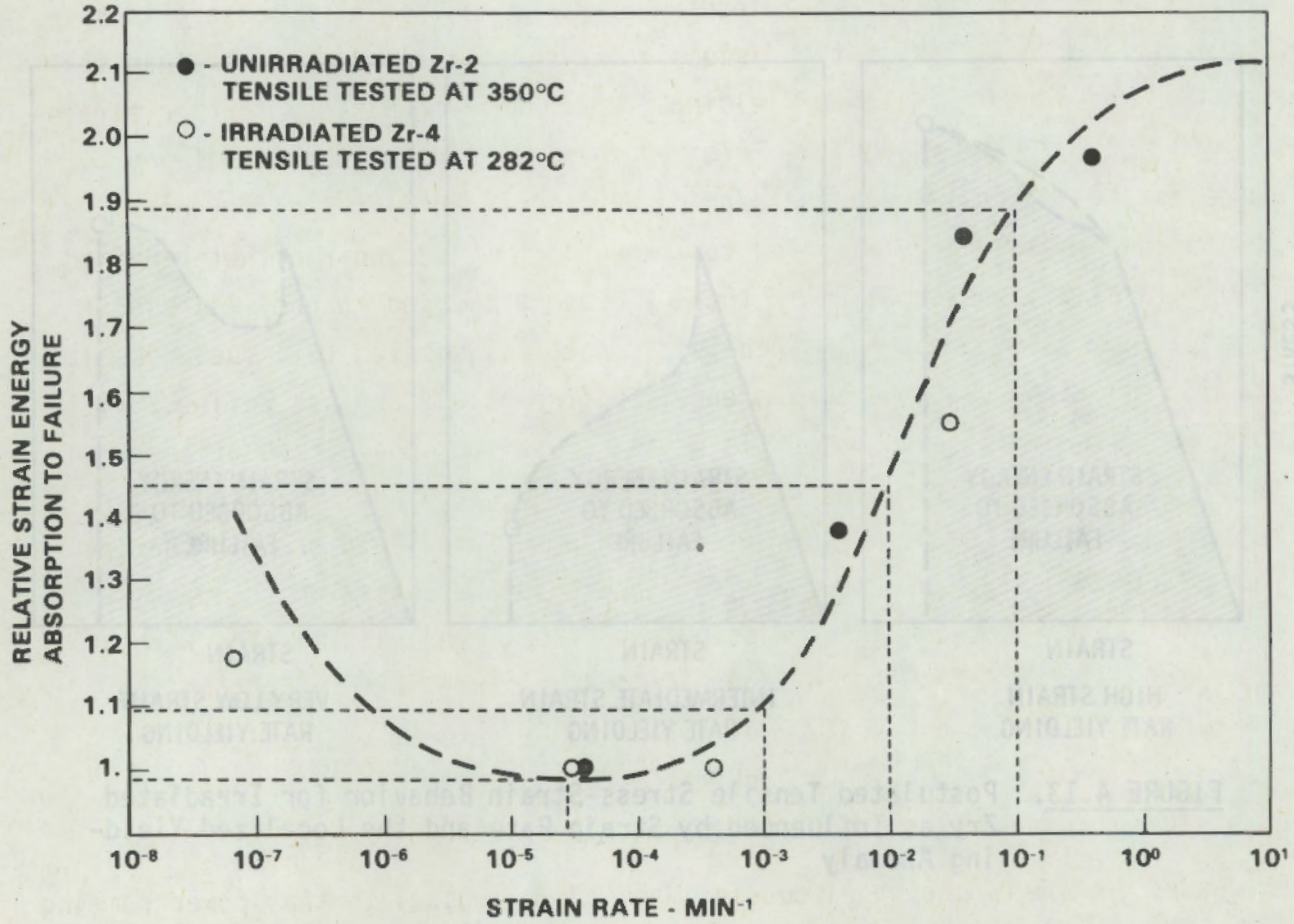

FIGURE 4.14. The Effect of Strain Rate on the Relative Strain Energy Absorption to Failure as Determined for Available Uniaxial Tensile Data.[42,44]

absorption to failure relative to the minimum strain energy absorption to failure, in each data set, is plotted as a function of strain rate. As a matter of interest, the strain energy absorption to failure for the irradiated condition is within the range of 1/6 to 1/7 of that for the unirradiated condition at all strain rates. This difference, however, represents, in part, the test temperature difference, as well as the irradiation effect on the strain energy absorption to failure.

Experimental observations, particularly, those of Bement[57] and Hardy[63] on irradiated Zry, of a yield point, yield drop, and localized strain to failure, strongly suggest that this stress-strain anomaly is of major importance in the PCI fuel failure phenomenon. The occurrence of a yield point and yield drop as a manifestation of dislocation channeling constitutes a mechanical instability wherein the external loading and/or displacement necessary to sustain plastic deformation in the dislocation cleared channels is less than that which was required to initiate yielding. Under this condition, further straining will occur in the dislocation cleared channels, in the absence of any change in the external loading and/or displacement, until the difference between the strain energy required for the initial yielding and that required to sustain plastic deformation in the dislocation cleared channels is dissipated in plastic deformation. When this concept is applied to a fuel rod, it must be recognized that the strain energy differential, as just defined, will be in direct proportion to the ratio of the cross-sectional areas of the fuel rod and the localized yielding zone(s) in the Zry cladding! These considerations suggest that the occurrence of a yield point and yield drop in the Zry cladding of a fuel rod provides a strain energy differential which is at least potentially greater than can be dissipated in localized plastic flow without incurring failure. As shown in Figure 4.14, the strain rate effect on the strain energy absorption to failure appears to be generally similar to the strain rate effects observed by Parkins[44] and others[46-49] in chemically aggressive environments.

Based on the foregoing discussions and the on postulate that power ramping rate ($\dot{P}$) is the operating corollary of strain rate dependent deformation and

failure mechanisms, it appears that the COSH failure and/or any other failure probability function should be modified to account for the strain rate SCC embrittlement and plastic deformation characteristics of the Zry cladding. Figure 4.15 shows the PCI fuel failure distribution about the statistical mean for all failure data (See Figure 4.10), adjacent to the strain energy absorption to failure versus strain rate for the Zry cladding (see Figure 4.14). Recognizing that the composite PCI fuel failure data base probably encompasses a range of power ramping rates, this juxtaposed view suggests that at least some of the failures, which occurred in the least severe of the transients represented in the data base, may have been the consequence of power ramping conditions (rates) corresponding to strain rates in the Zry cladding at which the strain energy absorption to failure is a minimum. By the same logic, some of those failures which occurred in the more severe transients may have been the consequence of power ramping/strain rate conditions for which the strain energy absorption capacity of the Zry cladding is comparatively large. These considerations therefore suggest that the likelihood of incurring PCI fuel failures in low severity transients could be significantly greater than in the more severe transients!

It must therefore be recognized that all failures that lie below the ΔP_{SM} surface/contour do not necessarily have a lower probability of failure than the failures that lie above ΔP_{SM} (shown in Figures 4.10 and 4.15). In short, there is likely to be a family of ΔP_{SM} surfaces/contours each with its own statistical distribution of failures and each corresponding to a specific strain/power ramping rate.

Power ramping rate ($\dot{P}$) information can be extracted only from Data Set 1. In Data Set 1, however, the range of power ramping rates is very narrow (less than an order of magnitude) and inadequate to define a power ramping/strain rate dependence for the PCI fuel failure phenomenon. If, as suggested above, there is some correspondence between the severity of the transient and the power ramping/strain rate dependent strain energy absorption to failure, then the COSH failure function must be modified to reflect the strain rate sensitive SCC embrittlement and plastic deformation characteristics of the Zry cladding.

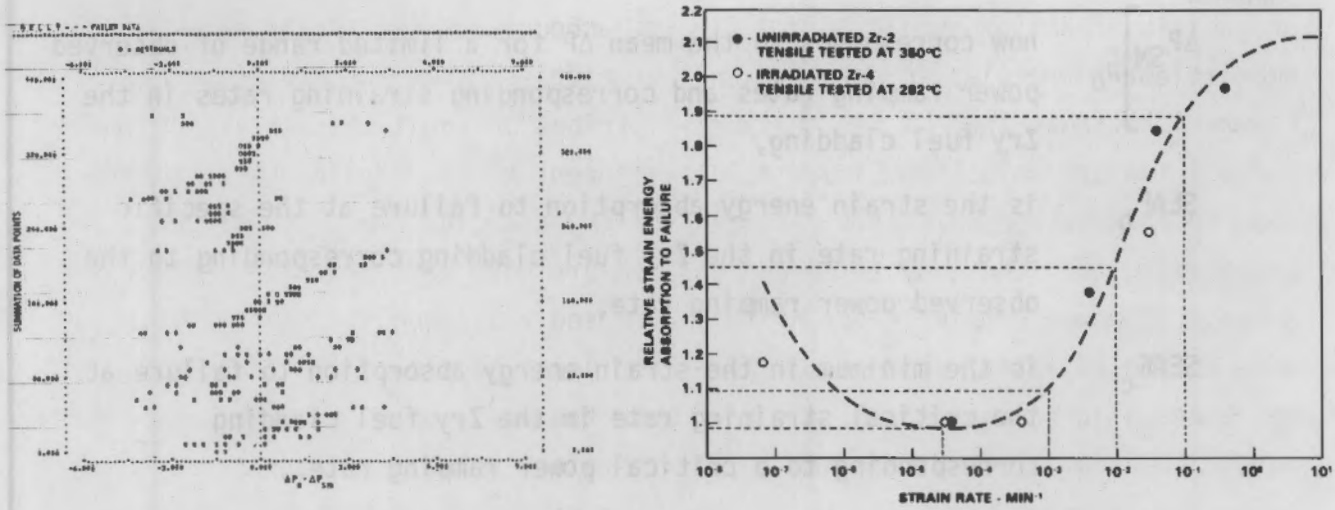

FIGURE 4.15. The Juxtaposition of Figures 4.10 and 4.14 to Suggest a Correspondence Between the Severity of the Transients in Which PCI Failures Were Observed and The Strain Rate Versus Strain Energy Absorption to Failure.

One possible approach is the use of a simple multiplier to the COSH failure function. One appropriate multiplier appears to be the ratio of the strain energy adsorption to failure, corresponding to the strain/power ramping rate in the actual transient, to the minimum strain energy absorption to failure corresponding to the critical strain/power ramping rate. Assuming that the above suggested approach may reasonably account for power ramping/Zry cladding strain rate effects for all of the failed data, the COSH failure function may then be modified as follows:

$$\Delta P_{SM}\Big]_{\dot{P}_o} = \frac{A}{2}\left(\frac{SEAF_o}{SEAF_c}\right) \cdot \text{COSH}\left(\frac{P_i - P_a}{A}\right) \qquad (4.6)$$

where:

$\Delta P_{SM}\Big]_{\dot{P}_o}$ now corresponds to the mean ΔP for a limited range of observed power ramping rates and corresponding straining rates in the Zry fuel cladding,

$SEAF_o$ is the strain energy absorption to failure at the specific straining rate in the Zry fuel cladding corresponding to the observed power ramping rate,

$SEAF_c$ is the minimum in the strain energy absorption to failure at the critical straining rate in the Zry fuel cladding corresponding to a critical power ramping rate.

The parameters P_i and P_a and the coefficient A are all the same as in Equation 4.1. The power ramping/strain rate/strain energy absorption to failure modification, as shown in Equation 4.6, was applied to the COSH failure function in the belief that many, if not all of the PCI failures in the composite data are likely to have occurred not only because of the severity of their transient increase in power, but also because their power ramping rate corresponded to a near critical range of cladding straining rates for which the strain energy absorption to failure is minimal. Conversely, it appears likely that failure in the remainder of the composite data was avoided because their power ramping rates corresponded to cladding straining rates for which the strain energy absorption to failure is comparatively large.

4.5 FAILURE PROBABILITY

Empirical methods have provided a basis for the development of at least some of the elements of a model of the PCI fuel failure phenomenon. The elements of this PCI failure model are:

- the COSH function (Equation 4.1 and 4.2) defining the relationship between the three operating variables P, ΔP and Bu for the composite PCI failure data

- a multiplier to account, at least in part, for the strain (power ramping) rate and strain energy absorption to failure behaviorial characteristics of the Zry fuel rod cladding. (Equation 4.6)

Assuming that these elements of the PCI failure model provide an acceptable representation of the PCI fuel failure phenomenon, they may then be combined with a model for estimating the probability of failure in transients.

Using standard statistical methods, a function based on the COSH failure function, may be defined mathematically such that it constitutes the surface/contour which best separates the failures from nonfailures. The probability of failure in transients (PROFIT) model is:

$$S = \beta_0 + \beta_1 P_o - \beta_2 \Delta P_{SM} \left(\frac{SEAF_o}{SEAF_c} \right) \tag{4.7}$$

where:

$$\Delta P_{SM} = \frac{A}{2} \text{COSH} \left(\frac{P_i - P_a}{A} \right)$$

$$P_a = B \left(1 + e^{-C \cdot Bu} \right)$$

The coeffients, β_0, β_1 and β_2, are selected so as to best separate the failures from non-failures. The parameters are as previously defined. Equation 4.7 may then be used in a logistic distribution function (Equation (4.8) to provide an estimate of the probability of failure in transients as follows: (See Appendix B)

$$POF = \frac{e^S}{e^S + 1} \tag{4.8}$$

where:

P_i = initial, pre-transient power - kW/ft

Bu = fuel burnup - GWd/MTM

ΔP_o = observed increase in power - kW/ft

ΔP_{SM} = statistical mean increase in power - kW/ft

$SEAF_o$ = strain energy absorption to failure for the Zry cladding at the strain rate corresponding to the observed power ramping rate.

$SEAF_c$ = the minimum in the strain energy absorption for the Zry cladding at the critical strain rate corresponding to a critical power ramping rate.

POF = probabability of failure

A = 8.23

B = 12.70

C = 0.34

β_o = -0.36

β_1 = 0.58

β_2 = 0.63

Figures 4.16 and 4.17 show the estimated probability of failure assuming a SEAF ratio of unity. Table 4.2 shows the postulated effect of strain/power ramping rate on the estimated probability of failure for several SEAF ratios. As shown in Table 4.2, the postulated effect of the strain/power ramping rate on the probability of failure is substantial, particularly for the less severe transients.

Inasmuch as the composite data provided very little power ramping rate ($\dot{P}$) information, additional data are needed to quantify the strain/power ramping rate and strain energy absorption to failure (SEAF) relationship before

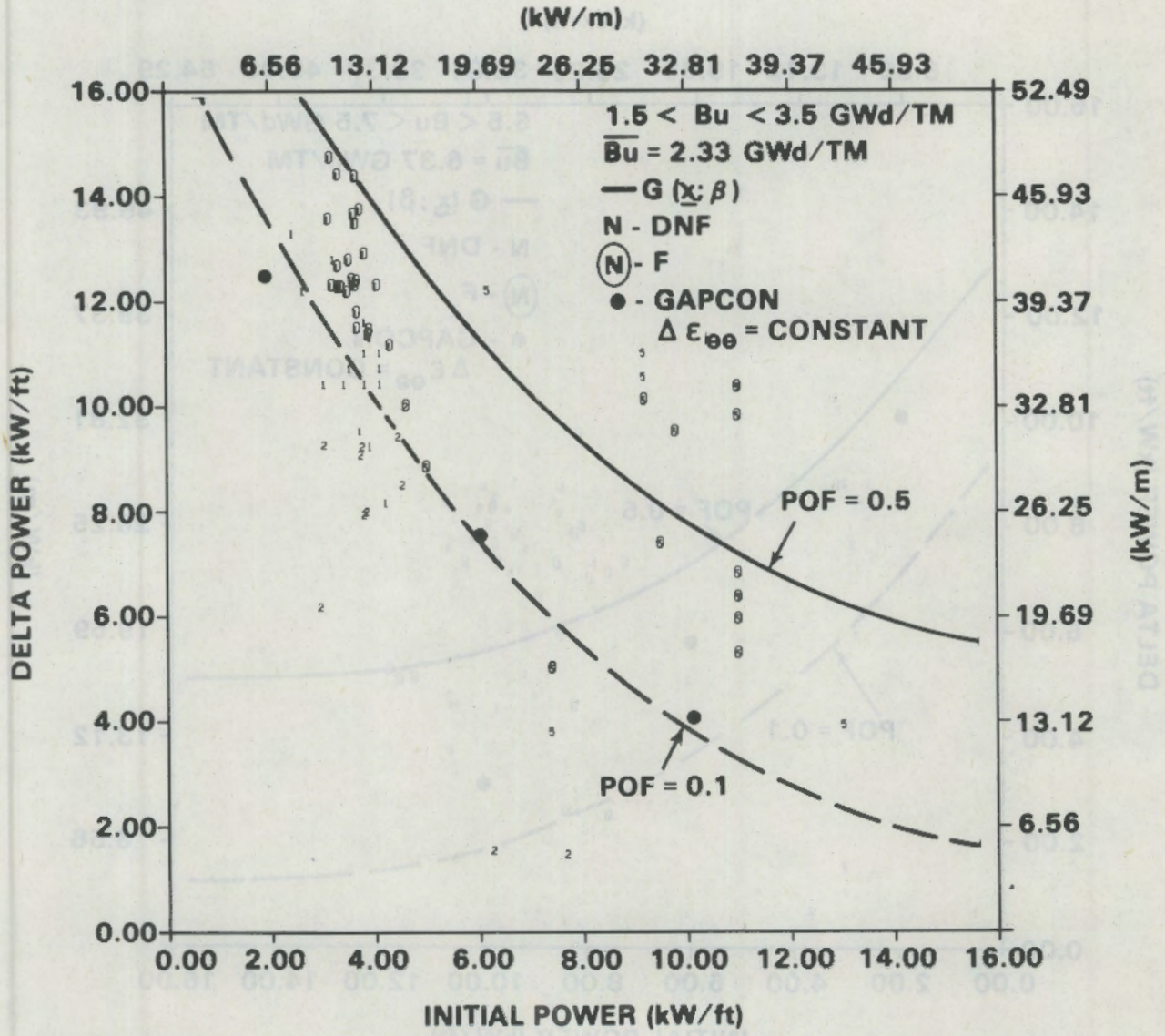

FIGURE 4.16. Shown Are All Fuel Data That Failed (F) and That Did Not Fail (DNF) for This Burnup Interval. Also shown are the 10% and 50% probability of failure (POF) curves and three simulated transients.

more accurate PCI failure probabilities can be estimated from PROFIT. The strain energy absorption to failure (SEAF) dependence on strain rate and environment appears to be the constitutive material property of first order importance in determining the likelihood of failure of the Zry cladding when

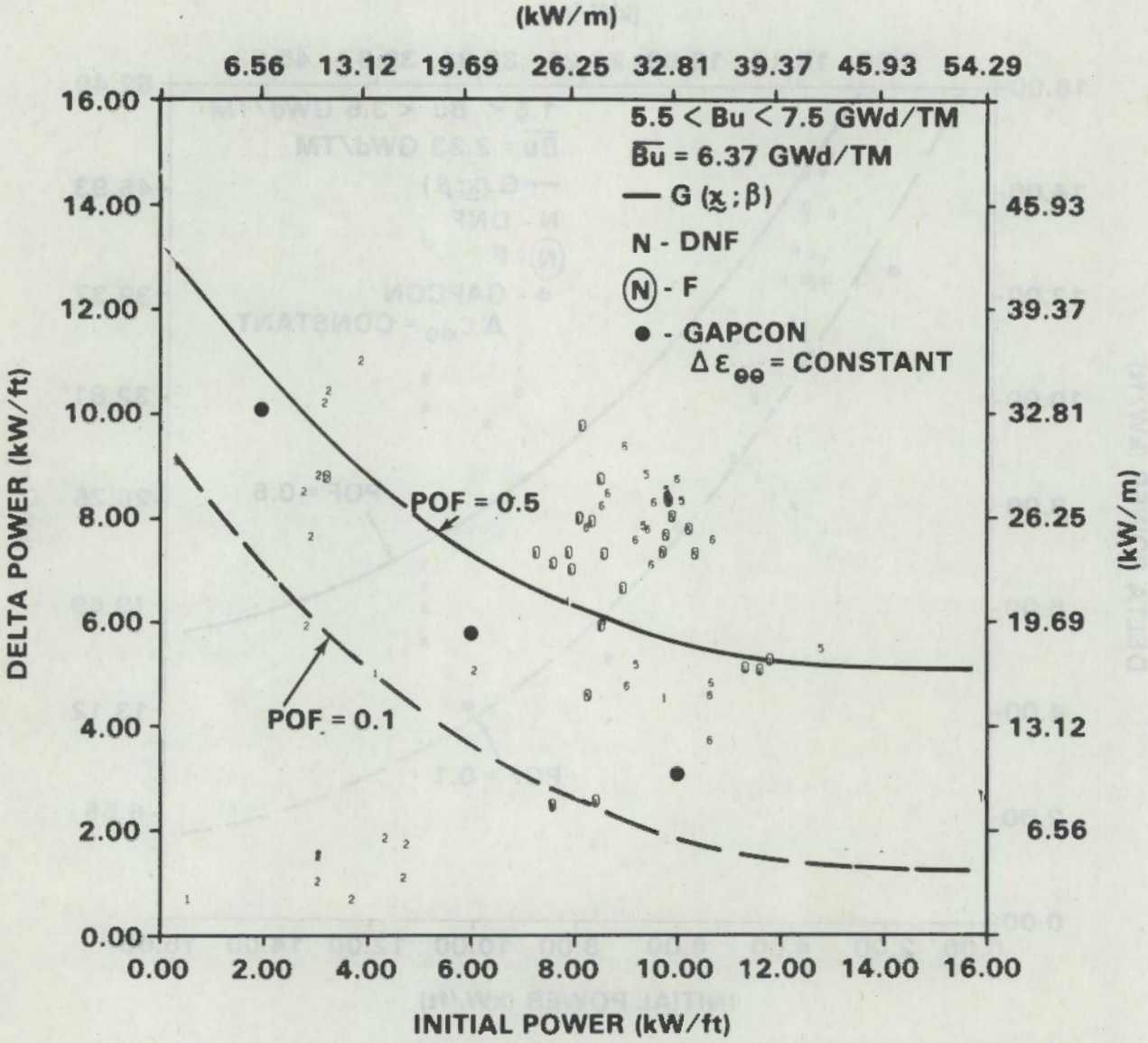

FIGURE 4.17. Shown Are All Failed (F) and Did Not Fail (DNF) Fuel Data for This Burnup Interval. Also shown are the 10% and 50% probability of failure (POF) curves and three simulated transients.

subjected to the differential thermal expansions of the fuel and cladding that accompany a transient increase in fuel rod power. Therefore, power ramping rate ($\dot{P}$), as the corollary operating parameter to strain rate in the Zry cladding, appears to be an operating variable of first order importance in PCI fuel failures.

TABLE 4.2. Postulated Effect of Strain/Power Ramping Rate on the Estimated Probability of Failure

Operating Parameters (Data Set 1)			Probability of Failure %		
			SEAF /SEAF		
Bu	Pi	ΔP			
GWd/MTM	kW/ft	kW/ft	1	1.25	1.5
2.13	3.17	12.25	10.4	1.24	0.14
2.42	3.51	14.39	49.4	11.6	1.75
6.04	8.44	8.66	79.9	63.6	43.5

4.6 SUMMARY

A detailed statistical analysis of the failed fuel data indicated that additional parameters besides P, ΔP, and Bu are needed to fully define PCI fuel failure in terms of failure probability estimates with known confidence limits. Additional variables are needed. The environmental and strain rate dependent, strain energy absorption to failure (SEAF) constitutive property of the Zircaloy cladding and power ramping rate ($\dot{P}$) as the corollary operating parameter, have been postulated as one additional variable of first order importance to the PCI fuel failure phenomenon. Time-to-failure (TTF) was also examined as a potential variable. Because there was very little information relative to TTF in the composite data, the order of its importance to the PCI fuel failure phenomenon, or its usefulness as an adjunct function in estimating the probability of failure, is uncertain.

PROFIT is the result of the application of standard statistical regression methods to all available PCI fuel failure data and an analysis of the environmental and strain rate dependent stress-strain properties of the Zry cladding. The PROFIT model introduces an environmental and strain-rate dependent strain energy absorption to failure (SEAF) concept as the mechanistic corollary of the operating variable, power ramping rate ($\dot{P}$), and as a criterion for failure of the Zry cladding. The modeling parameters are the operating variables:

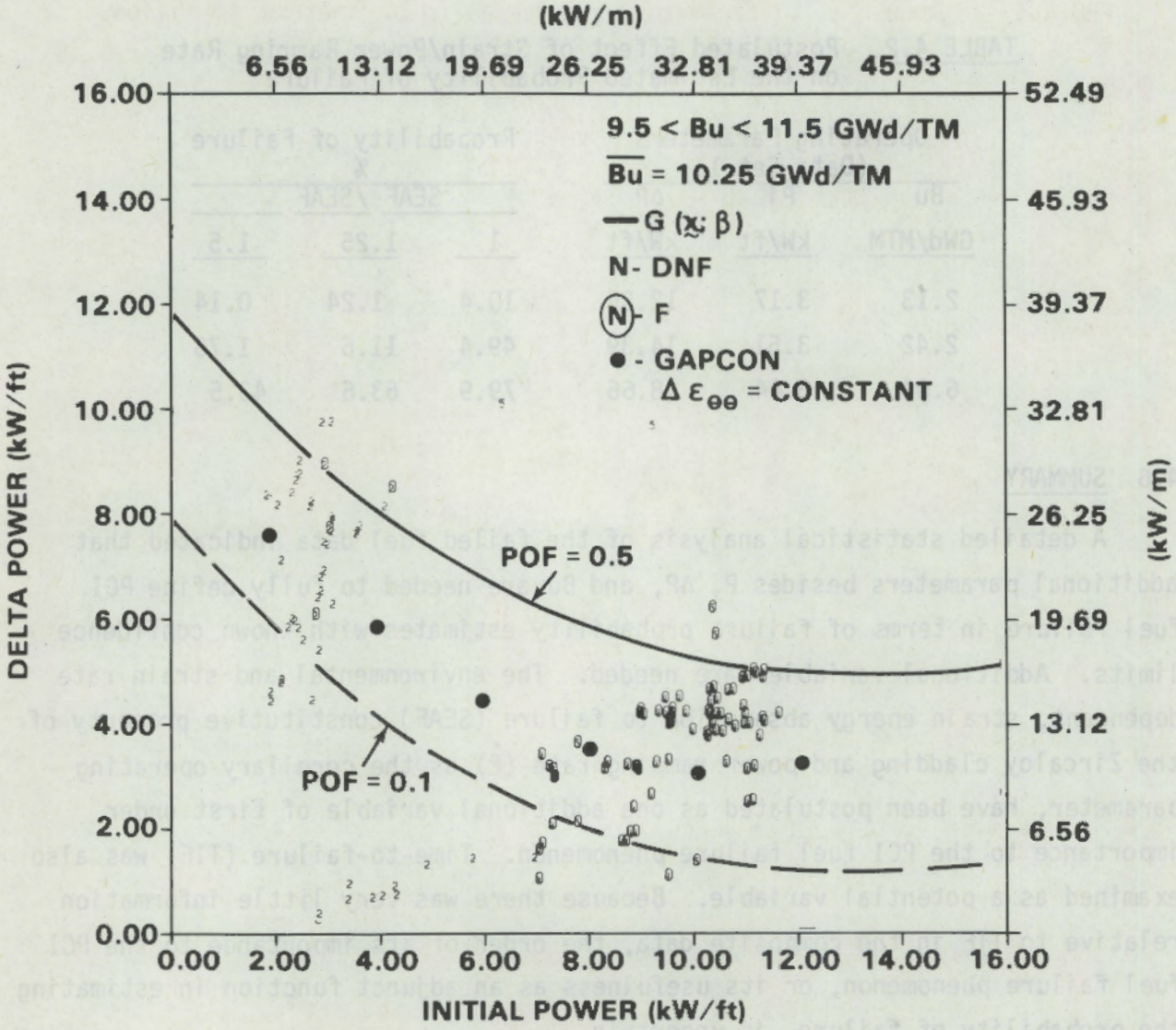

FIGURE 4.18. Shown are all Fuel Data That Failed (F) and That Did Not Fail (DNF) for This Burnup Interval. Also shown are the 10% and 50% probability of failure (POF) curves and six simulated transients.

- pre-transient power (P_i)
- transient increase in power (ΔP)
- fuel burnup (Bu)

and the constitutive material property:

- strain energy absorption to failure (SEAF).

PROFIT is summarized in terms of these modeling parameters as follows:

$$\Delta P_{SM} = \frac{A}{2} \cdot \cosh\left(\frac{P_i - P_a}{A}\right) \tag{4.1}$$

and:

$$P_a = B \left[1 + e^{-C \cdot Bu}\right] \tag{4.2}$$

$$TTF = \alpha \cdot e^{K (P_f - P_a)} \tag{4.5}$$

$$S = \beta_0 + \beta_1 \Delta P_o - \beta_2 \Delta P_{SM} \left(\frac{SEAF_o}{SEAF_c}\right) \tag{4.7}$$

$$POF = \frac{e^S}{e^S + 1} \tag{4.8}$$

where:

P_i = initial, pre-transient power - kW/ft

P_f = final, post-transient power - kW/ft

Bu = fuel burnup - GWd/MTM

ΔP_o = observed increase in power - kW/ft

ΔP_{SM} = statistical mean increase in power - kW/ft

$SEAF_o$ = strain energy absorption to failure for the Zry cladding at the strain rate corresponding to the observed power ramping rate

$SEAF_c$ = the minimum in the strain energy absorption for the Zry cladding at the critical strain rate corresponding to a critical power ramping rate

TTF = time-to-fail-minutes

POF = probabability of failure

$A = 8.23$

$B = 12.70$

$C = 0.34$

$\beta_0 = -0.36$

$\beta_1 = 0.58$

$\beta_2 = 0.63$

$\alpha = 48$

$K = -0.43$

Equation 4.5 is currently considered to be only an adjunct function, wherein failure is considered to be likely if and when TTF $\leq$ T/4 and unlikely when TTF >> T/4. Because the time-to-fail observations are sparse and statistically uncertain, Equation 4.5 must be used with considerable caution. Because the effects of strain/power ramping rate on the strain energy absorption to failure characteristics of the Zry cladding have not yet been systematically investigated, no attempt was made herein to provide any estimates of the $f(SEAF_o/SEAF_c)$ multiplier to be used in Equation 4.7.

5.0 COMPARISON OF PCI-OGRAM AND PROFIT PREDICTIONS

J. C. Wood, Contributing Author, CRNL

5.1 THREE-DIMENSIONAL PROBABILITY PLOTS

Defect probabilities for a variety of combinations of P, ΔP, and Bu as predicted separately by the PCI-OGRAM and PROFIT models are given in Table 5.1. At a given burnup, the predictions may be represented as pseudo-three-dimensional surfaces using as axes the three parameters defect probability, P, and ΔP. Figure 5.1 shows such a comparison for fuel that experienced power ramping after receiving a burnup of 300 MWh/kgU (12.5 GWd/MTM). The agreement in predictions between the two models is reasonable. Unfortunately, the overlapping of the respective defect probability surfaces on Figure 5.1 caused the diagram to become more complicated that desirable. Therefore, to avoid confusion, we have drawn the defect probability predictions of PCI-OGRAMS in mirror-image form in Figure 5.2 and arranged them to the right of the equivalent PROFIT predictions for ease of comparison.

5.2 SPECIFIC COMPARISON

The following are points of agreement between the two models:

1. Defect probabilities generally increased as ΔP was increased. Also, at the higher powers, defect probabilities increased as P was increased.
2. For a given P and ΔP, defect probabilities increased with increasing burnup. The change was largest at low burnup <300 MWh/kgU (<12.5 GWd/MTM).

The main points of disagreement between the two models:

1. At 100 MWh/kgU (4.2 GWd/MTM), PCI-OGRAM predicts defect probabilities half to one-third as high as PROFIT (Figure 5.2a).
2. When ΔP = 20 kW/m (6 kW/ft) PCI-OGRAMS suggest defect probabilities that are lower by a factor of 2 or 3 relative to PROFIT predictions. Note the sudden dip in the curves on the right of Figures 5.2b and 5.2c.

TABLE 5.1. Comparison of the Predictions of the PCI-OGRAM* and PROFIT Models

P_i		P_f		ΔP		Defect Probabilities %					
						100 MWh/kgU (4.2 GWd/MTM)		300 MWh/kgU (12.5 GWd/MTM)		500 MWh/kgU (20.8 GWd/MTM)	
kW/m	(kW/ft)	kW/m	(kW/ft)	kW/m	(kW/ft)	PCI-OGRAM	PROFIT	PCI-OGRAM	PROFIT	PCI-OGRAM	PROFIT
10	(3)	50	(15)	40	(12)	33	65	100	86	100	90
20	(6)	50	(15)	30	(9)	33	63	72	78	83	80
30	(9)	50	(15)	20	(6)	15	44	17	55	17.8	57
40	(12)	50	(15)	10	(3)	9	19	11	22	11.5	23
10	(3)	40	(12)	30	(9)	11	26	38	54	75	57
20	(6)	40	(12)	20	(6)	11	23	17	40	17.6	41
30	(9)	40	(12)	10	(3)	9	12	11	18	11.5	18
10	(3)	30	(9)	20	(6)	<1	6	11.5	17	15	19
20	(6)	30	(9)	10	(3)	<1	5	11	10	11.5	11.5
10	(3)	20	(6)	10	(3)	<1	1	<1	4	<1	4
15	(4.5)	20	(6)	5	(1.5)	<1	1	<1	3	<1	2

* Dwell Time $\geq$2.5 h at high power

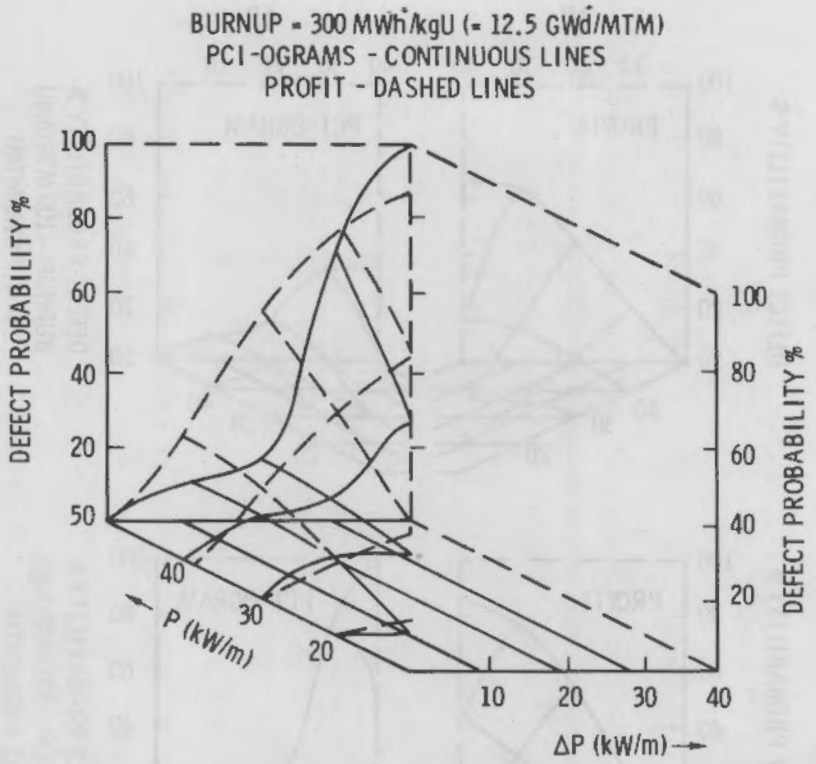

FIGURE 5.1. Comparison of the Predictions of Defect Probabilities from the PCI-OGRAM and PROFIT Models for Fuel Assemblies Whose Rods Have Received a Burnup of 300 MWh/kgU (12.5 GWd/MTM)

3. When ΔP exceeds 30 kW/m (9 kW/ft) PCI-OGRAM predicts lower defect probabilities than PROFIT at 100 MWh/kgU (4.2 GWd/MTM) but the trend reverses at higher burnup (Figure 5.2, compare a with b and c).

The reasons for relative differences will be discussed in subsections 5.3 and 5.4

5.3 LIMITATIONS IN METHODOLOGY AND SIMPLIFYING ASSUMPTIONS

Limitations of the models that contributed to the discrepancies are discussed as follows:

1. It was assumed for the PCI-OGRAM model that P_f and ΔP were independent parameters. In fact, they are related through the initial power before the ramp $P_i = P_f - \Delta P$. The positions of the threshold curves depend on

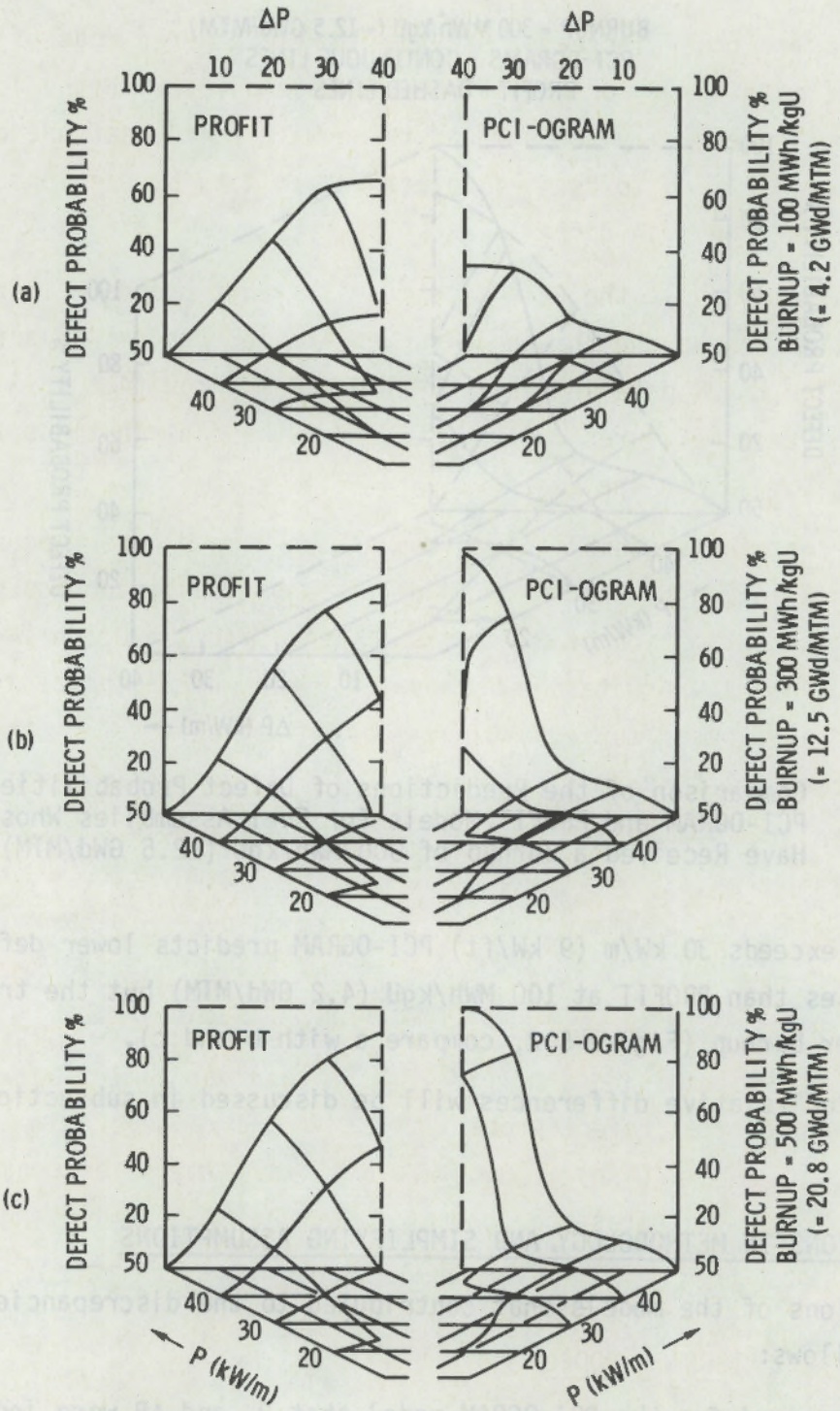

FIGURE 5.2. Comparisons of Predicted Defect Probabilities at Three Different Fuel Burnups. The PCI-DGRAM predictions on the right of each sketch are shown in "mirror image" form to prevent overlapping of the surfaces.

the powers and power increases of (the highest powered rods of) a few assemblies with low P_f or ΔP. Since the assemblies with the lowest P_f were not necessarily the same as those with the lowest ΔP, our assumption will tend to "smear" defect probability predictions by taking no account of possible differences in P_i.

Another assumption in the PCI-OGRAM model is that the defect probability distributions above the threshold curves are independent of burnup. This was true for CANDU data in the range 100 $\pm$60 MWh/kgU (4.2 $\pm$3.5 GWd/MTM), but inspection of Figures 3.1 and 3.2 shows the distributions to be variable with burnup for the LWR data.

2. The time that fuel assemblies resided at the ramped power was not taken into consideration by the PROFIT model. This simplifying assumption allowed the combination of Set 1 data (dwell time t = 0.3 h) with Data Set 2 (t > 2.5 h) and Data Sets 3 and 4 (t unknown) in the derivation of the statistical mean curves. Experience showed that defect thresholds shifted by 11 to 12 kW/m (3.5 kW/ft) on changing the dwell time from 0.3 h to $\geq$2.5 h. The assumption causes a "smearing" of defect probabilities such that the same defect probability is attributed after a short ramp as for fuel that resided many hours at the ramped power following the increase.
3. No account is taken of ramp rate in the PCI-OGRAM model. However, it would be possible to add a multiplying factor that varied between 0 and 1 to act on predicted defect probabilities in the range of ramp rates 0.2 kW/m/h (0.06 kW/ft/h) to $\geq$20 kW/m/h (6 kW/ft/h) to be consistent with known safe ramping rates and laboratory studies[17] simulating the problem.

5.4 GENERAL COMPARISON OF MODELS

We can gain a broader perspective on the predictions of the PROFIT and PCI-OGRAM models by viewing them against the predictions of other models. Three other models are available for such a comparison. They are the CANDU

FUELOGRAM[21] and two unpublished models which we will term "Model K" and "Model L." All these models are in current use by their originators. Figure 5.3 compares defect probability predictions for a given burnup of 150 MWh/kgU (5.25 GWd/MTM) and for a dwell time at the ramped power greater than 2.5 h. Salient characteristics are:

1. Model K was based on the assumption that the PCI defect mechanism is local mechanical overload. Therefore, the power shock that causes defects is closely related to ΔP, hence the strong dependence on ΔP (Figure 5.3a) and weak dependence on P.

2. Model L was derived using data with known gross differences in the time the fuel dwelled at the ramped power but time dependency was ignored. The resultant defect probability distribution (Figure 5.3b) was very different from Model K and depended very heavily on the ramped power rather than the power increase. At high powers, very high defect probabilities were predicted for modest power increases.

3. Defect probabilities predicted by the FUELOGRAM model depend with variable (sometimes equal) weighting on both P and ΔP. Predictions (Figure 5.3c) are based entirely on CANDU fuel data allowing for differences in dwell time at the ramped power.

4. The PCI-OGRAM model shares a common defect threshold with the FUELOGRAM model at low burnup but the defect probability distribution for PCI-OGRAMS is derived entirely from LWR data concentrated at burnups in the range $300 < Bu < 550$ MWh/kgU ($12.5 < Bu < 23$ GWd/MTM). Therefore, the PCI-OGRAM is more accurate at high burnups that at the burnup depicted in Figure 5.3d.

5. A plot of the average defect probability predictions of the FUELOGRAM and PCI-OGRAM models is shown in Figure 5.3e to provide a compromise taking account of both the LWR and CANDU defect distributions, using the defect thresholds common to both models. At higher burnups this averaging would not be valid and PCI-OGRAM predictions would be more appropriate.

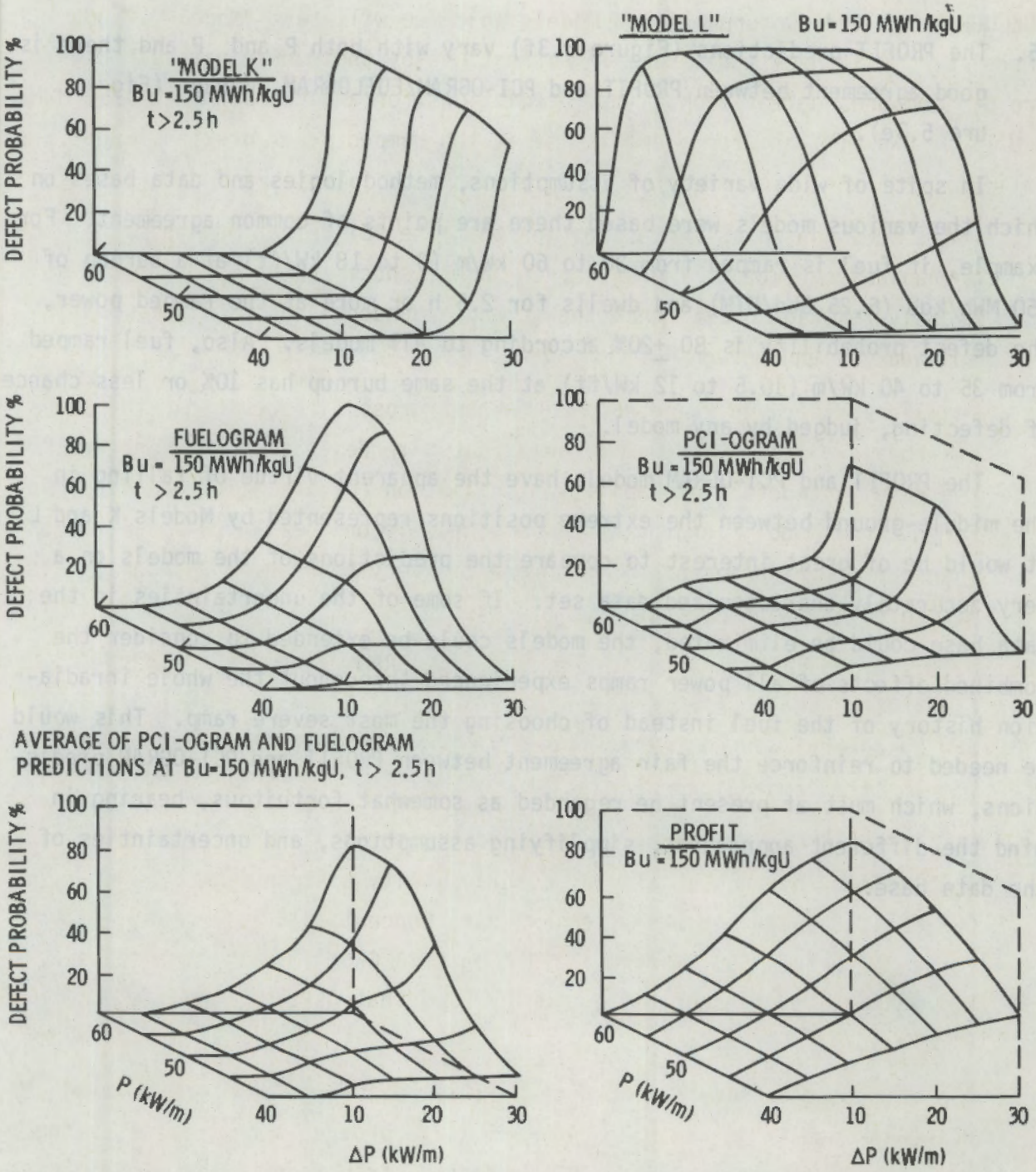

FIGURE 5.3. Comparison of Defect Probabilities at a Fuel Burnup of 150 MWh/kgU (6.25 GWd/MTM) by Various Models Over the Same Ranges of Ramped Power P (40 to 60 kW/m = 12 to 18 kW/ft) and Power Increase ΔP (D to 30 kW/m = 0 to 9 kW/ft).

6. The PROFIT predictions (Figure 5.3f) vary with both P and $\dot{P}$ and there is good agreement between PROFIT and PCI-OGRAM/FUELOGRAM average (Figure 5.3e).

In spite of wide variety of assumptions, methodologies and data bases on which the various models were based there are points of common agreement. For example, if fuel is ramped from 30 to 60 kW/m (9 to 18 kW/ft) at a burnup of 150 MWh/kgU (6.25 GWd/MTM) and dwells for 2.5 h or more at the ramped power, the defect probability is 80 $\pm$20% according to all models. Also, fuel ramped from 35 to 40 kW/m (10.5 to 12 kW/ft) at the same burnup has 10% or less chance of defecting, judged by any model.

The PROFIT and PCI-OGRAM models have the apparent virtue of falling in the middle-ground between the extreme positions represented by Models K and L. It would be of great interest to compare the predictions of the models on a very accurately characterized data set. If some of the uncertainties in the data base could be eliminated, the models could be extended to consider the combined effects of all power ramps experienced throughout the whole irradiation history of the fuel instead of choosing the most severe ramp. This would be needed to reinforce the fair agreement between PROFIT and PCI-OGRAM predictions, which must at present be regarded as somewhat fortuitous, bearing in mind the different approaches, simplifying assumptions, and uncertainties of the data base.

REFERENCES

1. Bailey, W. J. 1974. "Fuel Failures in Commercial Nuclear Power Reactors." Pacific Northwest Laboratory, Richland, WA 99352

2. Judge, F. J., H. E. Williamson and D. T. Weiss. 1975. "A General Electric Fuel Performance Update." Trans. Am. Nuclear Society 20:249.

3. Bobe, P. O. 1976. "Fuel Performance of Licensed Nuclear Power Plants Through 1974." NUREG-0032, Nuclear Regulatory Commission, Washington, D.C.

4. Pitek, M. T. 1976. "Utility Experience in LWR Fuel Performance." NUSCO-115. Joint ANS/CNA Meeting, June 13-18, 1976, Toronto, Canada.

5. Elkins, R. B. 1977. Experience With BWR Fuel Through December 1976. NEDO 21660, General Electric Company, San Jose, California.

6. Siegel, B. L. and H. H. Hagen. 1977. "Fuel Failure Detection in Operating Reactors." NUREG-0401, Nuclear Regulatory Commission, Washington, D.C.

7. Thomas, W. R. and A. S. Bain. 1972. "An Assessment of Defect Mechanisms Relating to Failures of Zirconium-Alloy Clad UO_2 Fuel." CRNL 808.

8. Wood, J. C. 1972-73. "Factors Affecting Stress Corrosion Cracking of Zircaloy in Iodine Vapor." J. Nuclear Materials 45:105-122.

9. Bain, A. S., J. C. Wood, C. E. Coleman. 1973. "Fuel Designs to Eliminate Defects on Power Increase." In Proceedings of the International Conference on Nuclear Fuel Performance, October 15-19, 1973. British Nuclear Energy Society.

10. Garlick, A. 1973-74. "Fracture of Zircaloy Cladding Under Simulated Power Ramp Conditions." J. Nuclear Materials 49:209-224.

11. Cox, B. and J. C. Wood. "Iodine Induced Cracking of Zircaloy Fuel Cladding--A Review." AECL-4936. (See also "Corrosion Problems in Energy Conversion and Generation." Electrochemical Society, pp. 275.)

12. Kreyns, P. H., G. L. Spahr and J. E. McCauley. 1975. An Analysis of Iodine Stress Corrosion Cracking of Zircaloy-4 Tubing. WAPD-TM-1203.

13. Robertson, J. A. L. 1975. "Nuclear Fuel Failures, Their Causes and Remedies." Joint ANS/CNA Topical Meeting on Commercial Nuclear Fuel Technology Today, April 28-30, 1975, Toronto, Canada.

14. Wood, J. C., B. A. Surette, I. M. London and J. Baird. 1975. "Environmentally Induced Fracture of Zircaloy by Iodine and Cesium: The Effects of Strain Rate, Localized Stresses and Temperature." J. Nuclear Materials 57:155-179.

15. Tucker, R. P., P. H. Kreyns and J. J. Kearns. 1976. "The Effects of Internal Surface Flaws, Iodine Concentration and Temperature on the Stress Corrosion Cracking Behavior of Zircaloy-4 Tubing." Presentation at the ERDA/Industry Meeting on UO_2 and ThO_2 Fuel Rod Performance, ERDA Headquarters, Germantown, Maryland, January 29-30, 1976.

16. Grubb, W. T. and M. H. Morgan, III. 1977. "Cadmium Embrittlement of Zircaloy-2." Proceedings in Conference on Water Reactor Fuel Performance, Chicago, Illinois. Amer. Nuclear Society, pp. 295-304.

17. Wood, J. C. and O. C. Hardy. 1977. "Characteristics and Interpretation of Power Ramping Defects." ANS Meeting on Water Reactor Fuel Performance, May 9-11, 1977, St. Charles, Illinois.

18. Cubicciotti, D. and R. L. Jones. 1978. EPRI-NASA Cooperative Project on Stress Corrosion Cracking of Zircaloys. Final Report. EPRI3NP-717,4 Standford Research Institute.

19. Hardy, D. G., J. C. Wood and A. S. Bain. 1978. "CANDU Fuel Performance and Development." AECL-6213, Chalk River Nuclear Laboratories, Chalk River, Ontario, K0J1J0.

20. Rolstad, E., et al. 1973. "Dimensional Changes of the Fuel and the Resulting Cladding Integrity Problems Under Irradiation." Transactions of CREST Specialist Meeting, October 1973, Saclay, France.

21. Penn, W. J., R. K. Lo and J. C. Wood. 1977. "CANDU Fuel - Power Ramp Performance Criteria." Nuclear Technology 34:249-268.

22. Strub, B. R. 1977. A Method for the Prediction of Boiling Water Reactor Fuel Failure. M. S. Thesis, Iowa State University.

23. Djurle, S. and H. Taylor. 1969. Post-Irradiation Evaluation of the Third Swedish Fuel Assembly, IFA-21, Irradiated in the Halden Boiling Heavy Water Reactor. HPR-114.

24. Djurle, S., G. Lysell and H. Morgard. "Some Irradiation Studies of Fuel Clad Interaction and Clad Cracking." A/CONF. 49/P/315, May 1971, Sweden.

25. Aas, S., K. D. Olshausen, K. Videm. 1973. "Fuel Failures Caused by Overpower Ramps." In Proceedings of the International Conference on Nuclear Fuel Performance, October 15-19, 1973, British Nuclear Energy Society.

26. Bozzoni, T., G. Pugnetti, and G. Valli. 1973. "Irradiation Experience in the Development of a Fuel Element for the Prototype CIRENE Reactor." In Proceedings of the International Conference on Nuclear Fuel Performance, October 15-19, 1973, British Nuclear Energy Society.

27. Chagrot, M., O. Ringot and H. Vidal. 1973. "The Behavior of Zircaloy-UO_2 Fuel Elements Working at Low Temperature (300°C)." In Proceedings of the International Conference on Nuclear Fuel Performance, October 15-19, 1973, British Nuclear Energy Society.

28. Knudsen, P., H. H. Hagen and J. Stiff. 1973. "Overpower Testing of UO_2-Zr Fuel Pins." Transaction of CREST Specialist Meeting, October 1973, Saclay, France.

29. Lysell, G. 1973. "Overpower Experiments on IFA-5 Fuel Rods in R2 at Studsvik." Transaction Enlarged Halden Programme Group Meeting, December 1973, Halden, Norway.

30. Lysell, G. and G. Valli. 1973. "Overpower Ramp Tests on CIRENE Prototype Fuel Pins." In Proceedings of the International Conference on Nuclear Fuel Performance, October 15-19, 1973, British Nuclear Energy Society.

31. Rolstad, E. 1976. "Model for Prediction of Fuel Failures." Trans. Am. Nuclear Soc. 24:163.

32. Rolstad, E. and K. Svanholm. 1973. "Overpower-to-Failure Experiment on a High Burnup Fuel Rod." In Proceedings of the International Conference on Nuclear Fuel Performance, October 15-19, 1973, British Nuclear Energy Society.

33. Fuhrman, N., V. Pasupathi and T. E. Hallowell. 1975. "Evaluation of Fuel Rod Performance in Maine Yankee Core I." Joint CE/EPRI Fuel Performance Evaluation Program, CENPD-221, December 1975.

34. Knudsen, P. and N. Kjaer-Pederson. 1975. "Performance Analysis of PWR Power Ramp Tests." ASME Transactions, December 1975, Houston, Texas.

35. Sipush, P. J. 1975. "Power Ramp Demonstrations in Westinghouse PWRs." WCAP-8531.

36. Furhman, N., et al. 1976. "Evaluation of Fuel Performance in Maine Yankee Core I." EPRI NP-218, Project 586-1.

37. Svanholm, K. 1977. "The Fourth Series of Overpower Tests in IFA-405." Paper presented at the Enlarged Halden Programme Group Meeting, March 8-12, 1976, Sanderstollen, Norway.

38. Borresen, S., D. L. Pomeroy, E. Rolstad and T. O. Sauar. 1977. "Nuclear Fuel Performance Evaluation." EPRI NP-409.

39. Cordall, D., R. M. Cornell, K. W. Jones and J. S. Waddington. 1977. "Fuel Failure in the Dodeward Boiling Water Reactor." Nuclear Technology 34.

40. Svanholm, K. 1976. "Overpower Tests in IFA-405." Paper presented at the Enlarged Halden Programme Group Meeting, March 8-12, 1976, Sanderstollen, Norway.

41. Rosenbaum, H. S. 1978. "Demonstration of Fuel Resistant to Pellet-Cladding Interaction." Second Semiannual Report, January-June 1978. GEAP-32773-1.

42. Pankaskie, P. J. 1978. The Impact of Pellet-Cladding Interaction on Fuel Integrity - A Status Report. PNL-2667, Pacific Northwest Laboratory, Richland, WA 99352

43. Lanning, D. D., C. L. Mohr, F. E. Panisko and K. B. Stewart. 1978. GAPCON THERMAL-3 Description. PNL-2434, Pacific Northwest Laboratory, Richland, WA 99352.

44. Parkins, R. N. 1977. "The Development of Strain Rate Testing and Its Implication." ASTM STP 655, pp. 5-24. ASTM Symposium on Evaluation Criteria for Determining the Susceptibility of Stainless Steels to Intergranular Corrosion, May 1-6, 1977, Toronto.

45. Reinoehl, J. E. and W. K. Boyd. 1971. "The Use of Slow Strain Rate Experiments in Evaluating Resistance to Environmental Cracking." AGARD-CP-98. Paper presented at the Structures and Materials AGARD, 33rd Meeting, October 5-6, 1971, Brussels, Belgium.

46. Wearmouth, W. R., G. P. Dean and R. N. Parkins. 1973. "Role of Stress in the Stress Corrosion Cracking of a MgAl Alloy." NACE 29:6.

47. Scully, J. C. and T. A. Adepoju. 1977. "Stress Corrosion Crack Propagation in A Ti-O Alloy in Aqueous and Methanolic Solutions." Corrosion Science 17:789-812.

48. Bradford, S. A. and T. Lee. 1978. "Effect of Strain Rate on Stress Corrosion Cracking of Brass." Corrosion, NACE.

49. Peehs, M., H. Stehle, E. Steinberg. 1978. "Out-of-Pile Testing of Iodine Stress Corrosion Cracking in Zry Tubing Under the Aspect of the PCI-Phenomenon." 4 ASTM Conf. on Zr in the Industry, June 1978.

50. Coffin, L. F. 1978. The Localized Ductility Method for Evaluating Zircaloy-2 Cladding. Report No. 78 CRD155, General Electric Company.

51. Tomalin, D. S. 1977. "Localized Ductility of Radiated Zircaloy-2 Cladding in Air and Iodine Environment." ASTM-STP-633.

52. Lee, D. and R. B. Adamson. 1977. "Modeling of Localized Deformation in Neutron Irradiated Zircaloy-2." ASTM-STP-633.

53. Zebroski, E. L. and J. T. A. Roberts. 1977. "EPRI Zircaloy Properties Program." Invited paper--Fifth Water Reactor Safety Research Information Meeting, November 7-11, 1977, UNSBS, MD.

54. Ramachandran, V., et al. 1973. "Dislocation-Solute Interactions and Mechanical Behavior of Zirconium and Titanium." Indian Journal of Technology II:485-492.

55. Veever, K., W. B. Rotsey and K. R. Snowden. 1969. "The Effect of Neutron Irradiation on Cold Work on the Strain-Aging Behavior of Zircaloy-2." Applications-Related Phenomena for Zirconium and Its Alloys, ASTM STP 548, American Society of Testing and Materials, pp. 194-209.

56. Pankaskie, P. J. "Irradiation Effects on the Mechanical Properties of Zirconium and Dilute Zirconium Alloys - A Review." BN-SA-618. (To be published in ASM Metals Handbook.)

57. Bement, A. L. 1967. "Symposium on Radiation Effects." American Institute of Mining, Metallurgical and Petroleum Engineers, 37:671.

58. Shober, F. R., et al. 1963. "Investigation of the Yield Pheonomeon in Zircaloy-2 at Elevated Temperatures." UC-25 Metals, Ceramics and Materials, (TID-4500, 18th Ed.) Report No. BMI-1616.

59. Weinstein, D. 1966. "Yield Point Occurrence in Polycrystalline Alpha-Zirconium." Electrochemical Technology 4:7-8.

60. Fearenough, G. D. and A. Cowan. 1967. "The Effect of Hydrogen and Strain Rate on the 'Ductile-Brittle' Behavior of Zircaloy." J. Nuclear Materials 22:137-147.

61. Sabol, G. P. and S. G. McDonald. 1976. "Strain-Rate Dependent Mechanical Response of Zircaloy-4." J. Nuclear Materials.

62. Thorpe, W. R. and I. O. Smith. 1978. "Tensile Properties of Zr-1 wt% Nb Alloy." J. Nuclear Materials 78:49-57.

63. Hardy, D. G. 1970. "The Effect of Neutron Irradiation on the Mechanical Properties of Zirconium Alloy Fuel Cladding in Uniaxial and Biaxial Tests." Irradiation Effects on Structural Alloys for Nuclear Reactor Applications. ASTM STP 484, American Society for Testing and Materials, pp. 215-158.

64. Pankaskie, P. J. 1962. "Creep Properties of Zircaloy-2 for Design Application." HW-75267.

65. Fidleris, V. 1975. "Summary of Experimental Results on In-Reactor Creep and Irradiation Growth of Zirconium Alloys." Atomic Energy Review 13:1.

66. Fidleris, V. 1978. "Primary Creep of Zircaloy-2 Creep Under Irradiation." Fourth International Conference on Zirconium in the Nuclear Industry, June 27-29, 1978, Stratford-Upon-Avon.

67. Lee, D. 1970. "The Strain Rate Dependent Plastic Flow Behavior of Zirconium and Its Alloys." Metallurgical Transactions 1:1607.

68. Azzarto, F. J., E. E. Baldwin, F. W. Wiesinger, and D. M. Lewis. 1969. "Unirradiated, In-Pile and Post-Irradiation Low Strain Rate Tensile Properties of Zircaloy-4." J. Nuclear Materials 30:208-218.

APPENDIX A

NUMERICAL CHARACTERIZATION OF EACH DATA SET

APPENDIX A

NUMERICAL CHARACTERIZATION OF EACH DATA SET

The raw data for each of the sets can be characterized using standard statistical techniques. These procedures given an indication of the grouping of the individual data points and the relative spread of each of the points. It also gives a means of looking at the individual data sets relative to each other and how they relate to total range of P, ΔP, and Bu.

It would be desirable if each of the data sets were uniformly distributed over the region of interest in the (Bu, P_i, ΔP) space. Such data would provide the most information about probability of failure and also allow the different data sets to be compared on similar terms. The data sets that were presented for this study do not fall in this classification.

The following statistics were calculated for each data set;

1) the mean location of the observations in the P, ΔP, Bu space
2) the standard deviations of each coordinate in the P, ΔP, Bu space
3) the minimum and maximum values attained by each coordinate
4) the correlation matrix of the individual parameters and the eigenvalue decomposition
5) histograms for each coordinate for both failed and non-failed data.

These statistical quantities have been computed for each of the 5 data sets (see Tables A.1 through A.5), where the general vector $X = [X_1, X_2, X_3]$ is used for Bu, P_i, and ΔP. The results of these calculations show that relative spacing of the individual data sets and give a measure of how well they might be expected to fit together in one common set.

The mean and standard deviation for each of the parameters characterizes the grouping of the data along the Burnup, Initial Power and Δ Power axis. These values are also used to compute the correlation matrix and the associated decomposition of this matrix into its eigenvalues and eigenvectors.

If the correlation between X_1, X_2, or X_3 is equal to unity then it is an indication that that particular variable of interest is linearly dependent on the other variable. A correlation value of zero shows that there is no relationship.

The eigenvalues for the correlation matrix give an indication of the grouping of the data about either a line or plane in X space. A very large eigenvalue for one direction with the other values very near zero gives an indication that the data are grouped about a line in X space.[(a)] If the eigenvalues are of approximately equal magnitude then the data are not grouped around a line but are in a ball. The eigenvector gives the direction cosines for each of the associated eigenvalues. The eigenvector associated with the largest eigenvalue can be considered as the major axis of an ellipsoid encompassing the data.

The absolute magnitude of the components of the correlation matrix, as well as the eigenvalues and eigenvectors are all normalized. The values then show the relative magnitude and the relationship between different axis or directions in X space. The correlation matrix is calculated from the covariance matrix which includes the variances reported in Tables A-1 through A-6.

The covariance matrix $S = [S_{ij}]$ of the vector $\underset{\sim}{X}(X_1, X_2, X_3)$ where X is the set of variables burnup, intial power, and delta power, is a positive semi-definite symmetric 3 x 3 matrix. It contains all of the covariances of the coordinate pairs in the vector $\underset{\sim}{X}$. This can be described in terms of an equation as:

$$S_{ij} = \text{Cov}\ (X_i, X_j) = E([X_i - E(X_i)]\,[(X_j - E(X_j)])$$

where:

$E(X_i)$ = mean of the variable X_i

X_i = variable for the coordinate i

(a) one zero eigenvalue indicates the data points lie on a plane, and, finally, if the three eigenvalues are about the same magnitude the data cluster is spherically shaped.

The covariance matrix provides information about the dispersion in the data and any linear dependencies that may exist between the coordinates in $\underset{\sim}{X}$. The values on the main diagonal of this matrix are the variances of the respective coordinates. The square root of the variances on the diagonal are the standard deviation reported in Tables A-1 through A-5.

When the coordinates X_i are not all of the same magnitude, it is better to normalize the coordinates by dividing by the standard deviation. This becomes the correlation matrix $R = r_{ij}$

where

$$r = \frac{s_{ij}}{\sqrt{S_{ii}}\ \sqrt{S_{jj}}}$$

$\sqrt{S_{ii}}$ = standard deviation for the X_i coordinate.

If, for example, coordinates X_2 and X_3 are linearly dependent, the $|r_{23}| = 1$. To locate the more subtle linear dependencies in the data, one must decompose the matrix R into its eigenvalues and eigenvectors. Any eigenvectors that are associated with a zero eigenvalue describe a linear dependency between the cordinates in $\underset{\sim}{X}$. That is, if $\underset{\sim}{V} = (V_1, V_2, V_3)$ is an eigenvector associated with zero then,

$$\frac{V_1[X_1 - E(X_1)]}{\sqrt{S_{11}}} + \frac{V_2[X_2 - E(X_2)]}{\sqrt{S_{22}}} + \frac{V_3[X_3 - E(X_3)]}{\sqrt{S_{33}}} = 0$$

for any vector $\underset{\sim}{X}$ in the data set.

The eigenvectors associated with non-zero eigenvalues also have a geometric significance. The eigenvector associated with the largesteigenvalue describes the direction in which the 3-dimensional point cluster is most elongated (after the data has been scaled by dividing each coordinate by its standard deviation). In general, each eigenvector represents a principal axis of an elipsoid that describes this scaled data.

TABLE A.1. Data Set 1

STATISTICAL CHARACTERIZATIONS
# of Observations = 104
# of Failures = 46
Proportion of Failures = 0.44

Coordinate Summary

Coordinate	Mean	Stnd. Dev.	Min.	Max.
Burnup(X_1)	4.054	1.52	2.	6.33
Initial Power(X_2)	6.124	2.54	.3	10.3
Delta Power(X_3)	8.284	3.33	.5	14.752

Analysis of Correlation Matrix

Correlation Matrix	X_1	X_2	X_3	Value	Eigenvalue/Vector Decomposition .1752	.1986	2.5262
X_1	1				.8000	-.0988	-.5919
X_2	.779	1		vector	-.3255	.7522	-.5663
X_3	-.806	-.703	1		.4041	.65457	.5735

Histogram of Burnup

Non-Failures

Middle of Interval	Number of Observations	
2.0	18	******************
2.5	0	
3.0	0	
3.5	0	
4.0	0	
4.5	3	***
5.0	27	***************************
5.5	6	******
6.0	4	****

Failures

Middle of Interval	Number of Observations	
2.0	9	*********
2.5	14	**************
3.0	0	
3.5	0	
4.0	0	
4.5	0	
5.0	6	******
5.5	13	*************
6.0	3	***
6.5	1	*

TABLE A.1. (contd)

Histogram of Initial Power

Non-Failures		Failures	
Middle of Interval	Number of Observations	Middle of Interval	Number of Observations
0.	1 *	0.	0
1.	1 *	1.	0
2.	1 *	2.	0
3.	5 *****	3.	11 **********
4.	13 **********	4.	12 **********
5.	1 *	5.	0
6.	3 ***	6.	0
7.	4 ****	7.	5 *****
8.	10 **********	8.	14 **********
9.	13 **********	9.	4 ****
10.	6 ******		

Histogram of Delta Power

Non-Failures		Failures	
Middle of Interval	Number of Observations	Middle of Interval	Number of Observations
0.	2 **	0.	0
2.	0	2.	0
4.	17 **********	4.	0
6.	15 **********	6.	9 *********
8.	7 *******	8.	13 **********
10.	10 **********	10.	1 *
12.	6 ******	12.	16 **********
14.	1 *	14.	7 *******

TABLE A.2. Data Set 2

STATISTICAL CHARACTERIZATIONS
# of Observations = 572
# of Failures = 67
Proportion of Failures = .12

Coordinate Summary

Coordinate	Mean	Stnd. Dev.	Min.	Max.
Burnup(X_1)	15.369	5.09	1.425	25.484
Initial Power(X_2)	2.916	1.13	.84	7.97
Delta Power(X_3)	5.503	2.77	-.11	11.54

Analysis of Correlation Matrix

Correlation Matrix	X_1	X_2	X_3
X_1	1		
X_2	.233	1	
X_3	-.223	-.307	1

Value	Eigenvalue/Vector Decomposition .4894	1.2028	1.3D78
vector	-.5336	-.8441	-.0526
	-.6014	.3350	-.7253
	.4947	.4184	.6864

Histogram of Burnup

Non-Failures

EACH * REPRESENTS 5 OBSERVATIONS

Middle of Interval	Number of Observations	
2.	8	**
4.	12	***
6.	13	***
8.	31	*******
10.	50	**********
12.	31	*******
14.	74	**********
16.	63	**********
18.	65	**********
20.	107	**********
22.	29	******
24.	19	****
26.	4	*

Failures

Middle of Interval	Number of Observations	
2.	0	
4.	2	**
6.	1	*
8.	6	******
10.	6	******
12.	4	****
14.	11	**********
16.	17	**********
18.	4	****
20.	9	*********
22.	2	**
24.	3	***

TABLE A.2. (contd)

Histograms of Initial Power

Non-Failures

EACH * REPRESENTS 5 OBSERVATIONS

Middle of Interval	Number of Observations	
1.0	16	****
1.5	22	*****
2.0	86	******************
2.5	149	*******************************
3.0	117	************************
3.5	34	*******
4.0	19	*****
4.5	27	******
5.0	5	*
5.5	4	*
6.0	12	***
6.5	5	*
7.0	5	*
7.5	4	*
8.0	1	*

Failures

Middle of Interval	Number of Observations	
1.0	0	
1.5	1	*
2.0	7	*******
2.5	19	******************
3.0	23	**********************
3.5	7	*******
4.0	7	*******
4.5	1	*

Histrograms of Delta Power

Non-Failures

EACH * REPRESENTS 2 OBSERVATIONS

Middle of Interval	Number of Observations	
0.	16	********
1.	78	**********************************
2.	37	******************
3.	7	****
4.	23	************
5.	42	**********************
6.	96	**
7.	91	***
8.	80	**
9.	25	*************
10.	8	****
11.	2	*
12.	1	*

Failures

Middle of Interval	Number of Observations	
0.	0	
1.	0	
2.	1	*
3.	1	*
4.	1	*
5.	7	*******
6.	8	********
7.	16	****************
8.	12	************
9.	11	***********
10.	7	*******
11.	1	*

TABLE A.3. Data Set 3

STATISTICAL CHARACTERIZATIONS
# of Observations = 518
# of Failures = 134
Proportion of Failures = 0.26

Coordinate Summary

Coordinate	Mean	Stnd. Dev.	Min.	Max.
Burnup(X_1)	11.210	1.62	5.5	12.0
Initial Power(X_2)	8.822	1.50	6.59	15.03
Delta Power(X_3)	2.776	1.12	.32	6.9

Analysis of Correlation Matrix

Correlation Matrix	X_1	X_2	X_3	Value	Eigenvalue/Vector Decomposition .61634	.8026	1.5811
X_1	1				-.6029	-.5441	-.5836
X_2	.208	1		vector	-.2406	.8214	-.5172
X_3	-.370	-.286	1		.7607	.1714	.6261

Histogram of Burnup

Non-Failures

EACH * REPRESENTS 10 OBSERVATIONS

Middle of Interval	Number of Observations
5.5	0
6.0	0
6.5	0
7.0	0
7.5	0
8.0	0
8.5	0
9.0	0
9.5	0
10.0	0
10.5	0
11.0	0
11.5	0
12.0	384 **************************************

Failures

EACH * REPRESENTS 2 OBSERVATIONS

Middle of Interval	Number of Dbservations
5.5	22 **********
6.0	4 **
6.5	1 *
7.0	0
7.5	0
8.0	3 **
8.5	11 ******
9.0	0
9.5	17 *********
10.0	60 ******************************
10.5	9 *****
11.0	7 ****

TABLE A.3. (contd)

Non-Failures

EACH * REPRESENTS 5 OBSERVATIONS

Middle of Interval	Number of Observations	
7.	93	**********
8.	85	**********
9.	166	**********
10.	20	****
11.	6	**
12.	0	
13.	0	
14.	0	
15.	14	***

Failures

Middle of Interval	Number of Observations	
7.	13	**********
8.	4	****
9.	48	**********
10.	35	**********
11.	31	**********
12.	3	***

Histogram of Delta Power

Non-Failures

EACH * REPRESENTS 5 OBSERVATIONS

Middle of Interval	Number of Observations	
.5	7	**
1.0	30	******
1.5	55	**********
2.0	56	**********
2.5	104	**********
3.0	50	**********
3.5	59	**********
4.0	12	***
4.5	3	*
5.0	0	
5.5	0	
6.0	0	
6.5	3	*
7.0	5	*

Failures

Middle of Interval	Number of Observations	
.5	0	
1.0	2	**
1.5	4	****
2.0	5	*****
2.5	7	*******
3.0	17	**********
3.5	32	**********
4.0	43	**********
4.5	15	**********
5.0	9	*********

TABLE A.4. Data Set 4

STATISTICAL CHARACTERIZATIONS
# of Observations = 481
# of Failures = 101
Proportion of Failures = 0.21

Coordinate Summary

Coordinate	Mean	Stnd. Dev.	Min.	Max.
Burnup(X_1)	11.696	.56	7.7	11.8
Initial Power(X_2)	6.186	.80	2.94	9.44
Delta Power(X_3)	4.232	2.13	1.2	10.45

Analysis of Correlation Matrix

Correlation Matrix	X_1	X_2	X_3	Value	Eigenvalue/Vector Decomposition .6079	.9914	1.4007
X_1	1				-.7011	-.1640	-.6940
X_2	.026	1		vector	-.0713	.9844	-.1606
X_3	-.390	-.066	1		.7095	.0632	.7019

Histogram of Burnup

Non-Failures

EACH * REPRESENTS 10 OBSERVATIONS

Middle of Interval	Number of Observations	
7.5	0	
8.0	0	
8.5	0	
9.0	0	
9.5	0	
10.0	0	
10.5	0	
11.0	0	
11.5	0	
12.0	380	********** ********** *******

Failures

EACH * REPRESENTS 2 OBSERVATIONS

Middle of Interval	Number of Observations	
7.5	2	*
8.0	3	**
8.5	0	
9.0	11	******
9.5	0	
10.0	0	
10.5	0	
11.0	0	
11.5	0	
12.0	85	********** **********

TABLE A.4. (contd)

Histogram of Initial Power

Non-Failures

EACH * REPRESENTS 5 OBSERVATIONS

Middle of Interval	Number of Observations	
3.0	1	*
3.5	0	
4.0	0	
4.5	2	*
5.0	28	******
5.5	81	******************
6.0	121	**************************
6.5	77	*****************
7.0	21	*****
7.5	21	*****
8.0	18	****
8.5	4	*
9.0	4	*
9.5	2	*

Failures

Middle of Interval	Number of Observations	
3.0	0	
3.5	0	
4.0	0	
4.5	0	
5.0	2	**
5.5	18	******************
6.0	50	************************** **************************
6.5	25	**************************
7.0	5	*****
7.5	0	
8.0	1	*

Histograms of Delta Power

Non-Failures

EACH * REPRESENTS 5 OBSERVATIONS

Middle of Interval	Number of Observations	
1.	7	**
2.	106	**********************
3.	95	*********
4.	97	**********
5.	33	*******
6.	24	*****
7.	9	**
8.	4	*
9.	4	*
10.	1	*

Failures

Middle of Interval	Number of Observations	
1.	1	*
2.	1	*
3.	3	***
4.	5	*****
5.	13	*************
6.	15	***************
7.	20	*********************
8.	18	******************
9.	17	*****************
10.	8	********

TABLE A.5. Data Set 5

STATISTICAL CHARACTERIZATIONS
# of Observations = 119
# of Failures = 57
Proportion of Failures = 0.48

Coordinate Summary

Coordinate	Mean	Stnd. Dev.	Min.	Max.
Burnup(X_1)	8.227	5.46	.88	31.592
Initial Power(X_2)	9.982	2.73	4.572	19.2D2
Delta Power(X_3)	6.579	3.04	.945	16.307

Analysis of Correlation Matrix

Correlation Matrix	X_1	X_2	X_3
X_1	1		
X_2	.021	1	
X_3	-.234	-.475	1

Eigenvalue/Vector Decomposition

Value	.4614	1.0169	1.5216
vector	-.3300	-.8971	-.2938
	-.6319	.4412	-.6372
	.7012	.0246	.7125

Histogram of Burnup

Non-Failures			Failures	
Middle of Interval	Number of Observations		Middle of Interval	Number of Observations
0.	5	*****	D.	4 ****
4.	19	*******************	4.	14 **************
8.	28	****************************	8.	23 ************************
12.	4	****	12.	6 ******
16.	1	*	16.	6 ******
20.	4	****	20.	5 *****
24.	0			
28.	0			
32.	1	*		

TABLE A.5. (contd)

Histogram of Initial Power

Non-Failures		Failures	
Middle of Interval	Number of Observations	Middle of Interval	Number of Observations
4.	2 **	4.	3 ***
6.	8 ********	6.	1 *
8.	11 **********	8.	11 **********
10.	26 **************************	10.	35 ********** **********
12.	6 ******	12.	1 *
14.	4 ****	14.	3 ***
16.	3 ***	16.	4 ****
18.	1 *		
20.	1 *		

Histogram of Delta Power

Non-Failures		Failures	
Middle of Interval	Number of Dbservations	Middle of Interval	Number of Observations
0.	1 *	D.	0
2.	6 ******	2.	13 **********
4.	7 *******	4.	6 ******
6.	12 **********	6.	11 **********
8.	25 ************************	8.	17 **********
10.	7 *******	10.	11 **********
12.	2 **		
14.	1 *		
16.	1 *		

APPENDIX B

STATISTICAL MODEL ANALYSIS

APPENDIX B

STATISTICAL MODEL ANALYSIS

B.1 FORMULATION OF THE OBJECTIVES

The primary objectives of this work is to develop a realistic estimate of the probability of failure for a fuel rod exposed to a given set of transient conditions. Probability of failure can most reasonably be considered to be a function of $p(\underset{\sim}{x})$ of certain variables:

$$\underset{\sim}{x} = \begin{bmatrix} x_1 \\ x_2 \\ . \\ . \end{bmatrix}$$

which describe the fuel rod and its environment.

If the form of the function $p(\underset{\sim}{x})$ is known except possibly for certain coefficients, then the problem of estimating $p(\underset{\sim}{x})$ is reduced to one of estimating these unknown coefficients. Under these circumstances p becomes a function both of $\underset{\sim}{x}$, the vector of independent variables and $\underset{\sim}{\beta}$, a vector of unknown parameters (coefficients). This relationship is made explicit by writing;

$$p\ (\underset{\sim}{x} \mid \underset{\sim}{\beta})$$

For example, one might suppose p has the following form;

$$p\ (\underset{\sim}{x} \mid \underset{\sim}{\beta}) = [1 + \exp\ (\beta_0 + \beta_1 x_1 + \beta_2 x_2 + \beta_3 x_3)]^{-1}$$

If a method can be found that will estimate the parameter vector $\underset{\sim}{\beta}$ from the available data, then these estimates can be substituted into $p\ (\underset{\sim}{x} \mid \underset{\sim}{\beta})$ to provide an estimate for probability of failure under each set of conditions described by $\underset{\sim}{x}$. In fact, once a specific form for $p\ (\underset{\sim}{x} \mid \underset{\sim}{\beta})$ is selected, there are several statistical methods that can be used to provide an estimate for the parameters $\underset{\sim}{\beta}$.

B.2 THE DATA

Many measurements may be required to completely describe the fuel rod and its operating environment. However, three variables have been provided by this study. They are:

x_1 = Bu = Fuel rod burnup
x_2 = P_i = Power experienced just before a transient
x_3 = ΔP = Power change experienced during a transient.

Additions to the above list have been suggested. For instance, dwell-time and rate of increase in power ($\dot{P}$) may possibly have an important effect on probability of failure.

These parameters could be built into the probability model by introducing a new variable x_4 and x_5 etc. The results of using such additional parameters would be to possibly improve the fit of the data and reduce some of the spread or scatter that was observed using the three parameters Bu, P_i, and ΔP.

In order to estimate the unknown parameters in the function $p(\underset{\sim}{x} \mid \underset{\sim}{\beta})$, the following information must be recorded for each fuel rod in the study.

- The fuel rod status. (Whether or not it failed after experiencing the transient.)
- The values of all variables in the vector $\underset{\sim}{x}$.

Fuel rod j will have, then, the values Y_j and $\underset{\sim}{x}_j$ associated with it where;

$$Y_j = \begin{bmatrix} 1 \text{ if fuel rod j failed after the transient.} \\ \\ 0 \text{ if fuel rod j did not fail.} \end{bmatrix}$$

$$\underset{\sim}{x}_j = \begin{bmatrix} x_{1j} \\ x_{2j} \\ x_{3j} \end{bmatrix} = \begin{bmatrix} Bu \\ P_i \\ \Delta P \end{bmatrix}$$ Burnup, initial power, delta-power environment experienced by fuel rod j

The dependent variable Y_j will have a binomial distribution determined by the probability $p\ (\underset{\sim}{x}_j \mid \underset{\sim}{\beta})$. Hence, Y_j will be distributed as;

$$p(\underset{\sim}{x}_j \mid \underset{\sim}{\beta})^{Y_j} [1 - p\ (\underset{\sim}{x}_j \mid \underset{\sim}{\beta})]^{1-Y_j}$$

The above distribution will play an important role in the formulation of a method to calculate estimates of $\underset{\sim}{\beta}$ from the data $\underset{\sim}{Y}$.

The raw data has been summarized by data sets in Tables B.2 through B.6. It would be desirable if the observations from each data set were more or less uniformly distributed throughout the region of interest in the $\underset{\sim}{x}$ space. Such data would tell us the most about $p\ (\underset{\sim}{x} \mid \underset{\sim}{\beta})$ and also allow the different data sets to be compared. To obtain some rough ideas concerning the location and dispersion of the point clusters in the $\underset{\sim}{x}$ - space, the following statistics were calculated for each data set and have been reported in Tables B.2 through B.6.

(1) Mean location of the observations in the $\underset{\sim}{x}$ space
(2) the standard deviations of each coordinate in $\underset{\sim}{x}$
(3) the maximum and minimum values attained by each coordinate in $\underset{\sim}{x}$
(4) the correlation matrix of $\underset{\sim}{x}$ and its eigenvector decomposition

The eigenvector decomposition of the correlation matrix tells whether or not the data almost lies on a plane in the $\underset{\sim}{x}$ - space. If the data lies on a plane, one of the eigenvalues will be zero. If two eigenvalues are zero and the third not zero the data lies on a line.

B.3 METHOD OF ESTIMATING $\underset{\sim}{\beta}$

The maximum likelihood method was used to obtain estimates for $\underset{\sim}{\beta}$. Maximum likelihood is a well known and versatile method for estimating unknown parameters of probability distributions. Two of the more important properties of maximum likelihood methods are:

1) The estimates $\hat{\underset{\sim}{\beta}}$, converge to the true vector $\underset{\sim}{\beta}$ rapidly as more data is taken.

2) $\hat{\underset{\sim}{\beta}}$ is asymptotically normally distributed and the covariance matrix of this distribution can be calculated.

This allows error bounds on $\underset{\sim}{\beta}$ to be calculated (see references 1, 2, 3 for further details). Using propogation of error formulas along with (2), one can calculate error bounds on the curve $p\ (\underset{\sim}{x} \mid \underset{\sim}{\beta})$. The maximum likelihood estimate $\hat{\beta}$ is obtained by maximizing the probability distribution (the likelihood) of the data with respect to $\underset{\sim}{\beta}$. In the present case, this requires the maximation of;

$$f\ (\underset{\sim}{Y} \mid \underset{\sim}{\beta}) = \prod_{j=1}^{N} p\ (\underset{\sim}{x}_j \mid \underset{\sim}{\beta})^{Y_j} [1 - p\ (\underset{\sim}{x}_j \mid \underset{\sim}{\beta})]^{1-Y_j} \tag{1}$$

or, equivalently, the mininization of;

$$-\ell\ (\underset{\sim}{\beta}) = -\sum_{j=1}^{N} \left[Y_j\ \ell n \left(p(\underset{\sim}{x}_j \mid \underset{\sim}{\beta}) \right) + (1 - Y_j)\ \ell n \left(1 - p(\underset{\sim}{x}_j \mid \underset{\sim}{\beta}) \right) \right] \tag{2}$$

Expression (2) is usually minimized, because this is an easier task and also yields results that can be used in hypothesis tests. $-\ell(\underset{\sim}{\beta})$ could be minimized using any one of many methods. Jennrich[4] presents one such method for dealing with this problem.

If replicate observations exist in the data (replicate observations are fuel rods that experienced the same conditions $\underset{\sim}{x}$), then one can modify (2) slightly to obtain a goodness of fit statistic. Under these circumstances, one can calculate a probability of failure $\hat{P}_j$ at each point x_j by forming the ratio

$$\hat{P}_j = \frac{\text{\# of fuel rods that failed under condition } x_j}{\text{\# of fuel rods that experienced condition } x_j}$$

The goodness of fit statistic is simply;

$$\chi^2 = 2 \sum_{j=1}^{N} \left[Y_j \ \ell n \left(\frac{\hat{P}_j}{p(\underset{\sim}{x}_j | \beta)} \right) + (1 - Y_j) \ \ell n \left(\frac{1 \ \hat{P}_j}{1 - p(\underset{\sim}{x}_j | \hat{\beta})} \right) \right] \qquad (3)$$

The above expression can be minimized instead of (2) to find the maximum likelihood estimates. When no replicates exist in the data, (2) and (3) are equivalent except for the factor 2. When the data $\underset{\sim}{Y}$ actually comes from a binomial distribution determined by the function $p(\underset{\sim}{x}|\underset{\sim}{\beta})$, the statistic χ^2 will have a χ^2 distribution with M degrees of freedom where

$$M = N - \text{dimension of } \underset{\sim}{\beta} \text{ vector.}$$

The statistic (Equation 3) could be used to gauge goodness of fit even when no replicates exist in the model but under these circumstances, it will be inaccurate. One could also create artificial replicates by dividing the $\underset{\sim}{x}$ - space into cubes of sufficient size to contain multiple observations. All observations in each cube could be considered to have experienced essentially the same transient and could be assigned a common $\underset{\sim}{x}$ - value, say the $\underset{\sim}{x}$ - value representing the center of the cube.

B.4 POSSIBLE CHOICES OF THE FUNCTION $p(\underset{\sim}{x}|\underset{\sim}{\beta})$

There are a great many different functional forms that have been suggested for $p(\underset{\sim}{x}|\underset{\sim}{\beta})$. However, many of the popular forms have, at least, a common structure. $p(\underset{\sim}{x}|\underset{\sim}{\beta})$ is constructed from two functions, a stress function $S(\underset{\sim}{x};\underset{\sim}{\beta})$ and a distribution function F(t).[4] It is assumed that the experimental unit (in our case, a fuel rod) fails only when the stress $S(\underset{\sim}{x};\underset{\sim}{\beta})$ exceeds the experimental unit's tolerance, T. The stress, $S(\underset{\sim}{x};\underset{\sim}{\beta})$, is assumed to be a function of the independent variables $\underset{\sim}{x}$ and can therefore be controlled by the experimenter. But the tolerence, T of the experimental unit is considered to be a random variable with distribution F(T). Thus, the probability that experimental unit j will fail when exposed to stress $S(\underset{\sim}{x}_j|\underset{\sim}{\beta})$ is just;

$$p(\underset{\sim}{x}_j|\underset{\sim}{\beta}) = Pr\left(T_j \leq S(\underset{\sim}{x}_j|\underset{\sim}{\beta})\right) = F\left(S(\underset{\sim}{x}_j|\underset{\sim}{\beta})\right)$$

The above structure concentrates attention on the stress function $S(\underset{\sim}{x}|\underset{\sim}{\beta})$ because it contains the unknown parameter vector. The distribution function $F(t)$ is frequently one of the following three distributions;

(a) standard normal $F(t) = \int_0^t \frac{1}{\sqrt{2\pi}} e^{\frac{-z^2}{z}} d z$

(b) exponential $F(t) = 1 - e^{-t}$

(c) logistic $F(t) = \frac{1}{1+e^{-t}}$ or $F(s) = \frac{1}{1+e^{-s}}$

Models that employ a normal, exponential, or logistic distribution are called, respectively, the probit, exponential and logistic models.

The most popular forms for the stress function are those that are simplest. Consequently, functions that are linear in the β's are most often used as stress functions. For instance;

$$S(\underset{\sim}{x};\underset{\sim}{\beta}) = \beta_0 + \beta_1 x_1 + \beta_2 x_2 + \beta_3 x_3$$

or

$$S(\underset{\sim}{x};\underset{\sim}{\beta}) = \beta_0 + \beta_1 x_1 + \beta_2 x_2 + \beta_3 x_1 x_2$$

or

$$S(\underset{\sim}{x};\underset{\sim}{\beta}) = \beta_0 + \beta_1 x_1 + \beta_1 x_1 + \beta_2 \ell n\ x_2$$

are all linear functions of $\underset{\sim}{\beta}$.

Of the three candidates for $F(t)$ discussed above, the logistic distribution appeared to be most reasonable for the present problem. First of all, the logistic distribution has a symmetric S-shape, and secondly, the

logistic distribution is mathematically simple; a great aid when calculating the maximum likelihood estimates. It is hoped that the use of the logistic distribution would give about the same results as any symmetric S-shaped distribution.

Several different forms of the stress function were fit to the data. They are;

(a) Cosh Failure Model;

$$S(\underset{\sim}{x};\underset{\sim}{\beta}) = \beta_0 + \beta_1 x_3 - \frac{\beta_2}{2} \cosh \frac{x_2 - \beta_3(1 + e^{-\beta_4 x})}{\beta_2}$$

(b) Main Effects Model;

$$S(\underset{\sim}{x};\underset{\sim}{\beta}) = \beta_0 + \beta_1 x_1 + \beta_2 x_2 + \beta_3 x_3$$

(c) Second Order Model;

$$S(\underset{\sim}{x};\underset{\sim}{\beta}) = \beta_0 + \beta_1 x_1 + \beta_2 x_2 + \beta_3 x_3 + \beta_4 x_1 x_2 + \beta_5 x_1 x_3 + \beta_6 x_2 x_3$$

The Cosh model is based on physical constraints and engineering judgment of the failure data. The main effects model is the simplest formulation that can be used to treat a three parameter model.

B.5 RESULTS OF FITS

Maximum likelihood fits for all three models are listed in Table B.1 through B.3. These tables contain the maximum likelihood estimates for the parameter vector $\hat{\underset{\sim}{\beta}}$, the standard deviations of these estimates and also the asymptotic covariance matrix for the vector of estimates $\hat{\underset{\sim}{\beta}}$. Finally, a goodness of fit statistic is calculated for each model along with the attained level of significance for this statistic. The results of this work shows that statistically all of the models fit the data about equally well and that the selection of one model over another must be made on some other basis.

The main effects or linear model was used to test the homogeneity of the data sets The purpose of this work was to determine the statistical justification for combining all of the data sets together. If the tests using the linear model indicated that the industrial data sets were a subset of the total population and not independent data sets it would lend credence to any further statistical analysis that could be performed.

B.6 TEST FOR HOMOGENIETY BETWEEN DATA SETS

To test whether the data sets k = 1, 2, 3, 4, 5 are homogeneous, one can perform the following test;

(1) Fit the model $p(\underset{\sim}{x}|\underset{\sim}{\beta})$ to each data set separately and calculate the loglikelihood for this fit. The loglikelihood associated with data set K will be denoted by ℓ_K.

(2) Fit the model to all data sets simultaneously and calculate the loglikelihod for this fit. Call this loglikelihood ℓ_T.

(3) For the statistic $T = 2\left[\sum_{j=1}^{5} \ell_j - \ell_T\right]$

(4) If the data sets are homogeneous, T should have a $X^2(4 \cdot P)$ distribution where P is the dimension of the parameter vector $\underset{\sim}{\beta}$. Thus, we conclude the data sets are not homogeneous when;

$$T \geq \chi^2_{1-\alpha}(4 \cdot P)$$

where α is the level of significance of the test.

Tables B.4 through B.5 give the results of the fits to the five sets of data. Table B.9 breaks the test statistic T into contributions from each difference data set. Since T = 686.27, and $\chi^2_{.99}(16) = 32$, we see that the data sets are not homogenous.

The conclusion that the data sets are not homogenous means that there is not a strong justification for combining all of the data into a unified set. It means that any further statistical calculations in terms of probabilities will be only an indication of the true probability.

It must be remembered however that the data sets in themselves contain much information which has not been quantified or included in the model development. The parameters such as ramp rate, time to failure are prime candidates for reducing the scatter in the results making the data sets homogeneous.

This would mean that it may be justifiable to combine the data sets and normalize the scatter by using these additional variables. The approach that has been taken in this work is to use the data in a combined mode and based on engineering judgment and a nonlinear regression of the failed data only develop a failure probability model.

The form of this model is the Cosh model. Three parameters in the model have been determined in a nonlinear regression analysis of the only failed data the remaining three coefficients have been determined by the methods outlined in this section. Statistically, interims of failed and non-failed data this model fits the data as well as any of the other two models. From an engineering judgment view point it is a reasonable choice for a stress function as will be indicated in the next section.

TABLE B.1. Fit of Cosh Model to Combined Data Set

Goodness of fit = 1446.31 | Degrees of freedom = 1749

Level of sig = 1.000 | # of free parameters = 3

Parameter Estimates

$\beta_0 = -.377 \pm 0.2511$ | $\beta_1 = 0.583 \pm 0.0385$

$\beta_2 = +0.631 \pm 0.0575$

Covariance Matrix

0.6308-01		
0.2099-02	0.1482-02	
-0.1145-01	-0.1639-02	0.3308-02

The Model is

$$S = \beta_0 + \beta_1 \Delta P - \beta_2 \Delta PSM$$

$$\Delta PSM = \frac{8.23}{2} \cosh \left(\frac{P_i - P_a}{8.23}\right)$$

$$P_a = 12.70 \left(1 - e^{-.34\ Bu}\right)$$

TABLE B.2. Fit of Second Order Model to Combined Data Set

Goodness of fit = 1488.90 Degrees of freedom = 1787

Level of Significance = 1.000 # of parameters = 7

Parameter Estimates

$\beta_0 = -1.250 \pm 0.905$ $\beta_1 = -0.4172 \pm 0.727$

$\beta_2 = 0.2943 \pm 0.878$ $\beta_3 = -0.0254 \pm 0.0853$

$\beta_4 = 0.0048 \pm 0.0056$ $\beta_5 = 0.0507 \pm 0.0071$

Covariance Matrix

β_0	β_1	β_2	β_3	β_4	β_5	β_6
.818388+000						
-.553843-001	.528404-002					
-.632081-001	.328707-02	.771068-002				
-.685634-001	.425028-002	.525171-002	.727503-002			
.339209-002	-.299512-003	-.372663-003	-.213033-003	.310964-004		
.438033-002	-.468538-003	-.160601-003	-.41378-003	.190433-004	.502423-004	
.308081-002	.164456-004	-.556572-003	-.460078-003	.850214-005	-.746873-005	.880519-004

TABLE 8.3. Fit of Main Effects Model to Combined Data Set

Goodness of fit = 1551.91 Degrees of freedom = 1790
Level of Significance = 1.000 # of parameters = 4

Parameter Estimates

$\beta_0 = -5.113 \pm 0.462$ $\beta_1 = -0.02011 \pm 0.0176$
$\beta_2 = 0.3165 \pm 0.0289$ $\beta_3 = 0.4020 \pm 0.031$

Covariance Matrix

Parameter	β_0	β_1	β_2	β_3
β_0	.213739+000			
β_1	-.635871-002	.308219-003		
β_2	-.113507-001	.241789-003	.833213-003	
β_3	-.117460-001	.250051-003	.567643-003	.96979-003

TABLE B.4. Fit of Main Effects Model to Data Set 1

Goodness of fit = 66.52 Degrees of freedom = 100

Level of Significance = 0.995 # of parameters = 4

Parameter Estimates

β_0 = -41.32 $\pm$ 0.462 β_1 = -0.9869 $\pm$ 0.477

β_2 = 2.338 $\pm$ 0.705 β_3 = 2.652 $\pm$ 0.593

Covariance Matrix

Parameter	β_0	β_1	β_2	β_3
β_0	.881103+002			
β_1	-.808085+000	.227258+000		
β_2	-.601840+001	.775217-001	.496471+000	
β_3	-.55420D+001	.452418-001	.378972+0D0	.351520+000

TABLE B.5. Fit of Main Effects Model to Data Set 2

Goodness of fit = 359.70 Degrees of freedom = 567

Level of Significance = 1. # of parameters = 4

Parameter Estimates

$\beta_0 = -6.847 \pm 1.21$ $\beta_1 = 0.0575 \pm 0.031$

$\beta_2 = 0.3325 \pm 0.177$ $\beta_3 = 0.4591 \pm 0.083$

Covariance Matrix

Parameter	β_0	β_1	β_2	β_3
β_0	.147013+001			
β_1	-.289823-001	.943277-003		
β_2	-.153308+000	.206352-002	.312862-001	
β_3	-.805768-001	.124618-002	.455848-002	.681520-002

TABLE 8.6. Fit of Main Effects Model to Data Set 3

Goodness of fit = 0.1 Degrees of freedom = 514

Level of Significance = 1. # of parameters = 4

Parameter Estimates

$\beta_0 = -226.9 \pm 1.61 \times 10^5$ $\beta_1 = -20.9 \pm 141$

$\beta_2 = 0.5349 \pm 38$ $\beta_3 = 0.9971 \pm 56$

Covariance Matrix

Parameter	β_0	β_1	β_2	β_3
β_0	.258021±007			
β_1	-.217491+006	.200044+005		
β_2	-.848134+004	.625193+003	.144733+004	
β_3	-.540854+004	.758815+003	.214374+003	.313333+004

TABLE B.7. Fit of Main Effects Model to Data Set 4

Goodness of fit = 277.38 Oegrees of freedom = 477

Level of Significance = 1. # of parameters = 4

Parameter Estimates

β_0 = 33.43 $\pm$ 6.43 β_1 = -3.3 $\pm$ 75.9

β_2 = 0.0505 $\pm$ 39.6 β_3 = 0.8829 $\pm$ 36.2

Covariance Matrix

Parameter	β_0	β_1	β_2	β_3
β_0	.413565+002			
β_1	-.488006+003	.575847+004		
β_2	-.252620+003	.298092+004	.156474+004	
β_3	-.221547+003	.261425+004	.134405+004	.131046+004

TABLE B.8. Fit of Main Effects Model to Data Set 5

Goodness of fit = 162.05 Degrees of freedom = 116

Level of Significance = .003 # of parameters = 4

Parameter Estimates

$\beta_0 = 1.44 \pm 1.23$ $\beta_1 = .0187 \pm .036$

$\beta_2 = -0.083 \pm .079$ $\beta_3 = -.1274 \pm .075$

Covariance Matrix

Parameter	β_0	β_1	β_2	β_3
β_0	.150706+001			
β_1	-.187618-001	.126441-002		
β_2	-.855588-001	.405936-003	.630603-002	
β_3	-.716421-001	.660561-003	.3D0603-002	.554692-002

APPENDICES REFERENCES

1. "Statistical Analysis in Biological Assay." 1964. D. J. Finney, Hafner, NY.

2. Cox, D. R. 1970. "Analysis of Binary Data." Methuen, London, England.

3. Rao, C. R. 1973. "Linear Statistical Inference and Its Applications." Wiley, NY.

4. Jennrich, R. I. and R. H. Moore. 1975. "Maximum Likelihood Estimation by Means of Nonlinear Least Squares." Princeton University, Educational Testing Service.

DISTRIBUTION

No. of Copies

OFFSITE

UNITED STATES

A. A. Churm
DOE Patent Division
9800 S. Cass Avenue
Argonne, IL 60439

360 Nuclear Regulatory Commission
Division of Technical Information and Document Control
7920 Norfolk Avenue
Bethesda, MD 20014

2 DOE Technical Information Center

D. E. Bessette
Advisory Committee on Reactor Safeguards
U.S. Nuclear Regulatory Commission
1717 "H" St., N.W.
Washington, DC 20555

F. D. Coffman
Reactor Safety Branch
Division of Operating Reactors
U.S. Nuclear Regulatory Commission
Washington, DC 20555

R. N. Duncan
Combustion Engineering
1000 Prospect Hill Road
Windsor, CT 06095

F. E. Gelhaus
Electric Power Research Institute
3412 Hillview Avenue
P.O. Box 10412
Palo Alto, CA 94304

No. of Copies

C. E. Crouthamel
Exxon Nuclear Company, Inc.
2955 George Washington Way
Richland, WA 99352

Don A. Hoatson
Fuel Behavior Research Branch
Division of Reactor Safety
Office of Nuclear Regulatory Research
U.S. Nuclear Regulatory Commission
Washington, DC 20555

Dr. W. V. Johnston
Chief, Fuel Behavior Research Branch
Division of Reactor Safety Research
Dffice of Nuclear Regulatory Research
U.S. Nuclear Regulatory Commission
Washington, DC 20555

W. M. Kiefer
Commonwealth Edison
72 W. Adams
Chicago, IL 60690

H. H. Klepher
General Electric Company
Nuclear Energy Division
175 Curtner Avenue
San Jose, CA 95126

K. Kniel
Chief, Core Performance Branch
Division of Systems Safety
Office of Nuclear Reactor Regulation
U.S. Nuclear Regulatory Commission
Washington, DC 20555

No. of Copies

Jerome Lee
Tennessee Valley Authority
1410 Commerce Union Bank Bldg.
Chattanooga, TN 37401

Rich Lobel
Oivision of Operating Reactors
Office of Nuclear Reactor Regulation
U.S. Nuclear Regulatory Commission
Washington, DC 20555

A. Lowe
Babcock and Wilcox Company
P.O. Box 1260
Lunchburg, VA 24505

George Marino
Fuel Behavior Research Branch
Division Reactor Safety Research
Office of Nuclear Regulatory Research
U.S. Nuclear Regulatory Commission
Washington, DC 20555

20 R. O. Meyer
Core Performance Branch
Division of Systems Safety
Office of Nuclear Reactor Regulation
U.S. Nuclear Regulatory Commission
Washington, OC 20555

P. A. Morris
Scandpower, Inc.
4853 Codell Avenue
Bethesda, MD 20014

T. Oldberg
Electric Power Research Institute
3412 Hillview Ave.
P.O. Box 10412
Palo Alto, CA 94304

No. of Copies

J. Owsley
Exxon Nuclear Company, Inc.
2955 George Washington Way
Richland, WA 99352

T. P. Papazoglou
Babcock and Wilcox Company
P.O. Box 1260
Lynchburg, VA 24505

G. W. Parry
Combustion Engineering
1000 Prospect Hill Road
Windsor, CT 06095

M. L. Picklesimer
Division of Reactor Safety Research
Fuel Behavior Research Branch
U.S. Nuclear Regulatory Commission
Washington, DC 20555

L. S. Rubenstein
Chief, Research Analysis Section
Office of Nuclear Reactor Regulation
U.S. Nuclear Regulatory Commission
Washington, DC 20555

A. E. Scherer
Combustion Engineering
1000 Prospect Hill Road
Windsor, CT 06095

G. G. Sherwood
General Electric Company
Nuclear Energy Division
175 Curtner Avenue
San Jose, CA 95125

B. L. Siegel
Division of Systems Safety
Office of Nuclear Reactor Regulation
U.S. Nuclear Regulatory Commission
Washington, DC 20555

No. of Copies

G. A. Sofer
Exxon Nuclear Company, Inc.
2955 George Washington Way
Richland, WA 99352

Victor Stello, Jr.
Director, Office of Inspection and Enforcement
U.S. Nuclear Regulatory Commission
Washington, DC 20555

R. L. Tedesco
Asst. Director for Reactor Safety
Division of Systems Safety
Office of Nuclear Reactor Regulation
U.S. Nuclear Regulatory Commission
Washington, DC 20555

20 M. Tokar
Core Performance Branch
Division of Systems Safety
Office of Nuclear Reactor Regulation
U.S. Nuclear Regulatory Commission
Washington, DC 20555

J. Tulenko
Babcock and Wilcox Company
P.O. Box 1260
Lynchburg, VA 24505

R. Van Houten
Fuel Behavior Research Branch
Division of Reactor Safety Research
U.S. Nuclear Regulatory Commission
Washington, DC 20555

J. C. Voglewede
Core Performance Branch
Division of Systems Safety
Office of Nuclear Reactor Regulation
U.S. Nuclear Regulatory Commission
Washington, DC 20555

No. of Copies

E. Zebroski
Electric Power Research Institute
3412 Hillview Avenue
P.O. Box 10412
Palo Alto, CA 94304

FOREIGN

M. J. F. Notley
Atomic Energy of Canada Ltd
Chalk River, Ontario
KOJ 1JO
CANADA

A. Hanevik
OECD Halden Reactor Project
Institutt for Atomenergi
P.O. Box 173
N-1751, Halden
NORWAY

K. D. Knudsen
OECD Halden Reactor Project
Institute for Atomenergi
P.O. Box 173
N-1751, Halden
NORWAY

R. W. Miller
OECD Halden Reactor Project
Institute for Atomenergi
P.O. Box 173
N-1751, Halden
NORWAY

5 J. C. Wood
Atomic Energy of Canada Ltd
Chalk River, Ontario
KOJ 1JO
CANADA

No. of
Copies

ONSITE

50 Pacific Northwest Laboratory

W. J. Bailey
J. O. Barner
E. R. Bradley
E. L. Courtright
M. E. Cunningham
S. D. Dahlgren
M. D. Freshley
R. L. Goodman
R. J. Guenther
C. R. Hann
P. L. Hendrick
P. G. Heasler (5)
K. A. Hsieh
D. D. Lanning
R. K. Marshall
R. P. Marshall
C. L. Mohr
C. Nealley
F. E. Panisko (5)
P. J. Pankaskie (10)
W. N. Rausch
R. E. Schreiber
R. H. Williams
R. E. Williford
C. L. Wilson
Technical Information (5)
Publishing Coordination RO (2)

NRC FORM 335 (7-77) U.S. NUCLEAR REGULATORY COMMISSION

BIBLIOGRAPHIC DATA SHEET

1. REPORT NUMBER *(Assigned by DDC)*
NUREG/CR-1163
PNL-2755

4. TITLE AND SUBTITLE *(Add Volume No., if appropriate)*
PCI Fuel Failure Analysis: A Report on a Cooperative Program Undertaken by Pacific Northwest Laboratory and Chalk River Nuclear Laboratories

2. *(Leave blank)*

3. RECIPIENT'S ACCESSION NO.

7. AUTHOR(S) P. J. Pankaskie Compiled by C. L. Mohr
P. G. Heasler
J. C. Wood

5. DATE REPORT COMPLETED
MONTH December YEAR 1979

9. PERFORMING ORGANIZATION NAME AND MAILING ADDRESS *(Include Zip Code)*
Pacific Northwest Laboratory
P. O. Box 999
Richland, WA 99352

DATE REPORT ISSUED
MONTH YEAR

6. *(Leave blank)*

8. *(Leave blank)*

12. SPONSORING ORGANIZATION NAME AND MAILING ADDRESS *(Include Zip Code)*
Core Performance Branch
Division of Systems Safety
U.S. Nuclear Regulatory Commission

10. PROJECT/TASK/WORK UNIT NO.
300A01038

11. CONTRACT NO.
EY-76-C-06-1830
TDO 875

13. TYPE OF REPORT
Technical, Formal

PERIOD COVERED *(Inclusive dates)*
FY-79

15. SUPPLEMENTARY NOTES

14. *(Leave blank)*

16. ABSTRACT *(200 words or less)*

Reactor fuel failure data sets for PWR, BWR and PHWR were evaluated and used as a basis for developing two predictive fuel failure models: PCI-OGRAM and PROFIT.

The PCI-OGRAM is an extension of FUELOGRAM developed by AECL. It is based on a critical threshold concept for stress dependent SCC. Thresholds are defined in terms of the minimum post-transient power and a critical minimum transient increase in power. PCI-OGRAM uses these two powers, burnup and dwell time at the peak post-transient power.

The PROFIT model, developed by PNL, is the result of applying standard statistical regression methods to the fuel failure data sets and an analysis of Zircaloy cladding properties. PROFIT uses pre-transient and transient increase powers and burnup and introduces a strain rate dependent strain energy adsorption to failure concept as the mechanistic corollary of the power ramp rate.

17. KEY WORDS AND DOCUMENT ANALYSIS

17a. DESCRIPTORS

PCI (pellet cladding interaction)
fuel rod failure analysis

17b. IDENTIFIERS/OPEN-ENDED TERMS

18. AVAILABILITY STATEMENT
National Technical Information Service

19. SECURITY CLASS *(This report)*

21. NO. OF PAGES

20. SECURITY CLASS *(This page)*

22. PRICE
$

NRC FORM 335 (7-77)